Mechanical Behavior of Hydrogels for the Use of Ionic Devices

Mechanical behavior of hydrogels for the use of ionic devices

A dissertation presented

by

Jianyu Li

to

The School of Engineering and Applied Sciences

in partial fulfillment of the requirements

for the degree of

Doctor of Philosophy

in the subject of

Engineering Sciences

Harvard University

Cambridge, Massachusetts

March 2015

Dissertation Advisors

Joost J. Vlassak, Zhigang Suo

Author

Jianyu Li

Mechanical behavior of hydrogels for the use of ionic devices

Abstract

Wearable and implantable devices hold great promise to transform the society by making healthcare continuous, personalized and affordable. They will enable mobile healthcare by monitoring continuously vital signals, and providing various stimulations on the human body. Conventional electronics face a primary challenge: their mechanical and electrical properties mismatch those of tissues. Stretchable electronics provide some remedies to the mechanical mismatch, but any interface between stretchable electronics and tissues must translate an electronic current into an ionic one (and vice versa). Whereas electronics struggle to solve many technical problems, ionic devices solve most of them readily.

Hydrogels are the materials of choice for the use of ionic devices. They mix water, mobile ions and polymer networks at molecular scales, and thus intrinsically integrate both ionic conductivity and high stretchability. Hydrogels resemble tissues biologically, mechanically and electrically. Although several ionic devices using hydrogels have been demonstrated, the mechanical behavior of hydrogels represents

one of main material constraints: complex chemomechanical interactions, poor mechanical properties and weak adhesion. To this end, this thesis focuses on the mechanical behavior of hydrogels for the use of ionic devices.

This thesis first presents theoretical and experimental approaches to characterize chemomechanical interactions of gels. How applied forces, mechanical constraints, crosslink density, solvents, pH and salt concentrations affect the properties of gels is investigated. The model of ideal elastomeric gels is extended and validated for polyacrylamide hydrogels, polyelectrolyte hydrogels and ionic liquid gels. A series of simple mechanical tests are developed to determine the equations of state.

Next, the thesis presents synthesis and characterization of hydrogels with superior mechanical properties. By engineering the molecular structure, harnessing crystallites as physical crosslinks, hybrid hydrogels achieve extremely high stiffness, strength and toughness. A new mechanism of strain-induced crystallization is also presented to toughen hydrogels.

The last part of the thesis focuses on adhesive property of hydrogels. Analytical and experimental methods are presented to quantify adhesion between highly stretchable materials. Despite of weak adhesion between hydrogels and elastomers, debonding can be retarded by reducing the hydrogel thickness. A facile method of adding nanoparticles at interface is also presented to improve the adhesion.

Table of Contents

Acknowledgements

This dissertation would not have been possible without supports from many people. First and foremost, I would like to express my deepest gratitude to my advisors, Professor Joost J. Vlassak and Professor Zhigang Suo. Thank them for their invaluable supports and guidance throughout this research. Joost has always been extremely knowledgeable and supportive, who cultivates me dedicatedly, encourages me sincerely, and helps me to tackle every difficulty in research. Zhigang has always been extraordinarily enthusiastic and enlightening, who teaches me critical, creative ways of thinking and exceptional insights into problems. Without their guidance or encouragement, I would have never stepped into the field of mechanics, where I have found different dimensions of potentials in myself. Joost and Zhigang have set a solid foundation and the best role models for my academic career, and their guidance will be a lifelong treasure for me.

I am also deeply grateful to the other members of my dissertation committee, Professor David J. Mooney and Professor Neel S. Joshi for their valuable suggestions and comments at every stage of this research. I enjoy every fruitful discussion with them, which has provided me strong impetus to carry on this research, and cultivated my research interests in the field of bioengineering. Thank David for his appreciation of my research, invaluable suggestions, and selfless supports for me to conduct experiments in his lab.

Special thanks also to Vlassak group members and Suo group members, in particular, Dr. Yuhang Hu, Widusha R.K. Illeperuma, Dr. Jeong-Yun Sun, Mingyu Li, Jingda Tang, Qihan Liu and Kechao Xiao. Dr. Yuhang Hu led me into the field of

experimental mechanics, and mentored me with care, when I started my own research at Harvard. Widusha R.K. Illeperuma and Jeong-Yun Sun are tremendously resourceful, who taught me synthesis and characterization of tough hydrogels. Mingyu Li and Jingda Tang are diligent experimentalists, without whom my research wouldn't have come into fruition. Qihan Liu and Kechao Xiao are very helpful both in research and in life. All the other groupmates offer me valuable suggestions through this research. I thank them from the bottom of my heart for the supports from various aspects.

I would also like to express thanks to professors and colleagues at Harvard. Thank Professor David A. Weitz and Center of Nanoscale Systems for the generous supports of experimental instruments. Thank Pai Wang, Hu Zhang, Sicong Shan, Han Liu, Jia Liu and many other friends at Harvard for accompanying me in the last five years. The fusion of all those talented people makes Harvard such a unique, wonderful and fantastic place to grow in wisdom, explore the new boundaries of science and technology.

Deepest love and gratitude to my families. My parents devote themselves to cultivating me at every moment of my life. Their encouragement, expectation and supports have been a perpetual driving force for my progress. Thank my sister for accompanying and sharing every happiness and sadness with me. Thank my parents in law for their countless supports and care. It is my greatest fortune to have them, and I love them as my own parents. Thank my beloved wife, Xiaozhe Wang. I cherish for you the liveliest feeling of affection and gratitude, thank you for supporting me in my dream, and standing by me in life's changing winds.

Chapter 1 Introduction

1.1 Motivation of the thesis

Mobile health promises to transform our society in yet another way—making healthcare continuous, personalized, and affordable.[1,2] This vision of mobile health raises many social, economic, and technological issues. A technological bottleneck is the ultimate objects of healthcare—human bodies—connect to the Internet primitively and indirectly. This bottleneck has inspired the development of wearable and implantable devices.[3] Wearable sensors are placed on the skin to collect various physiological data.[4-7] Implantable devices can monitor and stimulate living tissues.[8,9] Wearable and implantable devices will be essential components of mobile health.

A primary challenge in developing wearable and implantable devices is simple, but fundamental: tissues and electronics are *mismatched* in their mechanical and electrical behavior. Electronic devices are typically hard and rigid, whereas tissues are often soft and stretchable. Electronics transmit electrical signals using electrons, whereas tissues transmit electrical signals using ions. Any interface between these two systems must translate an electronic current into an ionic one (and vice versa). The mechanical mismatch can be solved partially with stretchable electronics: those devices can be stretched by using stretchable electronic conductors.[6,10-12] Commonly used electronic conductors include carbon in various forms (powders, fibers and sheets),

solid metals containing micro-cracks or patterned in serpentine shapes, and liquid metals. Although these stretchable conductors have demonstrated exciting applications, their limitations have been noted: low stretchability, limited transparency, degradation under cyclic loading, and leakage of liquid metals. Not to mention their charge carriers, electrons, are distinct from those of cells and tissues.

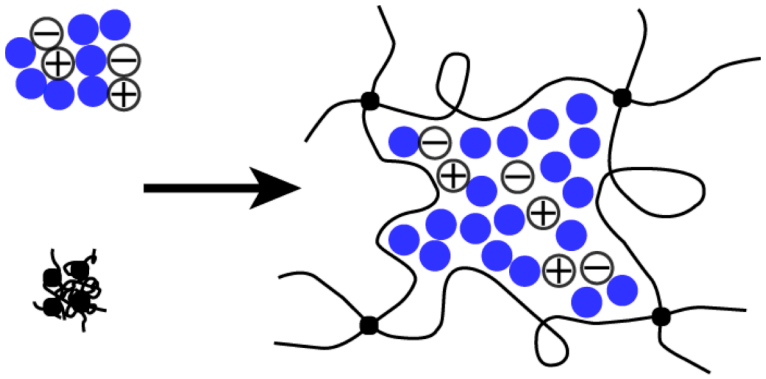

Figure 1.1 A crosslinked polymer network swells in an electrolyte solution, forming a hydrogel-based ionic conductor. The hydrogel integrate both stretchability and ionic conductivity.

Whereas electronic conductors struggle to solve these technical problems, ionic conductors (such as hydrogels) solve most of them readily. Hydrogels integrate two functions—stretchability and conductivity—at the molecular scale (**Figure 1.1**).[13] A hydrogel consists of a polymer network and water. The polymer network makes the gel a soft elastic solid, and water makes the gel a fast ionic conductor.[14] Hydrogels closely resemble soft tissues in molecular architecture; many hydrogels are biocompatible and widely used in tissue engineering[15] and drug delivery.[16] Hydrogels can be made even

softer than tissues, and be "mechanically invisible". Fundamental discoveries in the last decade have led to the development of hydrogels as tough as elastomers.

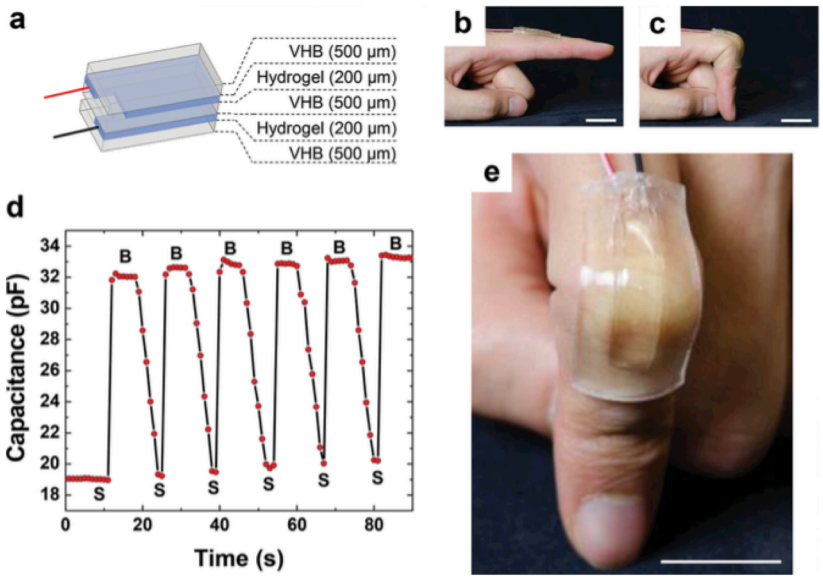

Figure 1.2 Ionic strain sensor. (**a**) A layer of stretchable dielectric is sandwiched between two layers of a stretchable ionic conductor (salt-containing hydrogel), which are then connected to two metallic electrodes. The device is covered with two additional layers of VHB. (**b, c**) The strain sensor is attached to a straight finger. The bending of the finger stretched the strain senor. (**d**) The capacitance is measured as the finger bent cyclically. 'B' denotes bent, and 'S' denotes straight. (**e**) The strain senor is fully transparent.

These unprecedented attributes have motivated the recent development of stretchable ionic devices. A dielectric elastomer sandwiched with salt-containing hydrogels forms an ionic strain sensor (**Figure 1.2**).[17] Subject to an external force, the sensor deforms and changes its capacitance, which is readily measured using a low voltage. The entire sensory sheet is fully stretchable and transparent. The sensor

monitors deformation, such as that generated by the bending of a finger. It detects stimuli with a wide dynamic range (strains from 1% to 500%) and measures pressures as low as 1 kPa.

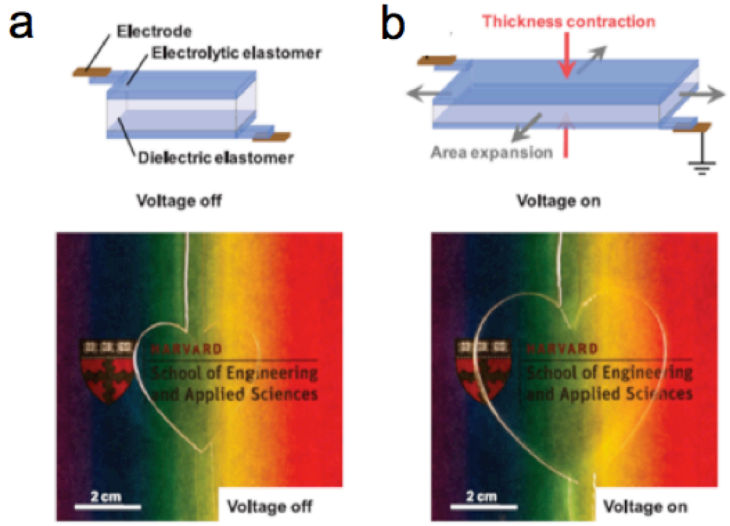

Figure 1.3 Transparent actuator capable of fast voltage-induced deformation. (**a**) A dielectric elastomer is sandwiched between two layers of an electrolytic elastomer. (**b**) When subjected to a voltage the two layers of the electrolyte spread ions of opposite signs on the two sides of the dielectric, causing the sandwich to reduce its thickness and expand in area.

A transparent actuator is also constructed with salt containing hydrogels and dielectric elastomers.[13] Subject to a voltage, the hydrogels spread ions of opposite signs on the two sides of the dielectric, resulting in an electric field that deforms the structure (**Figure 1.3**). This actuator is transparent to the entire visible spectrum, and capable of producing sounds across the entire audible spectrum.

The mechanical behavior of hydrogels is essential to the performance of ionic devices. Hydrogels mix water and polymer networks at molecular scales. The water, making a hydrogel a fast ionic conductor, is essential to the ionic conductivity.[18] Many factors affect the water content of hydrogels, including applied forces, mechanical constraints, pH, salinity, temperature and solvents.[19,20] The swelling of hydrogels involve complex chemomechanical interactions, which necessitates the development of experimental approaches to characterize the swelling behavior.

The polymer network makes a hydrogel a stretchable solid, and thus its mechanical properties are essential to the stretchability. Whereas dry elastomers like VHB have reasonable mechanical properties,[21] conventional hydrogels are soft, brittle and slippery.[22] Although tough hydrogels have been made, their fracture energy is typically on the order of $1{,}000\ Jm^{-2}$ lower than that of natural rubber (on the order of $10{,}000\ Jm^{-2}$).[23-25] Due to the interdependence of mechanical properties, a trade-off of properties seems inevitable.[26] In particular, it remains a big challenge to achieve high stiffness, strength and toughness simultaneously. It is even challenging that some hydrogels degrade significantly in electrolyte solutions.[27] Hydrogels of superior mechanical properties and chemical stability may open up many applications, including ionic devices, cartilage replacement and soft robotics.

1.2 Plan of the thesis

In this thesis, we will study the mechanical behavior of hydrogels for the use of ionic devices. We will also discuss broader impacts of the proposed methods and

materials in other fields ranging from biomedical applications like cartilage replacement, to engineering applications like soft machines. The plan of the thesis is as follow.

This thesis first presents theoretical and experimental approaches to characterize chemomechanical interactions of gels, especially the swelling behavior. We adopt the model of ideal elastomeric gels, and propose experimental methods to determine the equations of state of polyacrylamide hydrogels. To testify the method, we vary various experimental conditions, and reanalyze the data from the literature to compare them with our results. We then extend the theoretical and experimental methods for polyelectrolyte hydrogels and an ionic liquid gel. The effects of pH, salinity and non-Gaussian chain, ionic liquid are investigated.

Next, the thesis presents synthesis and characterization of hydrogels with superior mechanical properties. The toughness of hydrogels can be improved by introducing energy dissipation mechanisms. We first engineer ionic crosslinks of alginate-polyacrylamide hydrogels, and crystallites of polyvinyl alcohol-polyacrylamide hydrogels. By mixing short- and long-chain alginate, alginate-polyacrylamide hydrogels decouple strength and crosslink density, and achieve high stiffness and toughness, as well as compatibility with mobile calcium ions. By harnessing high-density crystallites as physical crosslinks, polyvinyl alcohol-polyacrylamide hydrogels achieve superior mechanical properties and chemical stability. We also discover a new toughening mechanism, strain-induced crystallization, for hydrogels. This effect leads to high toughness, and formation of anisotropic structure under deformation that results

in kinking and shape-memory property. Besides ionic devices, the resulting hydrogels will also open up new applications ranging from cartilage replacement to soft robotics.

The last part of the thesis focuses on adhesive property of hydrogels. We quantify the adhesive property with the interfacial toughness. Analytical and experimental methods are presented to measure adhesion between highly stretchable materials. We apply this approach to measure the interfacial toughness between polyacrylamide hydrogels and VHB elastomers. The effects of the thickness and crosslink density of hydrogels are investigated. We also demonstrate by introducing energy dissipation mechanisms at interface the interfacial toughness can be improved. One facial approach of adding nanoparticle solutions at interface is presented.

Chapter 2 Characterization of equations of states of hydrogels

2.1 Introduction

A hydrophilic polymer network can absorb water and swell, forming a hydrogel. The amount of swelling depends on the molecular interaction between the polymer and water, and changes greatly in response to external stimuli such as applied forces,[28] mechanical constraints,[29] temperature,[30] pH and salinity.[31-33] Hydrogels are being developed as scaffolds for tissue engineering,[34] vehicles for drug delivery,[16] sensors and actuators in micro-devices,[35] and packers in oilfields.[29] The hydrogels in devices are typically constrained by hard materials. The devices operate by exploiting the chemomechanical interaction of the hydrogels: how the mechanical constraint affects swelling, and how stimuli generate mechanical forces.[36] For applications of hydrogels in devices, it is desirable to develop experimental methods that characterize the chemomechanical behavior of gels without being constrained by models of statistical mechanics.

In this chapter, we will develop the model of ideal elastomeric gels to characterize thermodynamic properties of hydrogels. We will choose the polyacrylamide hydrogel as our focus, as it has been used extensively for stretchable ionic conductors. We will also study a stimuli-responsive hydrogel, polyacrylamide-co-polyacrylic acid hydrogel, to further extend the application of the model of ideal elastomeric gels.

2.2 Model of ideal elastomeric gels

The model of ideal elastomeric gels is based on two assumptions.[36] First, the volume of a gel is the sum of the volume of the dry network and that of the solvent. Second, the free energy of the gel is the sum of the free energy due to stretching the network and that due to mixing the polymer and the network. These assumptions lead to a set of equations of state, which can be tested experimentally without invoking specific models of statistical mechanics.

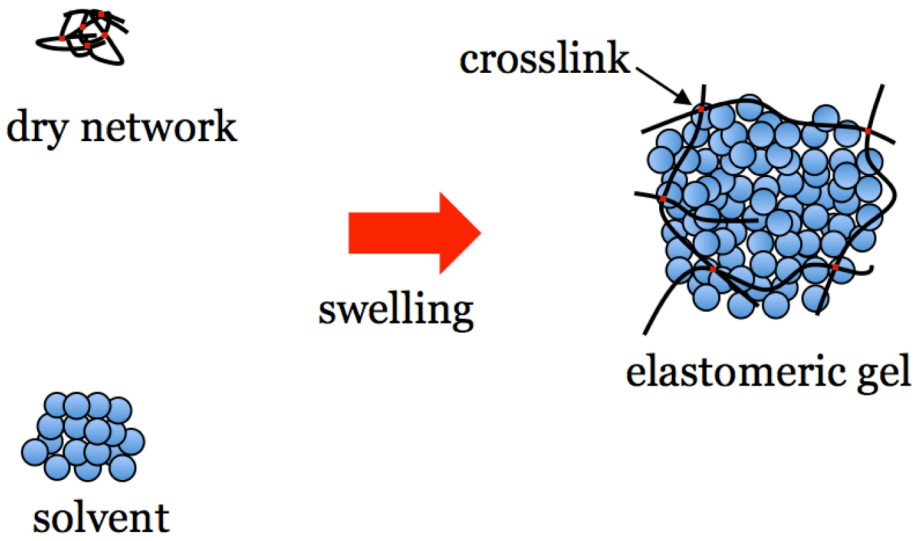

Figure 2.1 A polymer network absorbs a solvent and swells, forming an elastomeric gel.

To focus on the main ideas, here we consider deformation in principal directions (**Figure 2.1**). The equations of state for ideal elastomeric gels are derived as follows. In the reference state, the block is a unit cube of a dry network, containing no solvent and subject to no applied force. In the current state, submerged in a solvent-containing environment and subject to applied forces, the network absorbs C number of solvent

molecules, and stretches into a rectangular block of dimensions λ_1, λ_2 and λ_3. The ratio of the volume of the gel to the dry polymer, *J*, known as the swelling ratio, relates to the dimensions of the rectangular block by $J = \lambda_1\lambda_2\lambda_3$.

Recall the two basic assumptions of ideal elastomeric gels. First, the gel is a soft material; subject to the applied forces, the gel changes shape readily, but the volumes of individual polymer chains and individual solvent molecules remain nearly unchanged. The volume of the gel is related to the number of solvent molecules by a general form $J = J(C)$. Since the gels like hydrogels typically contain large amount of solvent, and the volume change due to mixing is very small.[37] Therefore, the volume of the gel is assumed to equal the sum of the volume of the dry network and that of the solvent:

$$J = 1 + \Omega C, \tag{2.1}$$

where Ω is the volume per solvent molecule.

Second, the density of crosslinks in the gel is typically very low; each polymer chain consists of a large number of monomers, so that the crosslinks negligibly affect the molecular interaction between the polymer and the solvent.[37] As an idealization, the Helmholtz free energy of the gel is assumed to be the sum of the free energy due to the stretching of the network and that due to the mixing of the polymer and the solvent:

$$W = W_{stretch}(\lambda_1, \lambda_2, \lambda_3) + W_{mix}(J). \tag{2.2}$$

The free energy of the gel, *W*, is defined as the excess in the gel relative to the sum of its constituents—that is, *W* is the free energy of the gel minus that of the dry polymer and that of the pure solvent.[37,38] The free energy due to the stretching of the network,

$W_{stretch}(\lambda_1,\lambda_2,\lambda_3)$, is a function of the stretches, and depends on the crosslink density. The free energy due to the mixing of the polymer and the solvent, $W_{mixing}(J)$, is a function of the swelling ratio, but is independent of the crosslink density.

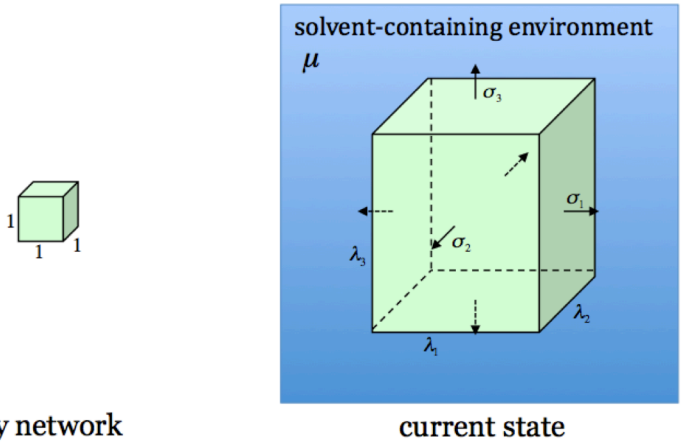

Figure 2.2 In the refenence state, a unit cube of a dry polymer network contains no solvent and is subject to no applied stress. In the current state, imersed in a solvent-containing enviroment and subject to applied stresses, the network absorbs solvent and is stretched into a rectangular block.

When a dry network is submerged in a solvent-containing environment and subject to applied forces, the network takes some time to absorb the solvent and attains a state of thermodynamic equilibrium. The condition of equilibrium is formulated as follows. Define the stresses σ_1, σ_2 and σ_3 as the applied forces divided by the areas of the faces of the rectangular block. Thus, the forces applied on the faces of the rectangular block are $\sigma_1\lambda_2\lambda_3, \sigma_2\lambda_3\lambda_1$ and $\sigma_3\lambda_1\lambda_2$ (**Figure 2.2**). The applied forces can be represented by hanging weights. Associated with a small change in the dimensions

of the rectangular block, the potential energy of the hanging weights changes by $-\sigma_1\lambda_2\lambda_3 d\lambda_1 - \sigma_2\lambda_3\lambda_1 d\lambda_2 - \sigma_3\lambda_1\lambda_2 d\lambda_3$. The gel is immersed in a solvent-containing environment such that the gel and environment can only exchange one species of molecules: the solvent. The chemical potential of the solvent in a saturated mixture of pure liquid and its vapor is set to be zero. Let μ be the chemical potential of the solvent in the environment—that is, μ is the increase of the Helmholtz free energy when the environment gains one solvent molecule from the pure solvent in the state of liquid-vapor mixture. Associated with the transfer of dC number of solvent molecules from the environment to the gel, the free energy of the environment changes by $-\mu dC$. The gel, the hanging weights and the environment together form a composite thermodynamic system. The Helmholtz free energy of the composite is the sum of the Helmholtz free energy of the gel, the potential energy of the weights, and the Helmholtz free energy of the environment. In equilibrium, the change of the Helmholtz free energy of the composite vanishes:

$$dW - \sigma_1\lambda_2\lambda_3 d\lambda_1 - \sigma_2\lambda_3\lambda_1 d\lambda_2 - \sigma_3\lambda_1\lambda_2 d\lambda_3 - \mu dC = 0. \tag{2.3}$$

A combination of (2.1)-(2.3) gives that

$$\begin{aligned} &\left[\frac{\partial W_{stretch}}{\partial \lambda_1} - \left(\sigma_1 + \Pi_{mix}(J) + \frac{\mu}{\Omega}\right)\lambda_2\lambda_3\right] d\lambda_1 \\ &+ \left[\frac{\partial W_{stretch}}{\partial \lambda_2} - \left(\sigma_2 + \Pi_{mix}(J) + \frac{\mu}{\Omega}\right)\lambda_3\lambda_1\right] d\lambda_2 \\ &+ \left[\frac{\partial W_{stretch}}{\partial \lambda_3} - \left(\sigma_3 + \Pi_{mix}(J) + \frac{\mu}{\Omega}\right)\lambda_1\lambda_2\right] d\lambda_3 = 0 \end{aligned} \tag{2.4}$$

with

$$\Pi_{mix}(J) = -\frac{dW_{mix}(J)}{dJ}. \tag{2.5}$$

The network, the solvent and the applied forces equilibrate when (2.4) holds for arbitrary and independent small changes in the three stretches, λ_1, λ_2 and λ_3. Consequently, the expression in the bracket in front of each of the three terms in (2.4) must vanish individually, giving three independent equations:

$$\sigma_1 = \frac{\partial W_{stretch}(\lambda_1, \lambda_2, \lambda_3)}{\lambda_2 \lambda_3 \partial \lambda_1} - \Pi_{mix}(J) - \frac{\mu}{\Omega}, \tag{2.6a}$$

$$\sigma_2 = \frac{\partial W_{stretch}(\lambda_1, \lambda_2, \lambda_3)}{\lambda_3 \lambda_1 \partial \lambda_2} - \Pi_{mix}(J) - \frac{\mu}{\Omega}, \tag{2.6b}$$

$$\sigma_3 = \frac{\partial W_{stretch}(\lambda_1, \lambda_2, \lambda_3)}{\lambda_1 \lambda_2 \partial \lambda_3} - \Pi_{mix}(J) - \frac{\mu}{\Omega}. \tag{2.6c}$$

The quantity $\Pi_{mix}(J)$ is the osmotic pressure in the gel in equilibrium with the pure solvent. The quantity μ/Ω is the additional osmotic pressure in the gel due to the chemical potential of the solvent in the environment. The applied stresses are balanced by the elasticity of the network, the osmosis due to the mixing of the polymer and the solvent, and the osmosis due to the chemical potential of the solvent in the environment. Equations (2.1) and (2.6) constitute four equations of state, relating the eight thermodynamic variables: λ_1, λ_2, λ_3, C, σ_1, σ_2, σ_3 and μ. (We do not count the swelling ratio J as a distinct additional variable because by definition $J = \lambda_1 \lambda_2 \lambda_3$.)

The equations of state involve two functions: $W_{stretch}(\lambda_1, \lambda_2, \lambda_3)$ and $\Pi_{mix}(J)$. The latter is derived from $W_{mix}(J)$ through (2.5). In the Flory-Rehner theory, the two functions are specified by models of statistical mechanics: the Gaussian-chain model

gives the free energy due to the stretching of the network, $W_{stretch}(\lambda_1,\lambda_2,\lambda_3)$,[39] and the Flory-Huggins model gives the free energy due to the mixing of the polymer and the solvent, $W_{mix}(J)$.[40] As an alternative approach, one does not calculate the two functions from any specific models of statistical mechanics; rather, one determines the function $W_{stretch}(\lambda_1,\lambda_2,\lambda_3)$ through experimental measurements of stress-stretch curves, and determines the function $W_{mix}(J)$ through experimental measurements of osmotic pressure. One can also adopt various combinations of models of statistical mechanics and experimental measurements.

The function $\Pi_{mix}(J)$ connects solutions and gels of the same polymer-solvent system. In the model of ideal elastomeric gels, the function $\Pi_{mix}(J)$ is independent of the density of crosslinks. In particular, when the density of crosslinks is so low that the free energy of stretching is negligible, the gel is indistinguishable from a solution, and (2.6) reduces to $\sigma_1=\sigma_2=\sigma_3=-\Pi_{mix}(J)-\mu/\Omega$. The solution and the gel have the same chemistry because the dilute crosslinks negligibly affect the molecular interaction between the solvents and the polymer. The solution and the gel have different mechanics because the solution is a liquid that can sustain only hydrostatic stress in equilibrium, while the gel is a solid that can sustain non-hydrostatic stress in equilibrium—an attribute that significantly increases the number of distinct methods to determine experimentally the function $\Pi_{mix}(J)$. In particular, $\Pi_{mix}(J)$ can be determined by free-swelling experiment of gels of different crosslink densities (Method 1 below), and by subjecting gels to a state of non-hydrostatic stresses (Methods 2 and 3

below). Furthermore, the function $\Pi_{mix}(J)$ can be determined by allowing gels to swell under stretches of different types, such as uniaxial tension, uniaxial compression and equal biaxial tension.

2.3 Characterization of polyacrylamide hydrogels

Here we test the model of ideal elastomeric gels by conducting experiments with polyacrylamide hydrogels, and by extracting from the literature four sets of data on polyacrylamide hydrogels and polyacrylamide-water solutions.[41] For an ideal elastomeric gel, the effect of mixing the polymer and the solvent is represented by the osmotic pressure as a function of the swelling ratio. We show that this function obtained by several distinct experimental methods is consistent. Specifically, the function obtained from a gel under different states of applied stress is the same, the function obtained from a free-swelling gel is the same as that obtained from the constrained-swelling gel, the function is independent of crosslink density, and the function obtained from the gels is similar to that obtained from the solutions. We further show that the Flory-Huggins model of mixing with a constant Flory-Huggins parameter does not fit the experimental data well, but does capture the trend of the data over four orders of magnitude in the osmotic pressure.[41]

We made polyacrylamide hydrogels by the following procedure. Acrylamide was dissolved in distilled water to 4.0 M in concentration, along with ammonium persulfate (0.012 × the weight of acrylamide) as polymerization initiators, N,N,N',N'-tetramethylethylenediamine (0.018 × the weight of acrylamide) as crosslinking

accelerators, and N,N-methylenebisacrylamide (MBAA, 0.007, 0.012, 0.017, 0.024, 0.035 and 0.041 × the weight of acrylamide) as crosslinkers. The MBAA-to-acrylamide ratio was varied to form gels of different crosslink densities. For each MBAA-to-acrylamide ratio, three batches of gels were prepared. The gels were cured for 2 hours at room temperature. They were then submerged in distilled water, subject no force, and kept at room temperature for a week, with a change of fresh distilled water every 48 hours.

We measured the swelling ratio *J* by using the gravimetric method. The gel was taken out of water, blotted with tissue paper to remove the water on the surface carefully. The gel was then immediately weighted on an analytical scale with an accuracy of $10^{-5}\mathrm{g}$ to obtain the mass of the gel, m_{gel}. For the mass of the dry network m_{dry}, the gel was dehydrated by the freeze-drying technique. A piece of the gel was frozen under $-80^{\circ}\mathrm{C}$ and transferred to a freeze dry system (Labconco Corporation), whose collector was kept a temperature of $-50^{\circ}\mathrm{C}$ and a vapor pressure of $0.040\mathrm{mbar}$. The freeze-drying process took 3 days. The dry network m_{dry} was weighted on an analytical scale. We calculated *J* from

$$J = 1 + \frac{(m_{\mathrm{gel}} - m_{\mathrm{dry}})/\rho_{\mathrm{water}}}{m_{\mathrm{dry}}/\rho_{\mathrm{PAAM}}}, \tag{2.7}$$

where the density of water is $\rho_{\mathrm{water}} = 1.000\mathrm{g/cm^3}$ and that of polyacrylamide is $\rho_{\mathrm{PAAM}} = 1.443\mathrm{g/cm^3}$.[42] We measured the swelling ratio *J* after free swelling, as well as after the force-relaxation experiment described below.

We performed the dynamical mechanical analysis (DMA) to measure viscoelastic moduli of the gels by using a Q800 dynamic mechanical analyzer (TA Instruments). Cylindrical samples were cut, 8 mm in diameter and 3 mm in thickness. The applied amplitude was 50μm, and the frequency ranged 0.01-10 Hz.

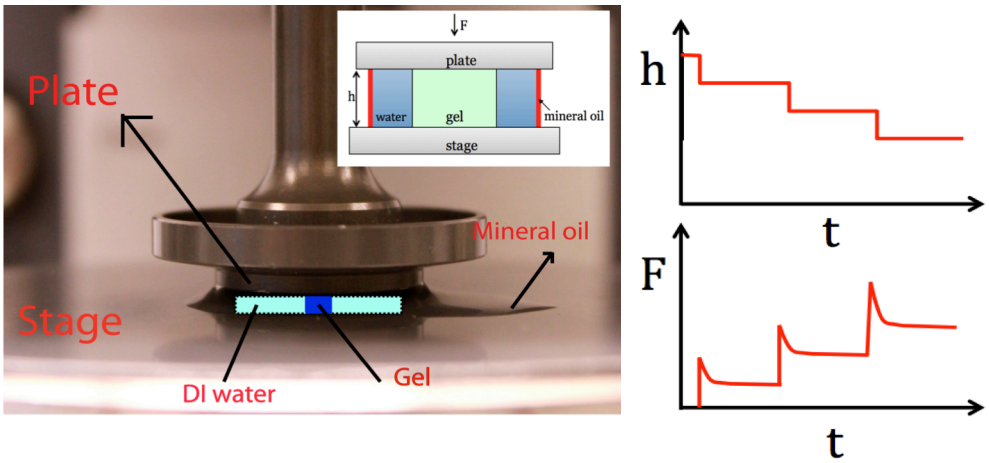

Figure 2.3 The setup for the force-relaxation experiment. A cylindrical sample of a gel is placed in water between a plate and a stage made of steel, and is sealed with mineral oil. While the plate is pressed on the gel and held at a fixed position, distance *h* above the stage, the force *F* applied on the plate is recorded as a function of time until the gel equilibrates with the force and the surrounding water. The experiment is run by adjusting the plate to several positions in succession. The gel is represented as a blue rectangle, and the water surrounding is represented as a cyan background.

We used an AR-G2 rheometer (TA Instrument) to perform uniaxial compression tests. A cylinder of the gel, 12mm in diameter and 9mm in thickness, was placed between the stage and plate made of steel, and submerged in distilled water. The plate approached the gel at a slow speed of 5μm/s till the force was detected to rise, indicating the contact between the plate and the gel. Upon the contact, the plate was

quickly loaded to a certain position within 90 seconds. During the loading process, both the force and height were recorded. The duration of this experiment was sufficiently short that the solvent had no time to redistribute in the gel, so that the gel behaved as an incompressible elastic material, and the experiment determined its stress-stretch curve.

We also performed force-relaxation experiments by using the AR-G2 rheometer. Cylindrical samples were cut, 3.0 mm in diameter and 0.5 mm in thickness. In each run of the experiment, a sample was placed between the stage and plate, and was submerged in distilled water (**Figure 2.3**). The gel was slippery, and was free to expand laterally when compressed between the stage and the plate. The gap between the stage and the plate was sealed with mineral oil to prevent the evaporation of water surrounding the gel. The plate was programmed to approach the gel at a speed of $5\mu m/s$. Once the contact between the plate and the gel was detected as the force began to rise, the speed of the plate was switched to $50\mu m/s$. After a certain height was reached, the plate was held stationary, and the force applied on the plate was recorded as a function of time. After some time, the force-time curve approached a plateau, indicating that the gel had reached a state of equilibrium under the constraint of the plate. Using a single sample, several force-time curves were obtained by holding the plate at multiple positions. We labeled the direction of the applied force as direction 3, and the two horizontal directions as 1 and 2. The stretch in the vertical direction was $\lambda_3 = h/H$, where H was the thickness of the dry network, and h was the thickness of the gel set by the spacing between the plate and the stage. It was inconvenient to

measure the diameter of the gel in the force-relaxation experiment. Consequently, we used the nominal stress s_3, defined as the applied force divided by the area of the dry network. The nominal stress s_3 relates to the true stress σ_3 by $s_3 = \sigma_3 \lambda_1 \lambda_2 = \sigma_3 J / \lambda_3$.

It is known that experimentally determined stress-stretch curves of polyacrylamide gels fit Gaussian-chain model well.[36] The free energy derived from the Gaussian-chain model is

$$W_{stretch}(\lambda_1, \lambda_2, \lambda_3) = \frac{1}{2} NkT\left[\lambda_1^2 + \lambda_2^2 + \lambda_3^2 - 3 - 2\log(\lambda_1 \lambda_2 \lambda_3)\right], \tag{2.8}$$

where N is the number of polymer chains per unit volume, and kT the temperature in the unit of energy.[39] As stated previously, chemomechanical interaction is specific to the polymer and solvent, and can be very complex. For the time being we do not specify any form of the function $W_{mix}(J)$. Inserting (2.8) into (2.6), one obtains that

$$\sigma_1 = \frac{NkT}{J}(\lambda_1^2 - 1) - \Pi_{mix}(J) - \frac{\mu}{\Omega}, \tag{2.9a}$$

$$\sigma_2 = \frac{NkT}{J}(\lambda_2^2 - 1) - \Pi_{mix}(J) - \frac{\mu}{\Omega}, \tag{2.9b}$$

$$\sigma_3 = \frac{NkT}{J}(\lambda_3^2 - 1) - \Pi_{mix}(J) - \frac{\mu}{\Omega}, \tag{2.9c}$$

Thus, a gel is fully characterized by a scalar NkT, and a single-variable function $\Pi_{mix}(J)$. Once NkT and $\Pi_{mix}(J)$ are obtained, the four equations of state, (2.1), (2.9a), (2.9b) and (2.9c) connect the eight thermodynamic variables: λ_1, λ_2, λ_3, C, σ_1, σ_2, σ_3 and μ.

Submerged in pure water and subject to no applied forces, the gel attains a state of equilibrium—the free-swelling state—characterized by isotropic stretches, $\lambda_1 = \lambda_2 = \lambda_3 = \lambda_o$. When the gel is subject to a force, in a short time the solvent in the gel has no time to redistribute, so that the concentration of the solvent in the gel remains fixed, and the gel behaves like an incompressible material. The gel changes shape to a state of stretches $\lambda_1, \lambda_2, \lambda_3$, but the volume of the gel remains unchanged, so that $J_o = \lambda_1\lambda_2\lambda_3 = \lambda_o^3$. Experimental data are often reported in terms of stretches relative to the free-swelling state, λ_1 / λ_o, λ_2 / λ_o and λ_3 / λ_o. In terms of these relative stretches, (2.9) is written as

$$\sigma_3 - \sigma_1 = \frac{NkT}{\lambda_o}\left[\left(\frac{\lambda_3}{\lambda_o}\right)^2 - \left(\frac{\lambda_1}{\lambda_o}\right)^2\right], \tag{2.10a}$$

$$\sigma_3 - \sigma_2 = \frac{NkT}{\lambda_o}\left[\left(\frac{\lambda_3}{\lambda_o}\right)^2 - \left(\frac{\lambda_2}{\lambda_o}\right)^2\right]. \tag{2.10b}$$

These are the stress-stretch relations of a gel when the concentration of the solvent in the gel is fixed. The stress-stretch relations are the same as those of the neo-Hookean model commonly used for incompressible elastomers. The pre-factor in (2.10) defines the shear modulus,

$$G = NkT / \lambda_o. \tag{2.11}$$

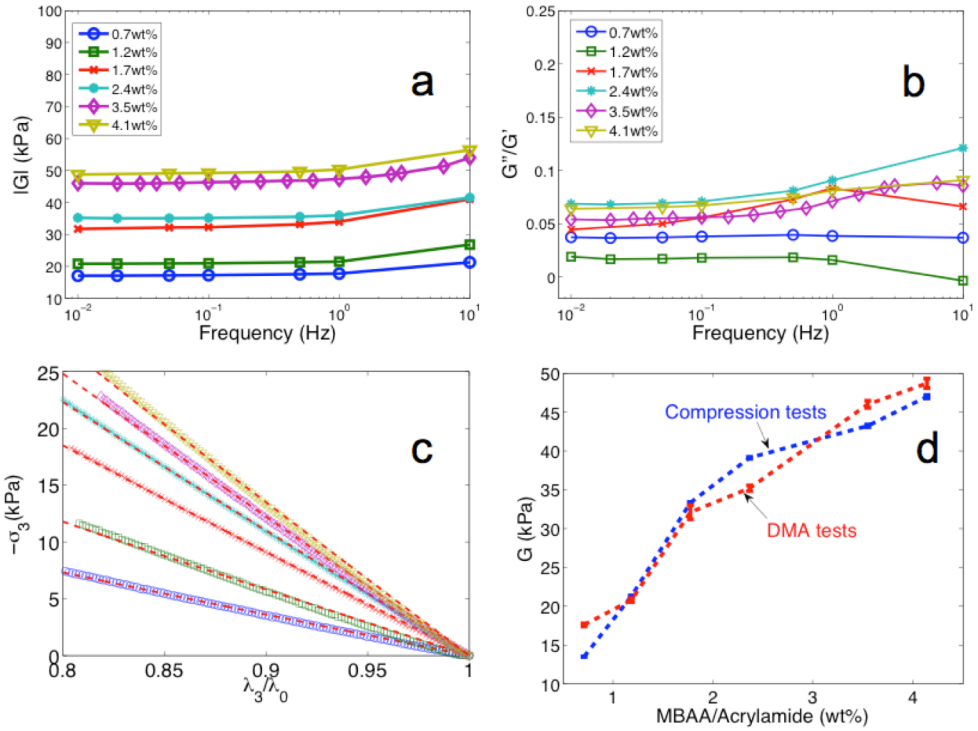

Figure 2.4 (**a**) Viscoelastic moduli for gels of various values of the MBAA-to-acrylamide ratio over a range of frequency. The amplitude of the modulus, $|G| = \sqrt{G'^2 + G''^2}$. (**b**) The ratio of the loss modulus to the storage modulus, G''/G'. (**c**) The stress-stretch curve measured under unidirectional compression is fitted with Equation (2.10), as shown by red dashed lines. (**d**) Comparison of the modulus obtained from compression tests and the storage modulus obtained from DMA tests.

Figure 2.4 illustrates the shear modulus G characterized with the viscoelastic measurements and the compression tests. Our viscoelastic measurements show that the polyacrylamide gels are highly elastic, with small viscous damping (**Figure 2.4a** and **2.4b**). Denote the storage modulus by G' and the loss modulus by G''. The magnitude

$|G| = \sqrt{(G')^2 + (G'')^2}$ increases with the concentration of the crosslinkers. The modulus remains nearly a constant and the ratio of the loss modulus to the storage modulus G''/G' remains low over the range of low frequency $(0.01\text{Hz} < f < 1\text{Hz})$. The increase of the modulus and loss at high frequency may be due to the entanglement of the polymer chains. These increases do not concern us here because we will focus on the behavior of gels in equilibrium, so that only the modulus determined at low frequency will be used. The stress-stretch curves determined by the compression test fit the neo-Hookean model (2.10) very well (**Figure 2.4c**). Furthermore, the shear moduli measured by two techniques—dynamic mechanical analysis (DMA) and compression test—match well in the entire range of the MBAA-to-Acrylamide ratio (**Figure 2.4d**).

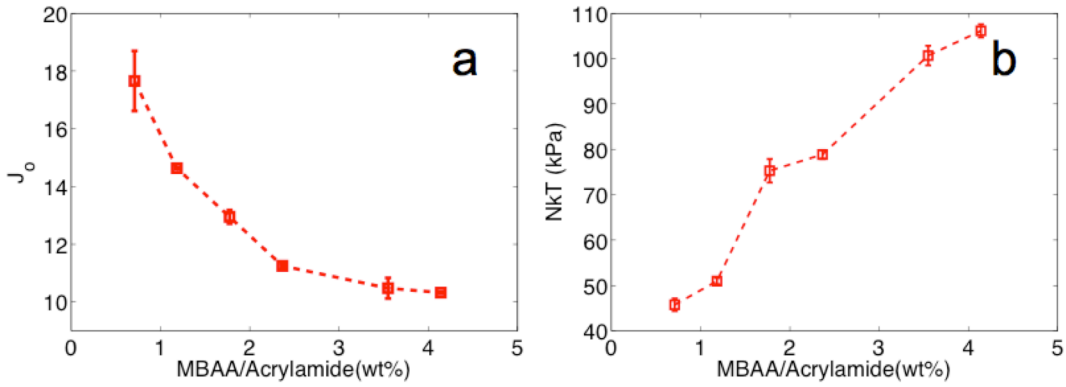

Figure 2.5 Properties of freely swolen gels of several values of MBAA-to-acylamide ratio. (**a**) The values of the swelling ratio J_o. (**b**) The values of *NkT*.

As expected, the swelling ratio J_o of the freely-swollen gel, determined by the gravimetric method, decreases as the concentration of the crosslinker increases (**Figure 2.5a**). We calculate the free-swelling stretch $\lambda_o = J_o^{1/3}$, and the number of chains per unit volume of the dry network from (2.11) using the storage modulus determined at

low frequency ($0.01\text{Hz} < f < 1\text{Hz}$). As expected, the value of NkT rises with the increasing concentration of the crosslinkers (**Figure 2.5b**).

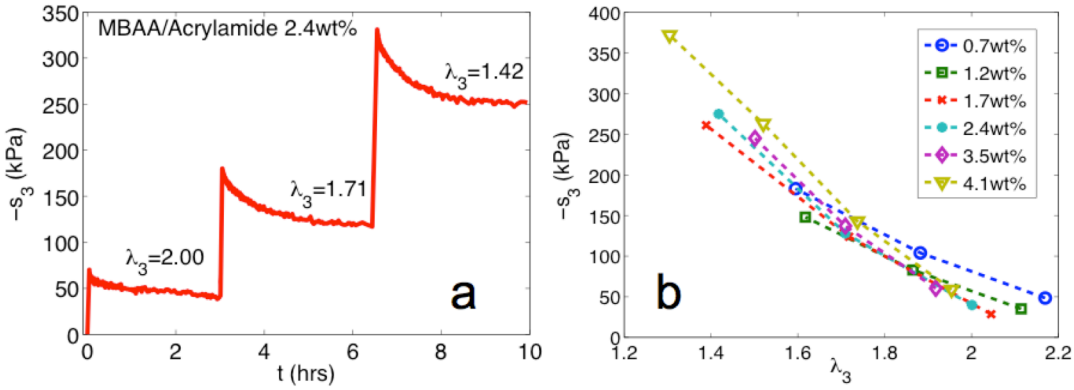

Figure 2.6 Data obtained from force-relaxation experiment. (**a**) Three stress-relaxation curves for a gel with a MBAA-to-acrylamide ratio of 2.4wt%. (**b**) For gels of various MBAA-to-acrylamide ratios, the nominal stress s_3 in equilibrium is plotted against the stretch λ_3.

In the force-relaxation experiment, once the plate is adjusted to a position, the force relaxes to attain a new state of equilibrium after some time (**Figure 2.6a**). When the position of the plate is high, the gel is not much deformed from the free-swelling state, so that the force applied on the plate is small. In such a case, a certain slope of the force-time is observed in experiment, possibly due to drift of the equipment. The force-relaxation curves do become flat when the gel is compressed significantly. It takes about $t_D = 2\text{hrs}$ to reach the state of equilibrium. For a sample of radius $R = 1.5mm$, the effective diffusivity of water in the polyacrylamide gel is estimated to be on the order of $D \approx R^2 / t_D \approx 10^{-10}\text{m}^2/\text{s}$, which is consistent with the literature.[28] The

measured nominal stresses in equilibrium are plotted against the stretches set by the positions of the plate (**Figure 2.6b**).

As pointed out by Cai and Suo,[36] the function $\Pi_{mix}(J)$ can be determined by multiple distinct experimental methods. Here we illustrate several methods using our experimental data. To determine a function of a single variable, $\Pi_{mix}(J)$, one needs to run an experiment that contains at least one independent variable. In Method 1, the independent variable is chosen as the MBAA-to-acrylamide ratio. By a combination of the compression test, gravimetric experiment and free-swelling experiment, we have already obtained *NkT* and J_o as functions of the MBAA-to-acrylamide ratio (**Figure 2.5**). When a gel swells freely in pure water, the stresses and the chemical potential vanish, $\sigma_1 = \sigma_2 = \sigma_3 = 0$ and $\mu = 0$. In equilibrium the stretches are isotropic and homogeneous in the gel, $\lambda_1 = \lambda_2 = \lambda_3 = \lambda_o$. Equation (2.9) reduces to

$$\Pi_{mix} = \frac{NkT}{\lambda_o^3}\left(\lambda_o^2 - 1\right). \tag{2.12}$$

This equation gives the osmotic pressure for a free-swelling gel. Consequently, we can determine pairs of the values (J, Π_{mix}) for gels of different values of the MBAA-to-acrylamide ratio.

In Method 2, the independent variable is chosen to be the position of the plate in the force-relaxation experiment. When a disk of a gel reaches a state of equilibrium in distilled water and subject to the constraint of the plate and stage, *J* can be determined by the gravimetric experiment, and λ_3 can be determined by the position of the plate.

The lateral stresses and the chemical potential vanish, $\sigma_1 = \sigma_2 = 0$ and $\mu = 0$. Recall that the lateral stretches are $\lambda_1 = \lambda_2 = \sqrt{J/\lambda_3}$. Equation (2.9a) reduces to

$$\Pi_{mix} = \frac{NkT}{J}\left(\frac{J}{\lambda_3} - 1\right). \tag{2.13}$$

This equation gives the osmotic pressure in the gel in equilibrium with the pure solvent and subject to the constraint of the plate and the stage.

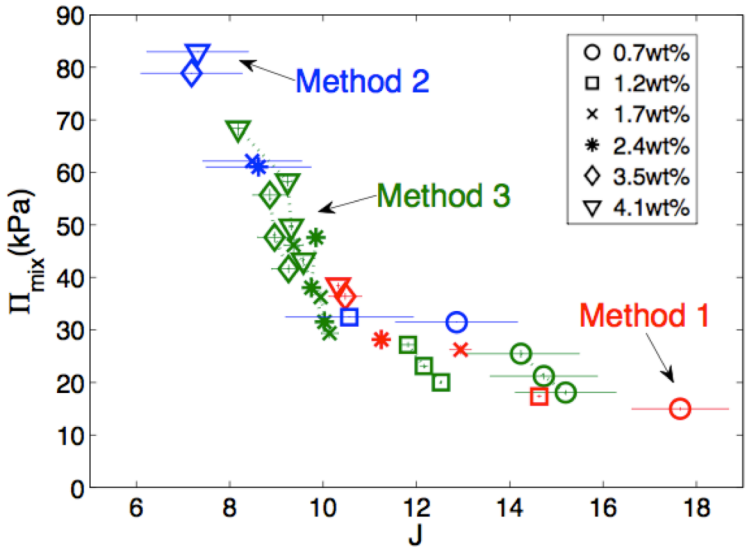

Figure 2.7 The function $\Pi_{mix}(J)$ determined by the three methods. Data points obtained with gels of different MBAA-to-acrylamide ratios are differentiated by symbols. Date points obtained by the three methods are differentiated by colors.

In Method 3, the independent variable is still chosen to be the position of the plate in the force-relaxation experiment, but we now use the measured stress in equilibrium. Subtracting (2.9b) from (2.9c), and recalling that $\lambda_2^2 = J/\lambda_3$ and $s_3 = \sigma_3 J/\lambda_3$, we obtain that

$$J = \lambda_3^3 - \frac{s_3 \lambda_3^2}{NkT}. \tag{2.14}$$

Once we determine NkT as before, and determine s_3 and λ_3 upon equilibrium from constrained swelling, we calculate J from (2.14), and Π_{mix} from (2.13).

The functions $\Pi_{mix}(J)$ determined by the three methods are indistinguishable (**Figure 2.7**). This agreement supports the hypothesis that polyacrylamide hydrogels are ideal elastomeric gels. The osmotic pressure due to mixing, Π_{mix}, decreases as the swelling ratio J increases. Note that some data were obtained from the free-swelling gels, and others were obtained from the force-relaxation experiment. In the free-swelling experiment, the swelling ratio was varied by varying the crosslink density (i.e., by varying the MBAA-to-acrylamide ratio). In the force-relaxation experiment, the swelling ratio is varied by both the crosslink density and the compression of the plate. The agreement indicates that the function $\Pi_{mix}(J)$ is independent how the swelling ratio is varied.

Our data is plotted in **Figure 2.8** along with the data marked as Konda,[28] which was extracted by using Methods 2 and 3 from the tensile tests of polyacrylamide hydrogels. The two sets of data were for different ranges of the swelling ratio, but both were obtained by using more than one method to determine the osmotic pressure. Thus, the function $\Pi_{mix}(J)$ is independent of the methods of its determination over a range of swelling ratio typical in the applications of polyacrylamide gels.

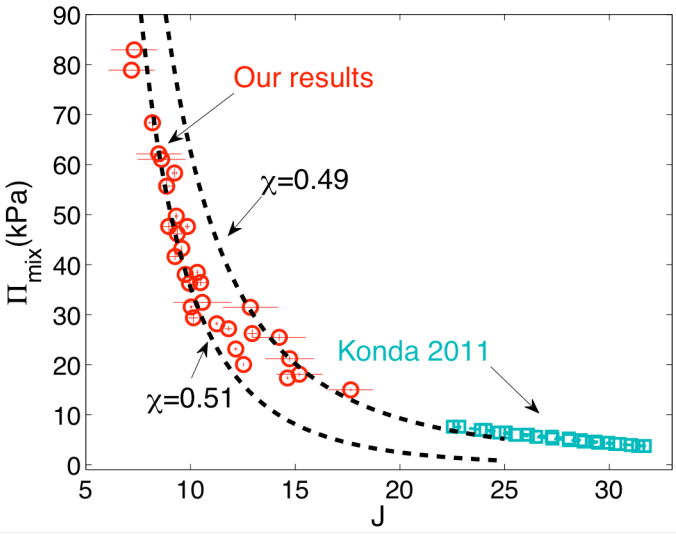

Figure 2.8 To fit the experimentally determined osmotic pressure over a range of swelling ratios to the Flory-Huggins theory (dashed lines), different values of the Flory-Huggins parameter χ are required.

These two sets of data are further compared with three other sets of data extracted from the literature (**Figure 2.9**). The data marked as Day[42] and Livney[43] were obtained by measuring the osmotic pressure of polyacrylamide-water solutions enclosed in semipermeable membranes. Relatively mono-dispersed polyacrylamide chains were used in the two experiments with molecular weight 100000g/mol and 237000g/mol respectively. The data marked as Mallam was measured by placing a polyacrylamide gel in a semipermeable bag submerged in certain polymer (e.g. polystyrene or polyvinyl acetate) solutions.[44] By changing the concentration of the polymer in the aqueous solution outside the bag, the chemical potential of water in the external solution was changed. (The relation between the chemical potential of water and the

concentration of the polymer was determined in a separate experiment.) The semipermeable bag was only permeable to water. When the gel inside the bag and the solution outside the bag attains the equilibrium, the chemical potential of water inside equals that outside. Setting $\sigma_1 = \sigma_2 = \sigma_3 = 0$ in (2.9), we obtain that

$$\Pi_{mix} = \frac{NkT}{\lambda^3}\left(\lambda^2 - 1\right) - \frac{\mu}{\Omega}. \tag{2.15}$$

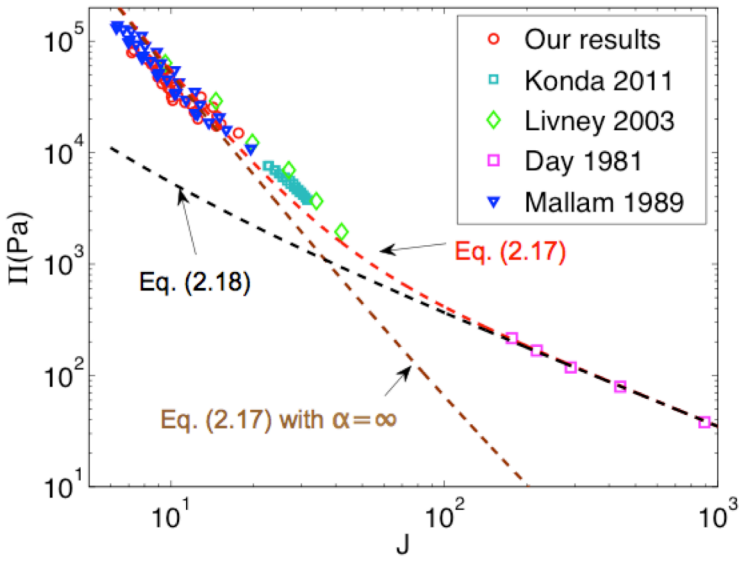

Figure 2.9 Comparison of the function $\Pi_{mix}(J)$ determined by various methods. The data is fitted to the Flory-Huggins theory. The fitting curves, as shown by dashes lines, are differentiated by colors, red for Equation (2.17), brown for Equation (2.17) with $\alpha = \infty$, and black for Equation (2.18).

Mallam et al. used the gravimetric method to determine $J = \lambda^3$ for gels equilibrated with solutions of several values of the chemical potential of water, μ.[44] Meanwhile, they did uniaxial compression measurements of the fully swollen gels for the shear

modulus, where we can recalculate NkT with (2.11). Once λ, NkT and μ are known, Π_{mix} can be calculated with (2.15).

All the data overlap within a range of the swelling ratio, within which the osmotic pressures measured by various methods agree. This agreement indicates that the function $\Pi_{mix}(J)$ is the same for polyacrylamide hydrogels and polyacrylamide-water solutions. The agreement further confirms that crosslinks negligibly affect the function $\Pi_{mix}(J)$. The data of Day et al. was obtained for dilute solutions,[42] and lie beyond the range of the four other sets of data.

Polyacrylamide gels are known to be temperature sensitive.[45] In this study we focus on isothermal processes. All the experiments were performed at room temperature, as well as those in the literature re-analyzed here to extract the function $\Pi_{mix}(J)$.

To highlight the model of ideal elastomeric gels, we have so far avoided invoking the Flory-Huggins model of mixing. We now discuss how the Flory-Huggins model fit the experimental data of polyacrylamide hydrogels and polyacrylamide-water solutions. The free energy of mixing derived from the Flory-Huggins model is[40]

$$W_{mix}(J)=\frac{kT}{\Omega}\left[(J-1)\log\left(1-\frac{1}{J}\right)-\frac{1}{\alpha}\log J+\chi\left(1-\frac{1}{J}\right)\right]. \qquad (2.16)$$

The first two terms in the bracket are due to the entropy of mixing, and the third term is due to the enthalpy of mixing. For uncrosslinked polymer chains, α is the volume per polymer chain divided by the volume per solvent molecule. The Flory-Huggins

parameter χ is a dimensionless measure of the enthalpy of mixing.[40] Inserting (2.16) into (2.5), one obtains the osmotic pressure due to mixing:

$$\Pi_{mix}(J) = -\frac{kT}{\Omega}\left[\frac{1}{J} + \log\left(1 - \frac{1}{J}\right) - \frac{1}{\alpha J} + \frac{\chi}{J^2}\right]. \tag{2.17}$$

For crosslinked polymer network, setting $\alpha = \infty$, only a single parameter χ is left to fit experimental data. We plot (2.17) with two values of χ, indicating that the Flory-Huggins theory does not fit the experimental data with any constant value of χ (**Figure 2.8**). A common practice is to fit (2.17) to experimental data by allowing χ to be a function of *J*, which will not be pursued here.

The Flory-Huggins model, however, does capture the trend of the large range of data on the log-log plot (**Figure 2.9**). We use the Flory-Huggins equation (2.17) to fit the five sets of data, giving $\chi = 0.4986$ and $\alpha = 3927$. This value of α may be compared with the following estimate. By definition, $\alpha = \Omega_{\text{PAAM}} / \Omega$, where the volume per water molecule is $\Omega = 2.99 \times 10^{-29} \text{m}^3$, and the volume per polyacrylamide chain is estimated by $\Omega_{\text{PAAM}} = x\Omega_{\text{AAM}}$, where $\Omega_{\text{AAM}} = 8.21 \times 10^{-29} \text{m}^3$ is the volume per acrylamide monomer around, and *x* is the number of acrylamide monomer per polyacrylamide chain ($x = 1400$ for the data by Day and Robb[42]). This estimate gives $\alpha = 3840$. Also plotted is (17) with $\chi = 0.49$ and $\alpha = \infty$, indicating that the finite value of α is needed to fit the data of dilute solutions.

The effect of the finite chain length of the polymer in a dilute solution is better appreciated as follows. Recall the Taylor series $\log(1-x)=-x-0.5x^2-...$ and write (2.17) as

$$\Pi_{mix}(J)=\frac{kT}{\Omega}\left(\frac{1}{\alpha J}+\frac{0.5-\chi}{J^2}\right). \tag{2.18}$$

This approximation retains the leading terms of the power series. The term of J^{-1} comes from the entropy of mixing when the polymer chains are of finite length, and the term of J^{-2} comes from the entropy of mixing and enthalpy of mixing. In a gel, the polymers are crosslinked, $\alpha=\infty$, and the term of J^{-1} vanishes. In a solution, $\alpha<\infty$, and for a dilute solution the term of J^{-1} can be significant compared to the term of J^{-2} . Equation (2.18) represents the dilute solution well, but not for gels of small values of the swelling ratio (**Figure 2.9**).

2.4 Extend model of ideal elastomeric gels to polyelectrolyte hydrogels

Following our previous work, we extend the model of ideal elastomeric gels for polyelectrolyte hydrogels. A polyelectrolyte gel is formed when a cross-linked polymer network carrying ionizable groups absorbs a solvent containing ionic species. Polyelectrolyte gels have the capacity to absorb large amounts of solvent, leading to their use in a broad range of applications in healthcare and personal hygiene.[46] The degree of swelling depends sensitively on environmental conditions such as temperature,[30] pH and salinity,[32,33] and in some cases even electric fields,[31] or light.[47]

Thus, polyelectrolyte gels can also be used as smart materials in sensors and actuators.[35,48-50]

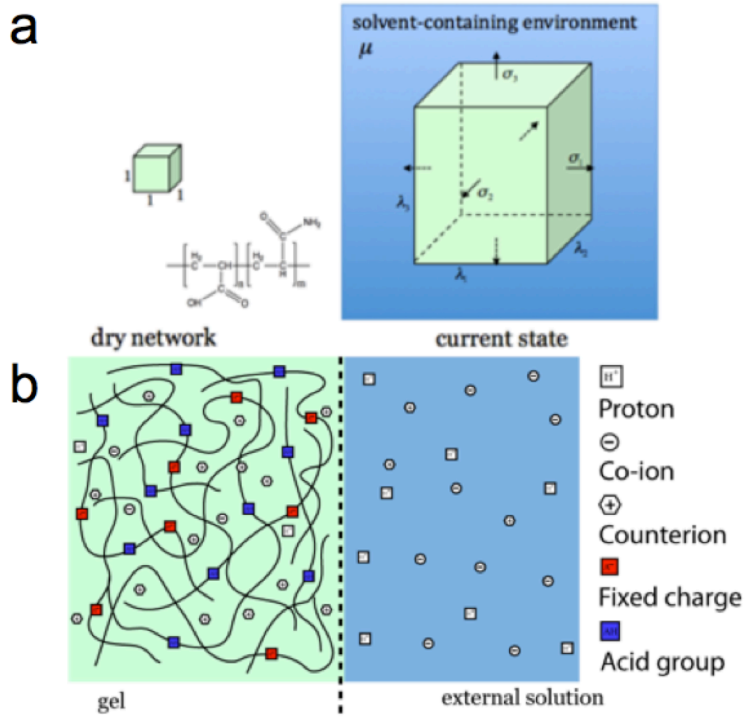

Figure 2.10 **(a)** A unit block of polyelectrolyte gel is submerged in a solution environment containing various ionic species. The inset is the structural formula of polyacrylamide-co-acrylic acid. **(b)** The polyelectrolyte gel, composed of cross-linked polymer chains with fixed charges and acidic groups, absorbs solvent and mobile ions, while the external solution contains solvent, protons, co-ions and counter-ions.

To focus on the main ideas, we consider deformation in the principal directions, although the theory is readily expanded to the more general case.[37] In the reference state, the gel is a unit cube of dry polymer, containing no solvent and subject to no applied forces (**Figure 2.10a**).[51] In the current state, submerged in a solution and

subject to applied forces, the gel absorbs solvent molecules and various ionic species, and stretches into a rectangular block of dimensions λ_1, λ_2 and λ_3. The volume ratio of gel to dry polymer, *J*, relates to the dimensions of the rectangular block by $J = \lambda_1\lambda_2\lambda_3$.

The gel and the external solution contain four mobile species: solvent molecules, protons, counter ions with charges opposite to the charges fixed on the polymer chains, and co-ions with charges of the same sign as the fixed charges (**Figure 2.10b**). We define the nominal concentration C_a of species α as the number of species α in the current state divided by the volume of the dry network. The same number divided by the volume of the gel in the current state defines the true concentration c_α. The two quantities are evidently related by $C_\alpha = c_\alpha J$. As part of the swelling process, the acidic groups *AH* on the polymer chains of the network may dissociate, leaving fixed charges A^- on the chains. This dissociation reaction, $AH \leftrightarrow A^- + H^+$, reaches equilibrium when

$$\frac{C_{H^+}C_{A^-}}{C_{AH}} = \frac{N_a K_a}{J} \tag{2.19}$$

where N_a is Avogadro's constant and K_a is the acid dissociation constant.[19]

Recall the two basic assumptions underlying the concept of an ideal elastomeric gel.[36,41] (1) Molecular incompressibility: the volume of the ideal elastomeric gel is equal to the sum of the volume of the dry network and that of the solvent,

$$J = 1 + \Omega_s C_s, \tag{2.20}$$

where Ω_s is the volume per solvent molecule *s*. In the case of polyelectrolyte gels, we assume further that the concentrations of the ionic species are generally much lower than that of the solvent species, so that Equation (2.20) remains valid. (2) Separability of the Helmholtz free energy: the Helmholtz free energy of the ideal elastomeric gel consists of one term that represents the elastic stretching of the polymer network and one term that is associated with mixing of polymer and solvent. In the case of polyelectrolyte gels, the fixed and mobile ions also contribute to the Helmholtz free energy. Therefore, we formulate the total Helmholtz free energy referred to a unit volume in the reference state as the sum of the following contributions:

$$W = W_{stretch} + W_{mix} + W_{ion} + W_{dis}\,, \tag{2.21}$$

where $W_{stretch}$ is the energy contribution due to the stretching of the network. This term is a function of the stretches ($\lambda_1, \lambda_2, \lambda_3$) and depends on the cross-link density of the network. The term W_{mix} is the contribution associated with the mixing of polymer and solvent. This term is a function of the swelling ratio, *J*, given by Equation (2.20) and is taken independent of the cross-link density. The term W_{ion} is associated with the mixing of mobile ions and generally takes the form $W_{ion} = W_{ion}(J, C_{H^+}, C_+, C_-)$, where the subscripts + and – refer to the counter ions and co-ions, respectively. If the concentrations of the ions are low and the polymer network is weakly charged, the electrostatic interactions between the ions in the gel is negligible,[52] and W_{ion} is determined mainly by the entropy of mixing of the mobile ions:

$$W_{ion} = kT[C_{H^+}(\log\frac{C_{H^+}}{c_{H^+}^{ref}J} - 1) + C_+(\log\frac{C_+}{c_+^{ref}J} - 1) + C_-(\log\frac{C_-}{c_-^{ref}J} - 1)], \tag{2.22}$$

where c^{ref} refers to the standard concentration, defined as 1 mol/L. For strongly charged polyelectrolyte gels, the energy contribution due to electrostatic interactions between mobile ions and fixed charges may be significant and needs to be considered.[53,54] The electrostatic effect can be readily added into this theoretical framework, but is not further considered in this study. The last term in Equation (2.21), W_{dis}, denotes the change in free energy caused by dissociation of the acidic groups on the polymer chains. This term contains both an entropic and an enthalpic term,

$$W_{dis} = kT[C_{A^-}\log(\frac{C_{A^-}}{C_{A^-}+C_{AH}}) + C_{AH}\log(\frac{C_{AH}}{C_{A^-}+C_{AH}})] + \gamma C_{A^-}, \qquad (2.23)$$

where γ is the increase in enthalpy when an acidic group dissociates. Under the constraints of mass conservation and electroneutrality, C_{A^-} and C_{AH} are readily expressed in terms of C_{H^+}, C_+ and C_-:

$$C_{A^-} = C_{H^+} + C_+ - C_- \qquad (2.24)$$

and

$$C_{AH} = f/v - (C_{H^+} + C_+ - C_-), \qquad (2.25)$$

where f is the number of the acidic groups attached to the network divided by the total number of monomers forming the network, and v is the volume per monomer. Consequently, the total Helmholtz free energy can be written as a function of six independent variables: the stretches ($\lambda_1, \lambda_2, \lambda_3$) and the concentrations of the protons, counter ions, and co-ions (C_{H^+}, C_-, C_+).

When a dry polymer network is submerged in a solution and subjected to forces, the network absorbs the mobile species and deforms, eventually attaining a state of thermodynamic equilibrium. The condition for equilibrium can be formulated as follows. Define the stresses σ_1, σ_2 and σ_3 as the applied forces divided by the areas of the faces of the block of gel in the current state (**Figure 2.10a**). Thus, the forces on the faces of the rectangular block are $\sigma_1\lambda_2\lambda_3$, $\sigma_2\lambda_3\lambda_1$ and $\sigma_3\lambda_1\lambda_2$. Associated with a small change in the dimensions of the gel, these forces perform work on the gel $\sigma_1\lambda_2\lambda_3 d\lambda_1 + \sigma_2\lambda_3\lambda_1 d\lambda_2 + \sigma_3\lambda_1\lambda_2 d\lambda_3$. The gel and the solution can also exchange four mobile species: solvent molecules, protons, counterions and co-ions. Let μ_α be the chemical potential of species α — since the gel and the solution are in a state of equilibrium, the chemical potential of each species is uniform in the system. When a number dC_a (per unit volume of dry gel) of species *a* are transferred from the solution to the gel, the free energy of the gel changes by $\mu_\alpha dC_\alpha$. This statement holds for solvent molecules, counter ions, and co-ions but not for protons because the number of protons in the gel can also change by dissociation of the acidic groups on the polymer chains. Consequently, in equilibrium the total Helmholtz free energy *W* obeys

$$\begin{aligned} dW = {} & \sigma_1\lambda_2\lambda_3 d\lambda_1 + \sigma_2\lambda_3\lambda_1 d\lambda_2 + \sigma_3\lambda_1\lambda_2 d\lambda_3 \\ & + \mu_s dC_s + \mu_{H^+}\left(dC_{H^+} - dC_{A^-}\right) + \mu_- dC_- + \mu_+ dC_+. \end{aligned} \tag{2.26}$$

Combining Eqs. (2.20)-(2.26) yields the following expression,

$$
\begin{aligned}
&[\frac{\partial W_{stretch}}{\partial \lambda_1} - (\sigma_1 + \Pi_{mix} + \Pi_{ion})\lambda_2\lambda_3]d\lambda_1 \\
&+[\frac{\partial W_{stretch}}{\partial \lambda_2} - (\sigma_2 + \Pi_{mix} + \Pi_{ion})\lambda_3\lambda_1]d\lambda_2 \\
&+[\frac{\partial W_{stretch}}{\partial \lambda_3} - (\sigma_3 + \Pi_{mix} + \Pi_{ion})\lambda_1\lambda_2]d\lambda_3 \\
&+[\frac{\partial W}{\partial C_+} - (\mu_+ - \mu_{H^+})]dC_+ + [\frac{\partial W}{\partial C_-} - (\mu_- + \mu_{H^+})]dC_- \\
&+\frac{\partial W}{\partial C_{H^+}}dC_{H^+} = 0
\end{aligned}
\tag{2.27}
$$

where

$$\Pi_{mix} = -\frac{dW_{mix}(J)}{dJ}, \tag{2.28}$$

$$\Pi_{ion} = -\frac{\partial W_{ion}(J, C_{H^+}, C_+, C_-)}{\partial J} + \frac{\mu_s}{\Omega_s}. \tag{2.29}$$

Here Π_{mix} is the osmotic pressure in the gel in equilibrium with the pure solvent, while Π_{ion} represents the osmotic pressure in the gel due to the mobile ions; μ_s / Ω_s is the osmotic pressure in the gel due to the chemical potential of the solvent in the external solution containing ionic species:

$$\mu_s = -kT\Omega_s(c^*_{H^+} + c^*_+ + c^*_-). \tag{2.30}$$

where c^*_α is the true concentration of species α in the external solution.[19] Substituting Eqs. (2.22) and (2.30) into (2.29) yields

$$\Pi_{ion} = kT(c_{H^+} + c_+ + c_- - c^*_{H^+} - c^*_+ - c^*_-). \tag{2.31}$$

The network, the solvent and the applied forces are in equilibrium, if Equation (2.27) holds for arbitrary and independent small changes in the three stretches (λ_1, λ_2 and λ_3)

and the three nominal concentrations (C_+, C_-, C_{H^+}). Consequently, the expressions in the brackets in front of each of the six terms in Equation (2.27) must vanish individually, yielding the following equations:

$$\sigma_1 = \frac{\partial W_{stretch}}{\lambda_2 \lambda_3 \partial \lambda_1} - \Pi_{mix} - \Pi_{ion}, \tag{2.32a}$$

$$\sigma_2 = \frac{\partial W_{stretch}}{\lambda_1 \lambda_3 \partial \lambda_2} - \Pi_{mix} - \Pi_{ion}, \tag{2.32b}$$

$$\sigma_3 = \frac{\partial W_{stretch}}{\lambda_1 \lambda_2 \partial \lambda_3} - \Pi_{mix} - \Pi_{ion}. \tag{2.32c}$$

$$\frac{\partial W}{\partial C_+} = \mu_+ - \mu_-. \tag{2.33a}$$

$$\frac{\partial W}{\partial C_-} = \mu_- + \mu_{H^+}. \tag{2.33b}$$

$$\frac{\partial W}{\partial C_{H^+}} = 0. \tag{2.34}$$

The applied stresses are balanced by the elasticity of the network, the osmotic pressure due to mixing of polymer and solvent, and the osmotic pressure due to mixing of ions. Equations (2.32) express mechanical equilibrium; Equations (2.33) provide the equilibrium conditions with respect to the exchange of counter ions and co-ions between the gel and its surrounding; Equation (2.34) formulates the equilibrium condition for dissociation of the acidic groups on the polymer chains. Substituting Eqs (2.21)-(2.23) into (2.34) leads to

$$N_A K_a = c_{H^+}^{ref} \exp(-\frac{\gamma}{kT}). \tag{2.35}$$

Equations (2.20), (2.32), (2.33), and (2.34) constitute the equations of state of the polyelectrolyte gel, relating the thermodynamic variables: λ_1, λ_2, λ_3, σ_1, σ_2, σ_3, C_+, C_-, C_{H^+}. Once the free energy contribution due to stretching of the network, $W_{stretch}$, and the osmotic pressure, Π_{ion}, have been characterized experimentally, the equations of state provide a complete description of the chemo-mechanical behavior of the polyelectrolyte gel. The energy contribution due to stretching is readily determined from stress-strain measurements. Characterizing Π_{ion} is less straightforward since that requires knowledge of the concentrations (C_{H^+}, C_+, C_-) inside the gel, which are difficult to measure in practice.[55] Instead, we adopt Donnan's theory,[19] which provides a relationship between the ion concentrations inside the gel and those in the external solution,

$$\frac{c_+}{c_+^*} = \frac{c_{H^+}}{c_{H^+}^*} = \left(\frac{c_-}{c_-^*}\right)^{-1}. \tag{2.36}$$

Tanaka et al. successfully applied Donnan's theory to capture the swelling behavior of an ionic gel quantitatively.[52] The concentrations of the three species inside the gel also satisfy the equilibrium condition (1) for dissociation of the acidic groups, yielding

$$\frac{c_{H^+}(c_{H^+} + c_+ - c_-)}{\frac{f}{vJ} - (c_{H^+} + c_+ - c_-)} = N_A K_a. \tag{2.37}$$

If f, J, $c_{H^+}^*$, c_+^*, c_-^*, and K_a are known, the concentrations (c_{H^+}, c_+, c_-) of the ionic species in the gel are solved readily from Eqs. (2.36) and (2.37).

2.5 Characterization of polyacrylamide-co-acrylic acid hydrogels

To testify the modified model of ideal elastomeric gels for polyelectrolyte gels, we chose polyacrylamide-co-acrylic acid gels as a model material system. A series of polyacrylamide-co-acrylic acid gels were synthesized according to the following protocol;[52] a summary of the composition and designation of each sample is provided in **Table 2.1**. Acrylamide (AAM), acrylic acid (AA), N,N'-methylenebis(acrylamide) (MBAA) and ammonium persulfate (APS) were acquired from Sigma Aldrich. The overall monomer (AAM + AA) concentration was *1000 mM*. As indicated in **Table 2.1**, the weight fraction of acrylic acid, *f*, was varied systematically, but kept small to ensure a low density of acidic groups on the polymer chains. Different cross-link densities were obtained by varying the weight percentage of MBAA (**Table 2.1**). APS (*7 mM*) was added as initiator for the free-radical polymerization. The chemicals (AAM, AA, MBAA and APS) were mixed with *10 mL* syringes. Part of the mixture (*6 mL*) was poured into a glass mold of *1mm* thickness. The rest of the solution (*4 mL*) was kept in the syringe to fabricate samples with a cylindrical shape.

Gelation occurred over a period of one hour on a hot plate at 70°C. To prevent hydrolysis of acrylamide and to precisely control the fraction of acidic groups, we did not use the usual accelerator, tetramethyl-ethylenediamine (TEMED). After gelation, the samples were stored at room temperature for 24 hours, and then transferred to a large body of distilled water to remove unreactive chemicals and other impurities, while the gels were allowed to swell freely to equilibrium. This step lasted around 10 days, during which fresh distilled water was added every *24* hours.

Notation	MBAA (wt%)	f	J_o	NkT (kPa)
AA01-080	0.80	0.01	140	2.33
AA02-080	0.80	0.02	590	3.62
AA04-080	0.80	0.04	654	3.71
AA01-216	2.16	0.01	71	10.83
AA02-216	2.16	0.02	79	10.22
AA04-216	2.16	0.04	88	10.07
AA01-433	4.33	0.01	36	15.96
AA02-433	4.33	0.02	37	22.22
AA04-433	4.33	0.04	61	17.39

Table 2.1. Composition and parameters of polyacrylamide-co-acrylic acid gels. f is the fraction of AA versus AAM, J_o is the equilibrium swelling ratio of the gel in distilled water, NkT is the crosslink density.

The masses of the fully swollen cylindrical samples (m_{gel}) were measured using an analytical scale with an accuracy of $10\,\mu g$. The samples were subsequently frozen at a temperature of -80°C and transferred to a freeze-dry system (Labconco Corporation) with a collector temperature of -50°C and a vapor pressure of *0.040 mbar*. This dehydration process took three days to complete, after which the mass of the dehydrated samples (m_{dry}) was measured. Swelling ratios were then calculated using

$$J = 1 + \frac{\left(m_{gel} - m_{dry}\right)/\rho_{water}}{m_{dry}/\rho_{dry}} \quad . \tag{2.38}$$

where ρ_{water} is the density of water taken as 1.000g/cm^3, and ρ_{dry} is the density of the dry polymer network taken as the density of polyacrylamide at 1.443g/cm^3.[42] The

swelling ratios, J_o, in distilled water are listed in **Table 2.1** for each of the samples. Swelling ratios in subsequent experiments were calculated from J_o and the change in diameter, $J = J_o(D_f / D_i)^3$, where D_i and D_f are the initial and final diameter of the sample.

The responses of the gels to changes in pH and salinity of the external solution were characterized using samples AA04-080 and AA04-433. Small gel cylinders of diameters 8 or 12 mm were punched out of fully swollen gel sheets. These samples were transferred to solutions of pH varying from *2.5* to *12*. Acidic solutions (pH<7) were prepared by adding HCl to distilled water, while KOH was used for alkaline solutions (pH>7). Gel cylinders were also transferred to solutions with NaCl concentrations varying from $10^{-7}M$ to $10^{-2}M$. The use of buffer solutions was avoided to not introduce additional electrochemically active species. The external solutions were renewed every 24 hrs. We recorded the diameters of the cylinders using a pair of calipers before and after reaching the new equilibrium state.

Small gel cylinders with 8 mm diameters were used for the mechanical tests. A series of uniaxial compression tests were performed using an AR-G2 rheometer (TA Instruments). The rheometer platen approached the samples at a speed of 5 μm/s until a rise in force was detected, indicating contact between the platen and the gel. Upon the contact, the displacement rate of the platen was increased to 20 μm/s until a pre-determined stretch ratio, typically *0.8-0.9*, was achieved. The entire loading process was finished within 2 minutes to avoid any redistribution of solvent inside the gel and

thus maintain incompressibility. Both force and displacement were recorded continuously throughout the experiment.

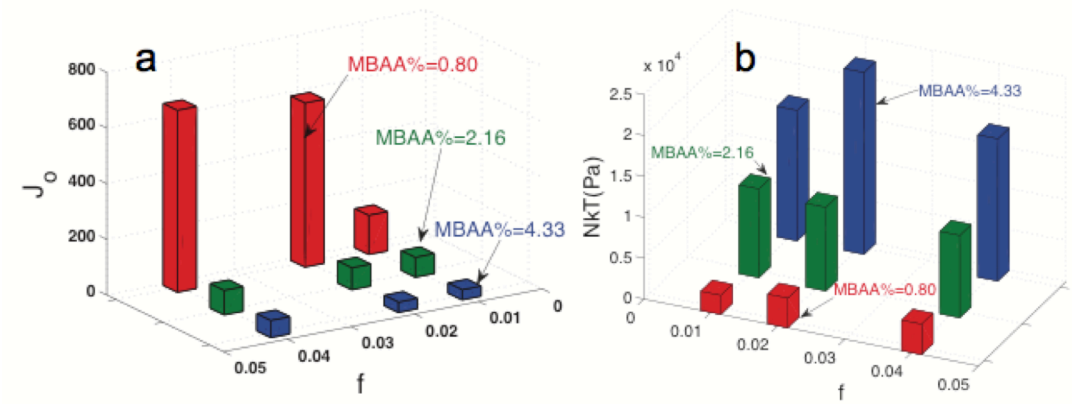

Figure 2.11 (a) The equilibrium swelling ratio of the gels fully swollen in distilled water (J_o) and **(b)** the crosslink density (NkT) of the gels, obtained from the stress-stretch measurements, is plotted versus the fraction of acidic groups (f) and the crosslinker input (MBAA%).

Figure 2.11a shows the swelling ratios in distilled water for each of the samples. Typical values are well in excess *50* so that the water content of most swollen gels is greater than *95%*. As illustrated in the figure, the swelling ratio changes rapidly with the fraction of acidic groups and the cross-link density. Even in distilled water, weakly charged and loosely cross-linked gels (e.g. AA02-080 and AA04-080) can swell to more than *500* times their dry volume.

The contribution of the free energy of stretching, $W_{stretch}$, was determined from uniaxial compression tests on samples fully swollen in distilled water. During the tests,

the gels behaved like incompressible solids ($\lambda_1\lambda_2\lambda_3 = \lambda_o^3$), because there was insufficient time for diffusion. We then used the Gaussian chain model,

$$\sigma_3 - \sigma_1 = \frac{NkT}{\lambda_o}\left[\left(\frac{\lambda_3}{\lambda_o}\right)^2 - \left(\frac{\lambda_1}{\lambda_o}\right)^2\right], \tag{2.39a}$$

$$\sigma_3 - \sigma_2 = \frac{NkT}{\lambda_o}\left[\left(\frac{\lambda_3}{\lambda_o}\right)^2 - \left(\frac{\lambda_2}{\lambda_o}\right)^2\right], \tag{2.39b}$$

to fit the experimental stress-stretch relations, where $\lambda_o = J_o^{1/3}$ is the stretch ratio after swelling in distilled water, N is the number of polymer chains per unit volume of the dry network, k is Boltzmann's constant, and T is the absolute temperature. Considering uniaxial compression along the x_3-direction, these equations reduce to a single equation

$$\sigma_3 = \frac{NkT}{\lambda_o}(\lambda^2 - \frac{1}{\lambda}), \tag{2.40}$$

where $\lambda = \lambda_3 / \lambda_o$ is the stretch relative to the freely swollen state. It is evident from Equation (2.40) that NkT / λ_o represents Young's modulus of the gels, while also allowing us to determine the cross-link density (N) from the initial slope of the stress-stretch curve. In our previous work on polyacrylamide gels, the Gaussian-chain model provided an excellent description of the mechanical behavior of the gels. As expected, the Gaussian-chain model also provides a very good fit for the experimental stress-stretch curves for the polyacrylamide-co-acrylic acid gels. Since the gels were swollen in distilled water, they had moderate swelling ratios and did not exhibit any non-Gaussian behavior. **Figure 2.11b** illustrates that NkT increases with increased cross-linker, but is independent of the fraction of acrylic acid, f. A correlation between the

modulus and the ionic components inside the gel has been reported in the literature,[56] a phenomenon attributed to the electrostatic interaction between the fixed ions on the polymer chain. In this study, the fraction of acidic group is intentionally maintained at a level below 5%, so that fixed ion are on average separated by at least 20 neutral segments resulting in weak electrostatic interaction between the ions.

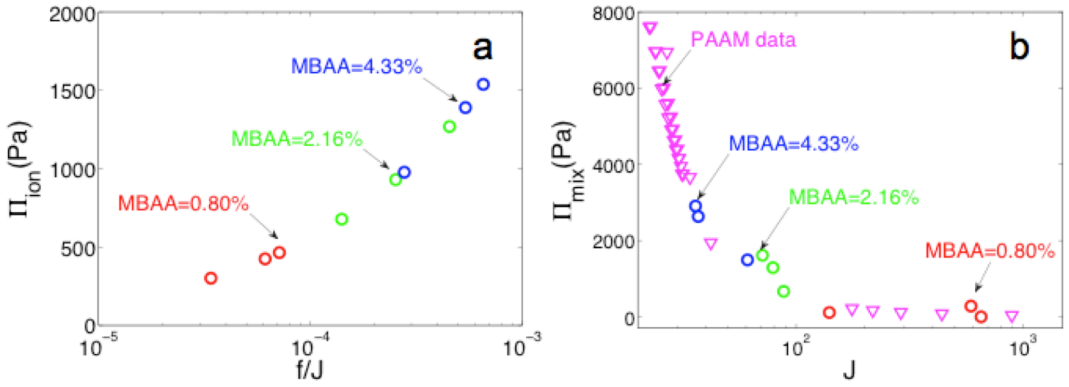

Figure 2.12 (a) The calculated osmotic pressure due to ions (Π_{ion}) versus the density of acidic groups (*f/J*), and **(b)** the osmotic pressure due to mixing (Π_{mix}) as a function of the swelling ratio (*J*), measured from gels fully swollen in distilled water. The same color implies the same input of crosslinker (MBAA) in the synthesis, while the fraction of acidic groups (*f*) is varied. The data points marked by PAAM data are extracted from the measurement on polyacrylamide gels.

The osmotic pressure Π_{ion} of the gel samples can be calculated by combining Equation (31) with Equations (36) and (37). The results for an external solution of distilled water with a slightly acidic pH of *6.5* are plotted as a function of *f/J* in **Figure 2.12a** – data for gels with different cross-link density and acid group content are shown, but they collapse into a single master curve because the ionic osmotic pressure

is a unique function of the current concentration of acid groups, *f/J*, and the pH of the external solution. The ionic osmotic pressure is shown to increase with acid group content and decrease with decreasing cross-link density. The former is caused by the higher concentration of active species, the latter occurs because the equilibrium swelling ratio is larger, which results in a lower concentration of active species.

Using the equations of state, it is now possible to derive the function $\Pi_{mix}(J)$ from our experiments without assuming a specific model for W_{mix}. The stress-strain curves suggest that $W_{stretch}$ is well described by the Gaussian-chain model, i.e.,

$$W_{stretch} = \frac{1}{2} NkT[\lambda_1^2 + \lambda_2^2 + \lambda_3^2 - 3 - 2\log(\lambda_1\lambda_2\lambda_3)]. \tag{2.41}$$

Under free-swelling conditions, the stretches are isotropic, $\lambda_1 = \lambda_2 = \lambda_3 = J_o^{1/3}$ and all applied stress components vanish, $\sigma_1 = \sigma_2 = \sigma_3 = 0$. Substituting into Equation (2.32) yields

$$\Pi_{mix} = \frac{NkT}{J_o}(J_o^{\frac{2}{3}} - 1) - \Pi_{ion}, \tag{2.42}$$

from which Π_{mix} can be obtained directly once J_o, NkT, and Π_{ion} have been determined experimentally. **Figure 2.12b** plots the function, Π_{mix}, as a function of swelling ratio for gels with different cross-link densities and acid contents. We have also included Π_{mix} measured for polyacrylamide (PAAM) hydrogels in our previous work.[26] Regardless of hydrogel cross-link density or acid content, Π_{mix} collapses into a single master curve over a large range of swelling ratios, i.e., Π_{mix} is a function of a single variable, *J*. This is a direct consequence of the low concentration of acid groups

in the hydrogels, which makes the overall chemistry of the polymer chains close to that of pure polyacrylamide.

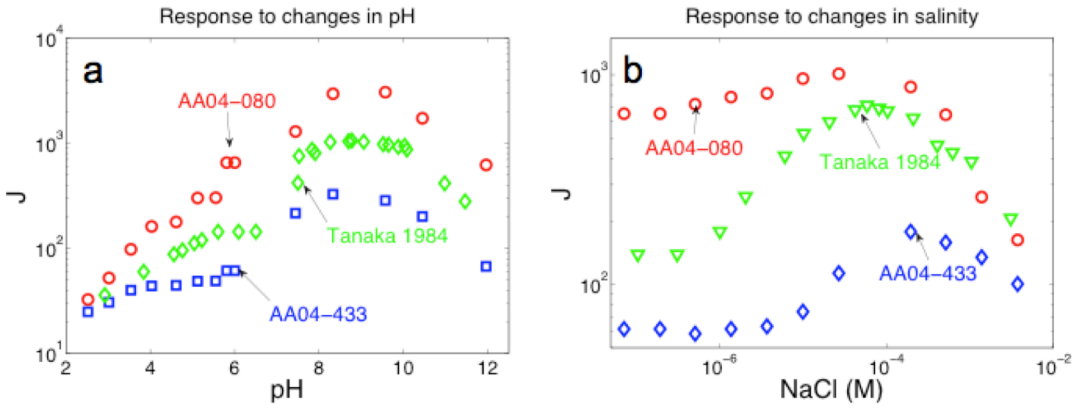

Figure 2.13 (a) Swelling ratio (*J*) of the gels as a function of pH in the external solution; HCl is added for pH values below 7, while KOH for pH values above 7. **(b)** Swelling ratio (*J*) of the gels as a function of salt concentration (NaCl) in the external solution. The data marked by Tanaka 1984 were obtained from an analysis of the results by Tanaka et al.[52]

The responses of the gels to changes in pH or salinity of the external solution were also characterized. **Figure 2.13a** plots the swelling ratio as a function of pH, along with experimental data obtained by Tanaka et al.[52] A qualitative understanding of the trends in the data is as follows. When the pH of the external solution is low, protons are abundant and the acidic groups on the polymer chains are fully protonated. The gel behaves like a neutral gel with a relatively small swelling ratio because of the absence of an ionic osmotic pressure Π_{ion}. As the pH approaches 8, the acidic groups dissociate and create fixed charges on the polymer chains. An imbalance of mobile ions builds up between the gel and the external solution, the increasing Π_{ion}, makes the gel swell. Once the pH increases further, the acidic groups are fully dissociated and

the ionic osmotic pressure Π_{ion} drops because of the abundant presence of mobile ions everywhere.

The response to the changes in salinity, the concentration of NaCl in the external solution, is shown in **Figure 2.13b**; an understanding similar to that for **Figure 2.13a** applies here. The gel acts as an ion exchanger. As the concentration of NaCl increases, protons in the gel are exchanged with Na^+ ions and the acidic groups continue to dissociate. At approximately 10^{-4} M of NaCl, the acidic groups are completely dissociated. The excess of NaCl reduces the ion imbalance between the gel and the solution, and the degree of swelling decreases. In the model we assumed an ideal ionic solution and insignificant effects due to electrostatic interactions between fixed and mobile ions, both valid for low concentrations ($<10^{-2}$ M) of ions in the external solution. For strong electrolyte solutions, the Debye-Huckel model may need to be invoked to calculate the activity of the ions.[52]

With known cross-link density, swelling ratio, and concentrations of ion species in the external solution ($c^*_{H^+}, c^*_+, c^*_-$), the ionic osmotic pressure Π_{ion} can be calculated from the model. We also used the model to re-analyze data from Tanaka et al.[52] Based on the concentration of MBAA in their gels, we estimated that NkT ~9 kPa for their gels.

Figures 2.14a and **2.14b** plot the ionic osmotic pressure versus equilibrium swelling ratio for external solutions of various pH and NaCl concentration, respectively. Results are shown for two hydrogels with identical acid content but different cross-link densities, along with the re-analyzed results from Tanaka et al.[52]

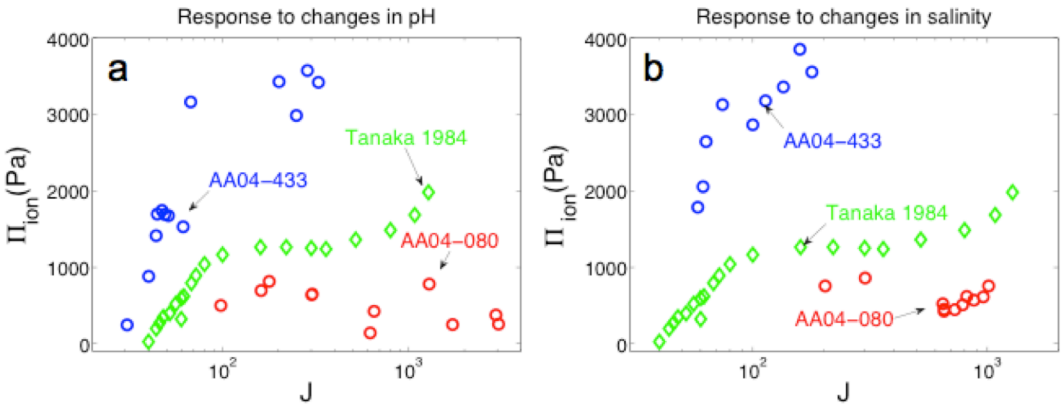

Figure 2.14 The osmotic pressure due to ions (Π_{ion}) as a function of the swelling ratio (J), determined from gels that were allowed to swell freely in an external solution of different pH values **(a)** and of different NaCl concentrations **(b)**.

Once the equilibrium swelling ratio and the ionic osmotic pressure have been determined, the osmotic pressure due to mixing can be calculated from Equation (2.42). The results are illustrated in **Figures 2.15a** and **2.15b**. It is evident that the osmotic pressure data for PAAM and AA04-080 form a single master curve that decays with swelling ratio. For AA04-433 and Tanaka's gel, however, we observe a discrepancy: the osmotic pressure functions drop below the master curve at large swelling ratios. We attribute this discrepancy to the use of the Gaussian chain model to describe the mechanical behavior of the network for the very large swelling ratios attained in **Figures 2.15a** and **2.15b**. At small swelling ratios, the polymer strands between two cross-links behave like Gaussian chains. At large swelling ratios, however, the polymer strands are highly extended in all three primary directions approaching their contour length; the network stiffens and no longer follows Gaussian elasticity. We

also conformed this point by performing compression tests on highly swollen gels, unlike the gel swollen in distilled water, the highly swollen gels didn't exhibit a plateau even at small strains in a Mooney-Rivlin plot. This stiffening effect is well known and has been characterized experimentally by measuring the shear modulus as a function of swelling ratio.[57,58] Consequently, using Equation (2.42) in the model is no longer appropriate and results in erroneous values for the osmotic pressure of mixing at large swelling ratios.

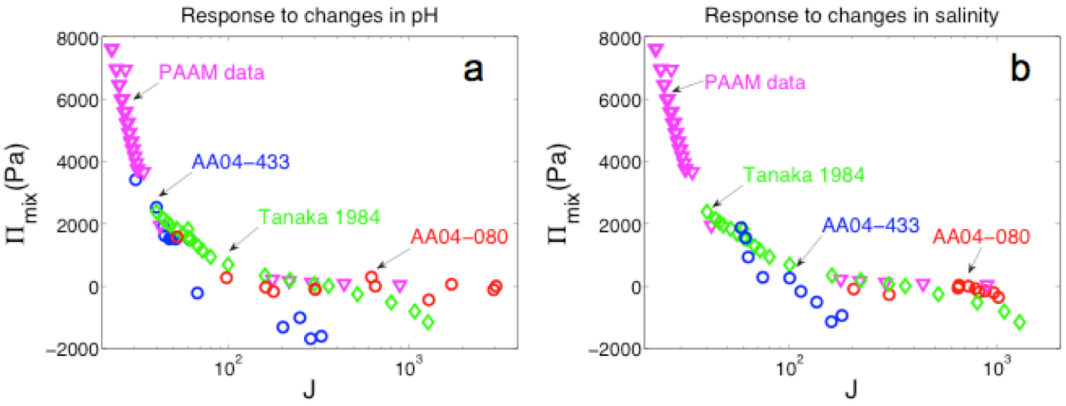

Figure 2.15 The osmotic pressure due to mixing (Π_{mix}) versus swelling ratio, determined from gels that were allowed to swell freely in an external solution of different pH values **(a)** and of different NaCl concentrations **(b)**. The results were calculated from Equation (2.42) using the Gaussian chain model for $W_{stretch}$.

To account for the non-Gaussian chain effect, many constitutive models have been proposed.[59-61] Among these models, the model by Gent[61] is an empirical two-constant constitutive relation that is essentially equivalent to the 8-chain model[59] without involving inverse Langevin relations. The compressible form of the Gent model yields the following expression for the stretching energy

$$W_{stretch} = -\frac{1}{2} NkT[J_{\lim} \log(1 - \frac{J_1}{J_{\lim}}) + 2\log(J)], \tag{2.43}$$

where J_1 is the first stretch invariant, defined by $J_1 = \lambda_1^2 + \lambda_2^2 + \lambda_3^2 - 3$, and J_{lim} denotes the maximum value of J_1.[62] At small strains, Equation (2.43) reduces to the Gaussian chain model Equation (2.41), but as J_1 approaches J_{lim}, the model captures the limited extensibility of the network. Due to its simplicity and robustness, the Gent model has been applied to a broad range of material systems.[60,63,64] Substituting Equation (2.43) into Equation (2.32), we obtain the following equations of state:

$$\sigma_1 = \frac{NkT}{J}[\frac{J_{\lim}\lambda_1^2}{J_{\lim} - (\lambda_1^2 + \lambda_2^2 + \lambda_3^2 - 3)} - 1] - (\Pi_{mix} + \Pi_{ion}) \tag{2.44a}$$

$$\sigma_2 = \frac{NkT}{J}[\frac{J_{\lim}\lambda_2^2}{J_{\lim} - (\lambda_1^2 + \lambda_2^2 + \lambda_3^2 - 3)} - 1] - (\Pi_{mix} + \Pi_{ion}) \tag{2.44b}$$

$$\sigma_3 = \frac{NkT}{J}[\frac{J_{\lim}\lambda_3^2}{J_{\lim} - (\lambda_1^2 + \lambda_2^2 + \lambda_3^2 - 3)} - 1] - (\Pi_{mix} + \Pi_{ion}) \tag{2.44c}$$

For free-swelling experiments ($\sigma_1 = \sigma_2 = \sigma_3 = 0$ and $\lambda_1 = \lambda_2 = \lambda_3 = \lambda_o$), we find the following expression for the osmotic pressure of mixing

$$\Pi_{mix} = \frac{NkT}{J}(\frac{J_{\lim}\lambda_o^2}{J_{\lim} - 3\lambda_o^2 + 3} - 1) - \Pi_{ion}. \tag{2.45}$$

We determine the values of J_{lim} for AA04-433 and for Tanaka's gel by fitting the osmotic pressure given by Equation (2.45) to the master curve obtained for PAAM. As illustrated in **Figure 2.16**, a good agreement is obtained between the PAAM data and the osmotic pressure based on the Gent model with J_{lim} values of 260 and 580 for AA04-433 and for Tanaka's gel, respectively. While the Gent model is empirical and it

is difficult to assign an exact quantitative interpretation to J_{lim}, it is possible to understand this result qualitatively: in a loosely cross-linked gel, the contour lengths of the polymer strands between cross-links are much larger than in a highly cross-linked gel, and the corresponding extensibility limit occurs at much larger strain. Thus the results are consistent with the fact that Tanaka's gels are more loosely cross-linked than AA04-433.

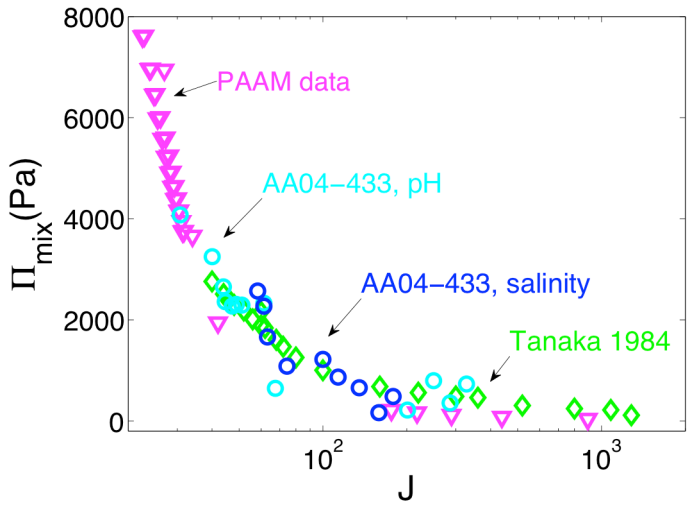

Figure 2.16 The osmotic pressure due to mixing (Π_{mix}) based on Gent model, with fitting parameters $J_{lim} \approx 260$ for AA04-433 and $J_{lim} \approx 580$ for the data marked by Tanaka 1984.

2.6 Summary

In this chapter, we have developed the model of ideal elastomeric gels, and testified this model with two material systems: (1) polyacrylamide hydrogels containing neutral polymers; (2) polyacrylamide-co-polyacrylic acid hydrogels

containing negative charged polymers. Their swelling behavior has been characterized experimentally as a function of applied forces, mechanical constraints, solvents, pH, and salinity.

In polyacrylamide hydrogels, the stresses applied on the gel are balanced by the elasticity of the network, the osmosis due to mixing the polymer and the solvent, and the osmosis due to the solvent-containing environment outside the gel. We showed that the functions of $\Pi_{mix}(J)$ obtained by several distinct experimental methods were consistent. Specifically, the functions obtained from the gel under different states of applied stress were the same, the function obtained from a free-swelling gel was the same as that obtained from the constrained-swelling gel, the function was independent of crosslink density, and the functions obtained from the gels was similar to that obtained from the solutions. We further showed that the Flory–Huggins model of polymer solutions with a constant Flory–Huggins parameter did not fit the experimental data well, but did capture the trend of the data over four orders of magnitude in the osmotic pressure.

In polyelectrolyte hydrogels, stresses applied to a polyelectrolyte gel are balanced by the elasticity of the network, the osmotic pressure due to mixing of the polymer and solvent, and the osmotic pressure due to ion distribution. The ion osmotic pressure was quantified using Donnan's theory, while the mixing osmosis was determined experimentally to yield a master curve that was valid for a broad range of polyacrylamide-co-acrylic acid hydrogels. We further demonstrated that non-Gaussian chain effects may need to be accounted for in the description of the mechanical

behavior of the polymer network, as polyelectrolyte gels can attain very large swelling ratios, and that these effects are well described by the Gent model.

We hope that the other elastomeric gels will be examined to ascertain the scope of applicability of the model of ideal elastomeric gels.

Chapter 3 Synthesis and characterization of ionic liquid gels

3.1 Introduction

The long-term performance of ionic conductors using hydrogels is severely limited by evaporation of water: as water evaporates, the hydrogel conductors dry out and lose functionality. Using an ionic liquid gel as an ionic conductor provides one potential solution to this problem: the ionic liquid in the gel enables ion transport and makes the gel non-volatile.[65] Ionic liquid gels, or ionogels, are formed by swelling a cross-linked polymer network in an ionic liquid. They possess both the mechanical integrity of a cross-linked polymer, and the ion conductivity and non-volatility of an ionic liquid.[66] Ionogels have been used in energy storage and conversion devices,[67-69] gate dielectrics for organic electronics,[70-73] gas and ion separation membranes,[74] and sensors and actuators.[75-77] With recent developments in the nascent field of soft machines, ionogels also have great potential for use as ionic conductors in transparent loudspeaker, active-noise-cancellation windows, and transducers.[13]

Along with good ion conductivity and non-volatility, ionogels used in these applications also need to be compliant, stretchable, and tough, so as to not constrain actuation, enable large deformation, and resist fracture. Many existing ionogels, however, have high stiffness[78,79] and rupture at small strains.[80] Much attention has been paid to the thermal and ion transport properties of ionogels,[81,82,83] but the complex chemo-mechanical interaction between the polymer network and the ionic liquid has

received little attention. Use of ionogels in applications where mechanical performance is critical requires models to describe and predict the mechanical behavior of these materials.

Here we present an ionogel prepared by swelling cross-linked poly(methyl methacrylate) (PMMA) in a 1-butyl-3-methylimidazolium bis(trifluoromethylsulfonyl) imide ([BMIM][NTf_2]) ionic liquid. This ionogel is representative of a larger class of ionogels based covalently cross-linked networks of neutral polymers swollen in ionic liquids. The resulting ionogels are compliant, highly stretchable, and relatively tough. We establish the effects of cross-link density on the swelling ratio, elastic modulus, stretchability, and toughness of the gels. We further demonstrate that the behavior of the ionogels is well captured by the model of the ideal elastomeric gel and that their fracture energy correlates inversely with cross-link density, in agreement with Lake-Thomas theory.[84] Because the cross-link density and the Flory interaction parameter fully determine the equations of state, we expect that the mechanical behavior observed in this study is representative of a broader class of ionogels obtained by swelling covalently cross-linked polymer networks in ionic liquids with physico-chemical parameters similar to those of [BMIM][NTf2].

3.2 Synthesis of the ionic liquid gel

In this study, we selected PMMA as host polymer, MBAA as cross-linker, and [BMIM][NTf_2] as ionic liquid (**Figure 3.1a**). The covalently cross-linked polymer network was selected, because of its greater chemical and thermal stability compared to

networks based on physical crosslinks.[79] The ionic liquid [BMIM][NTf_2] was selected because of its good miscibility with PMMA, low melting point, vanishing vapor pressure, low viscosity, and good ionic conductivity (3.9 mS cm^{-1}).[85] Furthermore, both PMMA and [BMIM][NTf_2] are hydrophobic and immiscible with water; the resulting ionogel absorbs less than 1% water by mass in a high-humidity environment. By contrast, ionogels formed by combining hydrophobic ionic liquids with hydrophilic polymers like polyethylene glycol readily absorb water, which may result in volume changes, phase separation, and a reduction in transparency.[86]

The ionic liquid, 1-butyl-3-methylimidazolium bis(trifluoromethylsulfonyl)imide ([BMIM][NTf_2]), was synthesized using an anion exchange reaction between 1-butyl-3-methylimidazolium chloride (BMIMCl, Sigma, 38899) and the lithium salt of bis(trifluoromethane)sulfonimide ($LiNTf_2$, Sigma, 449504). BMIMCl and $LiNTf_2$ were mixed together in equimolecular quantities in distilled water. The solution was kept at 70°C and stirred for 12 hours until it separated into two transparent layers: an aqueous solution on top and a hydrophobic oil-like ionic liquid at the bottom. The aqueous solution was removed and the ionic liquid was washed several times with distilled water. The ionic liquid was then dried at 100°C in a vacuum oven for 12 hours.

Ionogel are generally prepared in one of two ways: monomers can be polymerized in the presence of an ionic liquid,[81,85,86] or the polymer network can be formed first in a different medium and then swollen in an ionic liquid.[87] Using *in-situ* polymerization, it is difficult to synthesize ionogels with large swelling ratios and some ionic liquids have been shown to disrupt the polymerization process.[81,85,86] By contrast, the ex-situ

approach allows independent optimization of the polymerization process using established chemistries and the resulting networks have fewer defects,[57] but the swelling process can take a long time for a gel in bulk form.

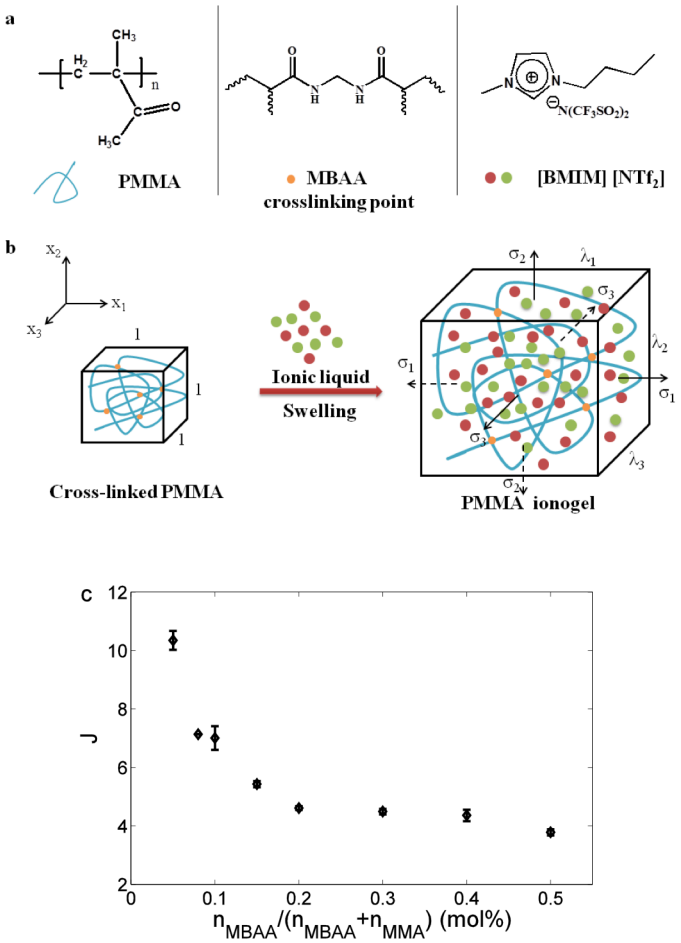

Figure 3.1 (a) Chemical structures of ionogel components. **(b)** Schematic diagram of the formation of the ionogels; (**c**) Swelling ratio of ionogels as a result of MBAA content. Error bars show one standard deviation; sample size N=3.

The ionogels in this study were synthesized using the ex-situ method. The polymer network of the ionogel was synthesized using methyl methacrylate (MMA; Sigma, M55909) as monomer, N, N'-methylenebisacrylamide (MBAA, Sigma, M7279)

as cross-linker, and benzoyl peroxide (BPO, Sigma, 33581) as initiator. MBAA, in quantities from 7.2 mg (0.05 mol %) to 72.8 mg (0.5 mol %), was dissolved in 10 ml MMA inside a 20 ml glass bottle. After bubbling nitrogen through the mixture of MBAA and MMA for 10 minutes, 0.033 g (0.1 mol%) BPO was added. The solution was then heated to 90°C, and kept at this temperature for 15-20 minutes to initiate the polymerization reaction. As soon as the solution turned into a viscous liquid, the solution was cooled to room temperature by immersing the bottle in water and poured into a glass mold with dimensions of 80×80×0.1 mm^3. The mold was then kept at 50 °C for 5 hours, after which the temperature was increased to 90 °C for one hour to finish the polymerization process. This protocol produced stiff, transparent films of cross-linked PMMA. The PMMA films were then submerged in [BMIM] [NTf_2] at 120°C until equilibrium was established. The mass of dry PMMA films was measured using an analytical scale before the swelling, and at various times during the swelling process. Typically, the swelling process reached equilibrium after 24 hours. The swelling ratio of the resulting gels, *J*, was calculated from

$$J = 1 + \frac{(m_{gel} - m_{dry}) / \rho_{IL}}{m_{dry} / \rho_{PMMA}}, \tag{3.1}$$

where the density of [BMIM] [NTf_2], ρ_{IL}, is 1.43 g cm^{-3} and that of poly(methyl methacrylate), ρ_{PMMA}, is 1.17 g cm^{-3}.[88] The resulting ionogels were highly transparent to the full spectrum of visible light and no phase separation was observed, confirming that PMMA and [BMIM][NTf_2] are highly compatible.

Figure 3.1b illustrates the swelling process schematically: a unit block of dry PMMA absorbs a large amount of ionic liquid, [BMIM][NTf_2] and forms a block of ionogel with dimensions ($\lambda_1, \lambda_2, \lambda_3$). The swelling ratio, *J*, denotes the ratio of the volume of the swollen ionogel to that of the dry network. Since the dry network is homogeneous and isotropic, the stretch ratio for the free swelling is independent of the direction, $\lambda_1 = \lambda_2 = \lambda_3 = J^{1/3}$. **Figure 3.1c** depicts the swelling ratio of the ionogels as a function of MBAA concentration. Evidently the swelling ratio is very sensitive to the cross-link density of the PMMA network. As the MBAA content increases, the equilibrium swelling ratio, *J*, decreases. At low cross-link densities, the volume fraction of ionic liquid is as high as 90 %.

3.3 Mechanical behavior of the ionic liquid gel

A series of mechanical tests were carried out at room temperature using an Instron tensile machine with a 50 N load cell. Samples were attached to polyacrylate grips with UV-curing acrylic glue (Loctite^R 3106 light cure adhesive). No debonding was observed during tensile testing of the ionogels using this type of glue. By contrast, glues based on cyanoacrylate (Krazy^R glue) or epoxy (Devcon^R epoxy 5 minute) did not provide adequate adhesion between the ionogels and the polyacrylate grips. The section of the tensile specimens between the grips was 5 mm in length and 30 mm in width. During the tests, the stretch rate was kept constant at 5 mm min^{-1}. All samples were stretched to rupture.

The stress-stretch curves of the ionogels are shown in **Figure 3.2a** for different MBAA concentrations. The nominal stress is the loading force divided by the cross-sectional area of the undeformed sample. The stretch ratio is the current length divided by the initial length of the undeformed sample. The figure clearly illustrates that the ionogels exhibit lower stiffness and larger stretchability with decreasing MBAA content. The most compliant ionogel can sustain a stretch ratio of 280% before rupture. On the time-scale of the experiments, the ionogels behave as elastic elastomers with negligible hysteresis between loading and unloading.

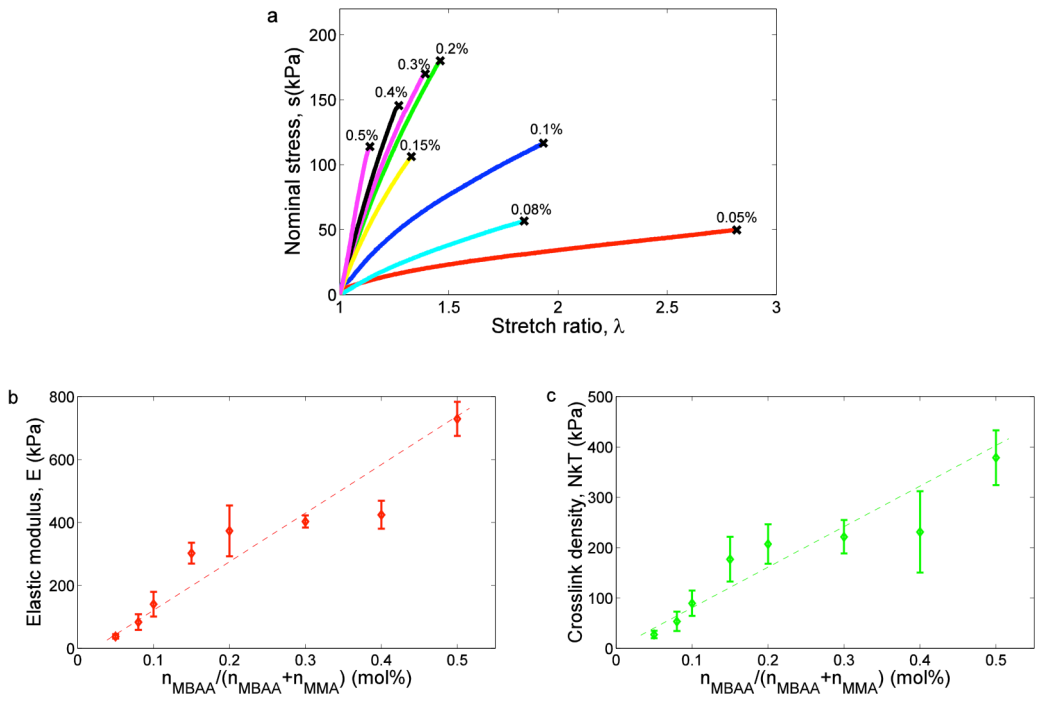

Figure 3.2 (a) Tensile curves of ionogels with various MBAA molar percentages as illustrated in the figure. **(b)** Elastic modulus as a function of MBAA content; (**c**) crosslink density. Error bars show one standard deviation; sample size N=3. The dashed lines are guides to the eye.

The plane-strain elastic moduli (M) of the ionogels can be determined as the slopes of the initial portions of the stress-stretch curves of the ionogels. The Young's moduli (E) were calculated from equation $E = M \times (1 - v^2)$, where v is Poisson's ratio. Because the ionic liquid is non-volatile and tests were performed in less than two minutes to prevent any re-distribution of the ionic liquid inside the sample, the ionogels behave like incompressible solids and Poisson's ratio can be taken as 0.5. The calculated elastic moduli of ionogels are shown in **Figure 3.2b**. As the MBAA concentration increases, the elastic modulus increases from 38 kPa to 729 kPa. The cross-link density N of the PMMA network is related to the elastic modulus and the swelling ratio of the ionogel by

$$NkT = \frac{E}{2(1+v)} J^{1/3}, \tag{3.3}$$

where kT the temperature in units of energy, and N is the cross-link density referred to the volume of the dry polymer.[89] Using the experimental values of the swelling ratios and elastic moduli, the cross-link densities of the ionogels can be calculated from Equation (3.3). The results are shown in **Figure 3.2c** as a function of MBAA concentration and, not surprisingly, the crosslink density increases with increasing MBAA concentration. Compared to the hydrogels used as ionic conductors on elastomeric actuators by Keplinger et al,[13] the ionogels in this work exhibit similar stretchability and stiffness, indicating that the ionogels can be used in the same application, but without the risk of desiccation.

The fracture energy of ionogels is critical in many applications involving soft machines. Ionic conductors, for example, often undergo large and frequent deformation. The fracture energy quantifies the resistance of a material to crack propagation, independent of the presence of any defects in the material; it is a material property that is independent of the test method.[25] Other parameters that are sometimes used to describe the resistance to fracture, such as fracture strain, work of loading before rupture, or breaking stress, depend on the flaws present in a particular sample, and are therefore less appropriate.[90-92] Many methods for measuring facture energy have been established, including the trouser tear test, the single-edge notch test, and the pure-shear test. Here we used the pure-shear test to measure the fracture energy. The pure-shear test was developed by Thomas to measure the fracture energy of elastomers.[93] J. Y. Sun et al recently demonstrated this method on hydrogels.[24]

The fracture energy of the ionogels was measured using the pure shear test.[94] The samples had a gauge section of 5 mm, a width of 30 mm, and a thickness in the 0.2-0.4 mm range. For each ionogel, two samples were tested: an un-notched sample and a notched sample with a 10 mm edge crack in the middle of specimen. The un-notched sample was used to record the load-extension curve. The notched sample was used to determine the critical extension l_c at which the crack started to propagate. The fracture energy of the ionogel was then calculated using

$$\Gamma = \frac{U(l_c)}{wt}, \tag{3.4}$$

where $U(l_c)$ is the work done by the applied force for the un-notched sample to reach the critical extension l_c; w and t are the width and thickness of the specimen gauge

section, respectively. The work $U(l_c)$ is readily determined by integrating the load-extension curve of the un-notched sample up to an extension l_c.

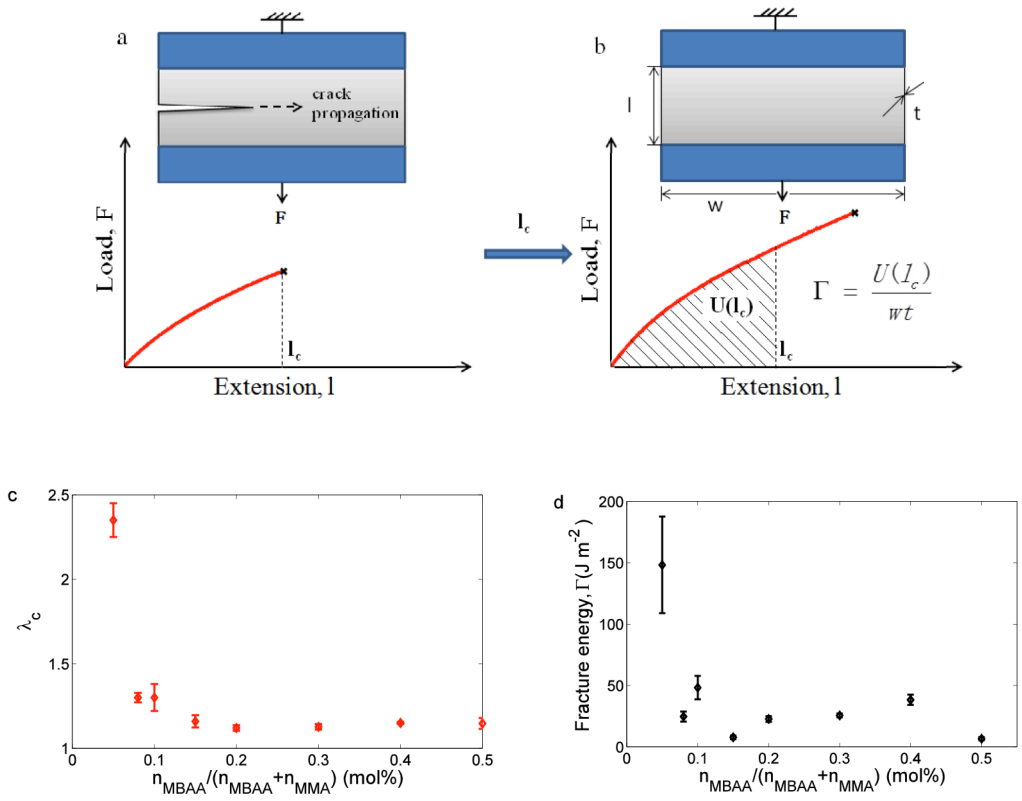

Figure 3.3 Illustration of pure-shear fracture energy measurement. **(a)** Load-extension curve for notched sample; **(b)** Load-extension curve for un-notched sample; **(c)** Stretch ratio at which pre-crack propagation starts as a function of MBAA content; **(d)** Fracture energy of ionogels as a function of MBAA content. Error bars show one standard deviation; sample size N=3.

Figures 3.3a and **3.3b** depict schematic load-extension curves of samples with and without pre-crack, respectively, and illustrate how the fracture energy is determined. **Figure 3.3c** shows as a function of MBAA content the stretch ratio at

which the pre-crack starts to propagate. It is clear from the figure that the critical stretch ratio is large for low cross-link densities and decreases with increasing cross-link density. The fracture energy of the ionogels follows a similar trend and is shown in **Figure 3.3d**. The inverse dependence on cross-link density is in agreement with the Lake-Thomas model for the fracture toughness of elastomers, and indeed the fracture energy of these ionogels is quite comparable to the threshold toughness of rubber, *40-80* J m^{-2}.[95] In accordance with the Lake-Thomas model, this fracture energy is associated mainly with the breaking of carbon-carbon bonds, without any other energy dissipation mechanisms.[84] To the best of our knowledge, this is the first measurement of the fracture energy of an ionogel. While the fracture energy of these ionogels is already relatively high, the fracture energy can be improved further through inclusion of energy dissipation mechanisms such as the rupture of sacrificial bonds or the unzipping of crystallites.[23,24,96-98] These strategies have been used to increase the fracture energy of hydrogels significantly, but further development is needed to adapt them to ionogels.

3.4 Extend model of ideal elastomeric gels to ionic liquid gels

We next derive the equations of state for ionogels based on the model of the ideal elastomeric gel.[41,51] This model provides a simple, robust, and general approach to characterize a gel and has been applied successfully to several types of hydrogels, including neutral hydrogels,[51] temperature-sensitive hydrogels,[99] and polyelectrolyte

hydrogels.[51] The model does not assume any particular mechanical model a priori, and can be calibrated via a set of straightforward experiments.

Recall the two basic assumptions of the ideal elastomeric gel.[36] First, the individual polymer chains and solvent molecules are taken to be incompressible; their volumes remain nearly unchanged on mixing. Consequently, we assume that the volume of the ionogel is equal to the volume of the polymer network plus the volume of the ionic liquid. There then exists a simple relationship between J and C.[36] Subject to charge balance, i.e., the number of cations must equal the number of anions $C_+ = C_- = \frac{1}{2}C$, where C is the total number of cations and anions divided by the volume of dry polymer network, the swelling ratio is given by

$$J = 1 + \frac{1}{2}C(\Omega_- + \Omega_+), \tag{3.4}$$

where Ω_+ and Ω_- refer to the atomic volumes of the cation and anion of the ionic liquid, respectively. Second, the density of crosslinks in the gel is assumed to be sufficiently low, that the effect of the cross-links on the molecular interactions between polymer and solvent is negligible.

As an idealization, the Helmholtz free energy of the ionogel is taken as the sum of the free energy due to stretching of the network and the free energy due to mixing of the polymer network and the ionic liquid:

$$W = W_{stretch}(\lambda_1, \lambda_2, \lambda_3) + W_{mix}(J). \tag{3.5}$$

The free energy of the gel, W, is defined as the excess energy of the gel relative to the sum of its constituents—that is, W is the free energy of the gel minus that of the dry

polymer and that of the pure ionic liquid. The free energy due to the stretching of the network, $W_{stretch}(\lambda_1,\lambda_2,\lambda_3)$, is a function of the stretches and depends solely on the cross-link density. The free energy due to the mixing of the polymer and the ionic liquid, $W_{mix}(J)$, is a function of the swelling ratio, but is independent of the cross-link density. The polymer backbone carries no charge; besides the mixing and stretching contributions, there are no additional energy terms.

Consider a block of ionogel subjected to Cauchy stresses σ_1, σ_2, and σ_3 in an ionic liquid (**Figure 3.1a**). If the gel is in equilibrium with its surroundings, the Helmholtz free energy of the ionogel satisfies the equation

$$dW = \sigma_1\lambda_2\lambda_3 d\lambda_1 + \sigma_2\lambda_3\lambda_1 d\lambda_2 + \sigma_3\lambda_1\lambda_2 d\lambda_3 + \mu_+ dC_+ + \mu_- dC_-, \tag{3.6}$$

where μ_+ and μ_- are the chemical potentials of the cations and anions in the ionic liquid, respectively. A combination of (3.4)-(3.6) then yields

$$\begin{aligned}
&\left[\frac{\partial W_{stretch}}{\partial\lambda_1} - \left(\sigma_1 + \Pi_{mix}(J) + \frac{\mu_+ + \mu_-}{\Omega_+ + \Omega_-}\right)\lambda_2\lambda_3\right] d\lambda_1 \\
&+\left[\frac{\partial W_{stretch}}{\partial\lambda_2} - \left(\sigma_2 + \Pi_{mix}(J) + \frac{\mu_+ + \mu_-}{\Omega_+ + \Omega_-}\right)\lambda_3\lambda_1\right] d\lambda_2 \\
&+\left[\frac{\partial W_{stretch}}{\partial\lambda_3} - \left(\sigma_3 + \Pi_{mix}(J) + \frac{\mu_+ + \mu_-}{\Omega_+ + \Omega_-}\right)\lambda_1\lambda_2\right] d\lambda_3 = 0
\end{aligned} \tag{3.7}$$

where the osmotic pressure due to mixing is given by

$$\Pi_{mix}(J) = -\frac{dW_{mix}(J)}{dJ}. \tag{3.8}$$

For the ionogel to be in equilibrium with its surroundings, Equation (3.7) must hold for arbitrary and independent changes in the three stretches, λ_1, λ_2 and λ_3.

Consequently, the coefficients of the variations of the stretches must vanish, giving three independent equations,

$$\sigma_1 = \frac{\partial W_{stretch}}{\lambda_2 \lambda_3 \partial \lambda_1} - \Pi_{mix}(J) - \frac{\mu_+ + \mu_-}{\Omega_+ + \Omega_-}, \tag{3.9a}$$

$$\sigma_2 = \frac{\partial W_{stretch}}{\lambda_1 \lambda_3 \partial \lambda_2} - \Pi_{mix}(J) - \frac{\mu_+ + \mu_-}{\Omega_+ + \Omega_-}, \tag{3.9b}$$

$$\sigma_3 = \frac{\partial W_{stretch}}{\lambda_1 \lambda_2 \partial \lambda_3} - \Pi_{mix}(J) - \frac{\mu_+ + \mu_-}{\Omega_+ + \Omega_-}. \tag{3.9c}$$

For polymer networks with relatively low cross-link density, the Gaussian chain model provides a good description of the mechanical behavior. The free energy for stretching derived from the Gaussian-chain model is given by[39]

$$W_{stretch}(\lambda_1, \lambda_2, \lambda_3) = \frac{1}{2} NkT\left[\lambda_1^2 + \lambda_2^2 + \lambda_3^2 - 3 - 2\log(\lambda_1 \lambda_2 \lambda_3)\right]. \tag{3.10}$$

The chemical interaction between a polymer and an ionic liquid can be very complex. Thus, for the time being, we do not specify the function $W_{\text{mix}}(J)$. Instead, we will show that $W_{\text{mix}}(J)$ is readily determined experimentally. With Equation (3.10), the expressions for the stresses finally become

$$\sigma_1 = \frac{NkT}{J}\left(\lambda_1^2 - 1\right) - \Pi_{mix}(J) - \frac{\mu_+ + \mu_-}{\Omega_+ + \Omega_-}, \tag{3.11a}$$

$$\sigma_2 = \frac{NkT}{J}\left(\lambda_2^2 - 1\right) - \Pi_{mix}(J) - \frac{\mu_+ + \mu_-}{\Omega_+ + \Omega_-}, \tag{3.11b}$$

$$\sigma_3 = \frac{NkT}{J}\left(\lambda_3^2 - 1\right) - \Pi_{mix}(J) - \frac{\mu_+ + \mu_-}{\Omega_+ + \Omega_-}. \tag{3.11c}$$

Thus, the ionogel is fully characterized by the scalar quantity *NkT* and a single-variable function $\Pi_{mix}(J)$. Once *NkT* and $\Pi_{mix}(J)$ are known, the four equations of state, (3.3), (3.11a), (3.11b) and (3.11c) connect eight thermodynamic variables: l_1, l_2, l_3, *C*, σ_1, σ_2, σ_3, and $\mu = \mu_+ + \mu_-$.

Under free-swelling conditions in an ionic liquid, the stretches of the ionogel are isotropic, $\lambda_1 = \lambda_2 = \lambda_3 = J^{1/3}$, and all applied stress components vanish, $\sigma_1 = \sigma_2 = \sigma_3 = 0$. If the ionic liquid is pure, the chemical potentials of the ionic species in the liquid are equal to zero, $\mu_+ = \mu_- = 0$. Substituting these expressions into Equation (3.11a) yields

$$\Pi_{mix} = \frac{NkT}{J}(J^{\frac{2}{3}} - 1). \tag{3.12}$$

from which the osmotic pressure Π_{mix} can be calculated once *J* and *NkT* have been measured experimentally. **Figure 3.4** shows the osmotic pressure as a function of the swelling ratio for the various ionogels synthesized in this study. Under the assumption that the cross-link density is sufficiently low that the cross-links do not affect the chemical interaction between polymer and ionic liquid, the graph in **Figure 3.4** provides a complete description of the energy of the interaction between PMMA and [BMIM][NTf_2]. Evidently, the osmotic pressure decreases as the concentration of the [BMIM][NTf_2] in the PMMA increases. This behavior is also observed for hydrogels.[41]

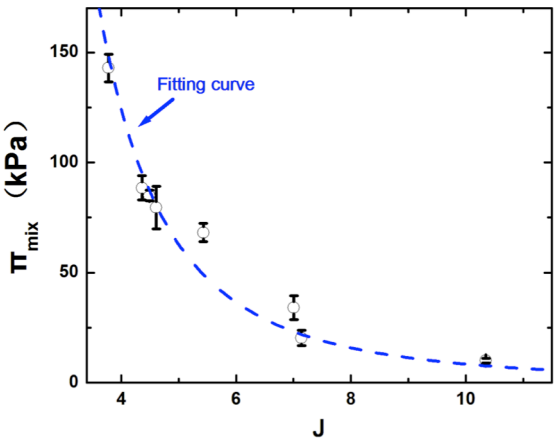

Figure 3.4 The experimental osmotic pressure as a function of swelling ratio (open circles); the dashed curve represents the Flory-Huggins model, Equation (3.19), with $\chi' = 0.48$, yielding a correlation coefficient $R^2 = 0.97$.

We next adopted the Flory-Huggins approach to derive an expression for the mixing contribution to the free energy of ionogels.[38,40,100] The ionic liquid is treated as a two-component solvent containing cations and anions. According to the regular solution model, the free energy (per site occupied by an ion) of the ionic liquid, F_{IL}, containing cations and anions in equimolecular quantities is given by

$$\frac{F_{IL}}{kT} = \ln\frac{1}{2} + \frac{1}{4}\chi_{+-}, \tag{3.13}$$

where χ_{+-} is the Flory interaction parameter for the anions and cations. The free energy F (per site) of a mixture of the ionic liquid and the polymer network is

$$\frac{F}{kT} = \Phi_+ \ln\Phi_+ + \Phi_- \ln\Phi_- + \frac{\Phi_p}{n}\ln\Phi_p + \chi_{+-}\Phi_+\Phi_- + \chi_+\Phi_+\Phi_p + \chi_-\Phi_-\Phi_p \tag{3.14}$$

where n is the number of sites occupied by the network, and where F_+, F_-, and F_p are the volume fractions of the cations, anions, and polymer in the ionogel, respectively. The Flory interaction parameters between the polymer and the cations, and between the polymer and the anions are denoted by χ_+ and χ_-. The mass and charge balances require that $\Phi_+ = \Phi_- = \frac{1}{2}\Phi$ and $\Phi_p = 1-\Phi$, so that

$$\frac{F}{kT} = \Phi \ln\frac{\Phi}{2} + \frac{(1-\Phi)}{n}\ln(1-\Phi) + \chi(1-\Phi)\Phi + \chi_{+-}\frac{\Phi^2}{4}, \tag{3.15}$$

where $\chi = \frac{1}{2}(\chi_+ + \chi_-)$. The free energy of mixing, F_{mix}, is then

$$F_{mix} = F - F_{IL} = kT\left[\Phi \ln\Phi + \frac{1-\Phi}{n}\ln(1-\Phi) + \chi'(1-\Phi)\Phi\right], \tag{3.16}$$

where $\chi' = \chi - \frac{1}{4}\chi_{+-}$. For a cross-linked network, $n\to\infty$ and

$$F_{mix} = kT\left[\Phi\ln\Phi + \chi'(1-\Phi)\Phi\right]. \tag{3.17}$$

From the definition of J, it follows that $\Phi = 1-\frac{1}{J}$. Writing F_{mix} as a function of J and per unit volume, we eventually find

$$W_{mix}(J) = \frac{kT}{\Omega}[(J-1)\ln(1-\frac{1}{J}) + \chi'(1-\frac{1}{J})], \tag{3.18}$$

leading to the following equation for the osmotic pressure

$$\Pi_{mix} = -\frac{kT}{\Omega}[\frac{1}{J} + \ln(1-\frac{1}{J}) + \frac{\chi'}{J^2}], \tag{3.19}$$

where $\Omega = \frac{1}{2}(\Omega_+ + \Omega_-)$. This expression for the osmotic pressure is shown as a dashed curve in **Figure 3.4**, where χ' was used a fitting parameter and where Ω_+=1.26×10^{-28} m^{-3} and Ω_- =3.54×10^{-28} m^{-3} were calculated from the respective ionic radii in references.[101,102] The experimental data in the figure is well captured by the Flory-Huggins model; evidently, the only materials parameters required for the equations of state of this class of ionogels are the elastic modulus and the Flory interaction parameter $\chi' = 0.48$.

3.5 Summary

Ionogels hold great promise for the use of ionic conductors. In this chapter, we have presented synthesis and mechanical characterization of a hydrophobic ionogel. The ionogel was prepared by swelling covalently cross-linked poly(methyl methacrylate) in 1-butyl-3-methylimidazolium bis (trifluoromethylsulfonyl) imide. The resulting ionogel is transparent, compliant, stretchable, and relatively tough. The inverse dependence of the fracture energy on the cross-link density agrees with the Lake-Thomas model and suggests that energy dissipation during fracture arises mainly from the fracture of carbon-carbon bonds. We anticipate that the toughness of these ionogels may be further improved by including other energy dissipation mechanisms.

The chemo-mechanical behavior of the ionogels may be complex, but described nicely with the model of ideal elastomeric gels combined with the Flory-Huggins model for the free energy of mixing. Only two material parameters are required for the

equations of state for these ionogels: the elastic modulus of the gel and a single Flory interaction parameter. Thus we expect that the mechanical behavior of the ionogel in this work is representative of a larger class of ionogels based on covalently cross-linked networks of neutral polymers.

Chapter 4 Toughening hydrogels with covalent and ionic crosslinks

4.1 Introduction

Hydrogels are used as scaffolds in tissue engineering,[34] carriers for drug delivery,[16] valves in microfluidics,[35,103] and superabsorbent polymers in disposable diapers.[46] Many other applications require hydrogels of exceptional mechanical properties. Examples include biomedical applications such as materials for cartilage replacement,[104] engineering applications such as swellable packers for oil and gas recovery,[29] and artificial muscles and artificial nerves in the nascent field of soft machines.[13,105-107] These load-bearing applications of hydrogels are often limited by low stiffness and toughness. Hydrogels for cartilage replacement, for instance, require high stiffness and toughness to retain shape and to resist fracture, respectively.[108] Several approaches have been reported to improve the toughness of hydrogels,[23,24,98,109,110] but simultaneously achieving high stiffness and toughness remains a challenge. Stiffness and toughness of polymer networks are often inversely related. According to the Lake-Thomas model, for example, as the crosslink density decreases, toughness increases, but stiffness decreases.[84,111] Most hydrogels are either stiff and brittle with low fracture energies on the order of 10 J m^{-2}, or tough and compliant with low elastic moduli on the order of 10 kPa. To place these values in

context, note that cartilage has elastic moduli on the order of 1,000 kPa and fracture energies on the order of 1,000 J m^{-2}.[108]

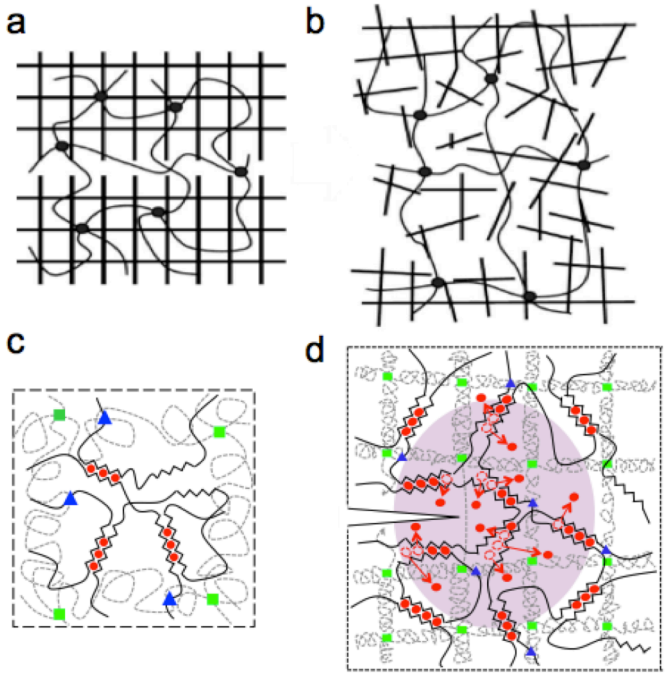

Figure 4.1 Energy dissipation in double network gels and alginate-polyacrylamide hydrogels. (**a**) A loosely crosslinked network is interpenetrating inside a highly crosslinked network. (**b**) When the double network is subject to large deformation, the highly crosslinked network ruptures and dissipate a large amount of energy whereas the loosely crosslinked network maintains the physical integrity. (**c**) Alginate-polyacrylamide hydrogels contain ionic and covalent crosslinks. (**d**) When the gel deforms, ionic crosslinks in a large plastic zone unzip and dissipate significant amount of energy.

J. P. Gong and her coworkers discovered that double network hydrogels can achieve fracture energy of 1,000 J m^{-2}.[23,103,111] The underlying mechanism for this high toughness is an effective energy dissipation by breaking sacrificial bonds under

deformation (**Figure 4.1a** and **4.1b**). In this benchmark work, covalent crosslinks serve as sacrificial bonds, which leads to negligible recovery of the polymer network after a single loading.[103]

A recent work has shown that by replacing the covalent bonds with ionic crosslinks, alginate-polyacrylamide hydrogels can achieve fracture energy of 9,000 J m^{-2} (**Figure 4.1c**). Such hydrogel has an interpenetrating network of ionically crosslinked alginate and covalently crosslinked polyacrylamide. The extremely high toughness is due to two synergetic mechanisms: covalent crosslinks bridge the crack, while ionic crosslinks unzip, dissipate energy in a large area of plastic zone at crack tip (**Figure 4.1d**). After deformation, the unzipped ionic crosslinks can reform quickly at elevated temperature.[24] Tests of biocompatibility have shown that alginate-polyacrylamide hydrogels have minimal effects on cells *in vitro* and *in vivo*, encouraging further exploration of the potential of these hydrogels as biomaterials.[23,112] This combination of high toughness, stretchability, recoverability and biocompatibility makes these hydrogels ideal candidates for further investigation. For example, these hydrogels have been infused into a scaffold of woven fibers to mimic cartilage.[113]

Although the alginate-polyacrylamide hydrogels have achieved exceptionally high toughness, their limitation has been noted: the mechanical properties deteriorate with high input of ionic crosslinker, e.g. Ca^{2+} ions.[24] This constraint leads to modest stiffness, and lacking of mobile ions for ionic conductivity. To overcome this constraint, there exist 3 obstacles. First, the concentration of alginate in the hydrogel is low; any attempt to significantly raise the concentration of alginate is frustrated by the

high viscosity, making it difficult to mix the ingredients to form a homogeneous hydrogel. Second, the crosslink density of alginate is low because the crosslinker, calcium sulfate, has low solubility. Third, as mentioned above, stiffness and toughness are often inversely related. As the stiffness increases, the toughness decreases significantly.

In this work, we report that alginate-polyacrylamide hydrogels can simultaneously achieve high stiffness and toughness. We increase the concentration of alginate while maintaining relatively low viscosity by using both short- and long-chain alginates. We increase the crosslink density of alginate while maintaining homogeneous distribution of alginate by using a combination of calcium sulfate and calcium chloride as crosslinkers. This approach breaks the inverse relation between stiffness and toughness. The resulting hydrogels achieve stiffness and toughness significantly beyond those of existing hydrogels. More importantly, the mechanical properties are compatible with high concentration of mobile ions, which may open up the use of alginate-polyacrylamide hydrogels as ionic conductors.

4.2 Hybrid hydrogels with high stiffness and toughness

An alginate-polyacrylamide hydrogel consists of two interpenetrating polymer networks. Polyacrylamide forms a covalently crosslinked network (**Figure 4.2a**). Alginate is a linear block copolymer of 1,4-linked β-D-mannuronic acid (M) and α-L-guluronic acid (G) residues. This block copolymer forms crosslinks via ionic interactions between the G residues on the chains and chelating ions such as Ca^{2+}

(**Figure 4.2b**).[114] The high toughness results from the synergy of two mechanisms: crack bridging by the covalently crosslinked polyacrylamide network and energy dissipation by unzipping ionic crosslinks in the alginate network over a large region of the hydrogel (**Figure 4.2c**).[24]

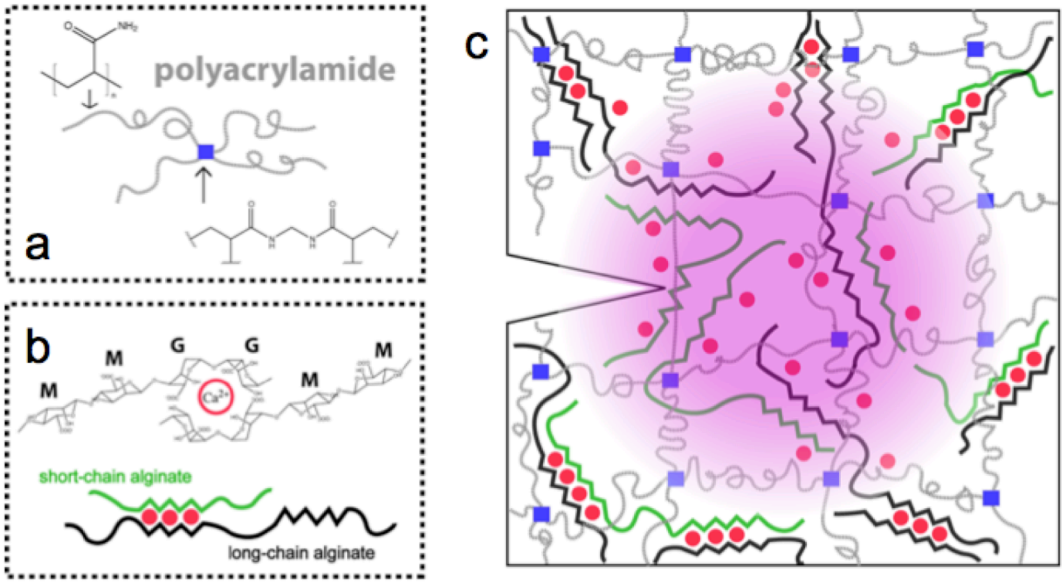

Figure 4.2 Structure and toughening mechanism of hybrid hydrogels. (**a**) Polyacrylamide (PAAm; grey dashed lines) forms covalent crosslinks through N,N`-methylenebisacrylamide (MBAA; blue squares). (**b**) Short- and long-chain alginate chains (green and black solid lines, respectively) with G blocks that form ionic crosslinks through Ca^{2+} (red circles). (**c**) A large area of plastic zone (pink region) presents ahead of the notch where ionic crosslinks unzip to dissipate energy.

The viscosity of an aqueous solution of alginate depends on both the concentration and chain length of the alginate.[115-117] Alginate is a natural product

available only with specific chain lengths. Modification of the chain length requires special treatments such as g-ray irradiation, which may also introduce changes in the distribution of the uronate residues.[118] We used two types of biologically derived alginates that differ in the chain length, but not in the distribution of the uronate residues: LF20/40, a long-chain alginate with a molecular weight of 200 kg mol^{-1}; and LFR5/60, a short-chain alginate with a molecular weight of 30 kg mol^{-1}.[119] Both alginates are commercially available (FMC BioPolymer).

We prepared aqueous alginate solutions containing various fractions of short-chain alginate. The total alginate content was fixed at 2.8 wt%. The viscosity of these solutions was measured with steady-state shear test on an AR-G2 rheometer. The viscosity reduces as the fraction of the short-chain alginate increases (**Figure 4.3a** and **4.3b**). We next prepared two series of aqueous alginate solutions, one containing long-chain alginate (LF20/40), the other containing short-chain alginate (LFR5/60). The weight ratio of alginate to water was varied. The long-chain alginate solution has a large viscosity when the alginate concentration exceeds 4wt%, while the short-chain alginate solution maintains a low viscosity throughout the experiment (**Figure 4.3c** and **4.3d**). When the alginate concentration is 12 wt%, alginate floccules appear, indicating that the solubility of alginate in water is around 10 wt% (**Figure 4.3d**).

We increase the ionic crosslink density by using a combination of calcium sulfate and calcium chloride. The crosslinker used in our previous work, $CaSO_4 \cdot 2H_2O$, has low solubility in water (2.4 g L^{-1} at 20°C);[24] $CaSO_4 \cdot 2H_2O$ cannot supply sufficient dissolved Ca^{2+} ions to achieve a high cross-link density. We prepared

hybrid hydrogels with various contents of $CaSO_4$. The alginate content was fixed at 6.4%, and the ratio of $CaSO_4$ to alginate was varied from 16% to 23%. These gels all had similar stress-stretch curves and elastic moduli (200±20 kPa) independent of $CaSO_4$ content; at the same time, these gels contained undissolved $CaSO_4$ particles. The results demonstrate that $CaSO_4$ cannot supply sufficient dissolved Ca^{2+} ions to achieve a high cross-link density.

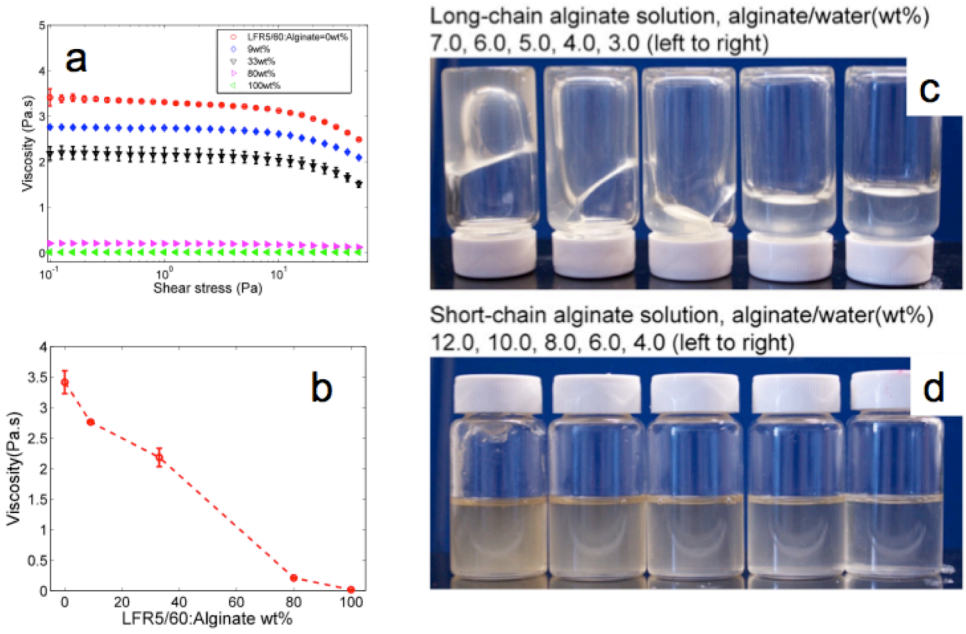

Figure 4.3 Viscosity of alginate solutions. (**a, b**) Steady-state shear test. Viscosity of alginate solutions containing various fractions of short-chain alginate (LFR5/60). Flow curves (**a**) and viscosity (**b**) at 10^{-1} Pa shear stress as a function of the fraction of the short-chain alginate (LFR5/60). (**c, d**) Vial test. Aqueous solutions of various alginate concentrations. (**c**) Long-chain alginate (LF20/40). (**d**) Short-chain alginate (LFR5/60).

The solubility of $CaCl_2$ is high, but the direct use of $CaCl_2$ as crosslinker causes inhomogeneous distribution of alginate in pure alginate hydrogels.[120] Here we show that $CaCl_2$ can be used to synthesize alginate-polyacrylamide hydrogels with homogeneous distribution of alginate. Our new protocol of synthesis is as follows. A homogeneous alginate-polyacrylamide hydrogel was first formed with $CaSO_4 \cdot 2H_2O$; the crosslink density of G blocks was low, but alginate chains were immobilized in the network. Subsequently, the hydrogel was immersed in a large volume of a 1.0 M $CaCl_2$ solution to achieve full crosslinking of G blocks, while retaining the homogeneous distribution of alginate in the hydrogel. This observation is consistent with a recent report.[121]

We demonstrate that the concentration of alginate strongly affects the properties of alginate-polyacrylamide hydrogels. In a series of experiments, we fixed the ratio of polyacrylamide to water at 16.8 wt% and fixed the ratio of short-chain to long-chain alginates at 4:1, but varied the concentration of alginate from 2.3 % to 6.4 %; the swelling ratio, defined as the ratio of the volume of the hydrogel to that of the dry polymer, changed from 7.0 to 6.0 with increasing alginate content. We soaked the hydrogels in a large reservoir of concentrated $CaCl_2$ solutions (1.0 M) for at least 3 days. The diffusion coefficient of Ca^{2+} ions in hydrogels (D) is typically on the order of 10^{-9} m^2s^{-1}; the thickness of specimen (H) is 3 mm; the diffusion time is estimated, $t=H^2/D$=2.5 hours. This soaking time is sufficient for diffusion of Ca^{2+} ions into the hydrogels.

To further confirm that the G blocks were fully crosslinked, we performed the following experiment: two specimens were soaked in $CaCl_2$ solutions (1.0 M) for 3 and 4 days, respectively; the results showed that the additional 24-hour soaking time made no difference in the stress-stretch curves, indicating the G blocks had been saturated in the soaking step.

We then performed a series of tensile tests on both unnotched and notched

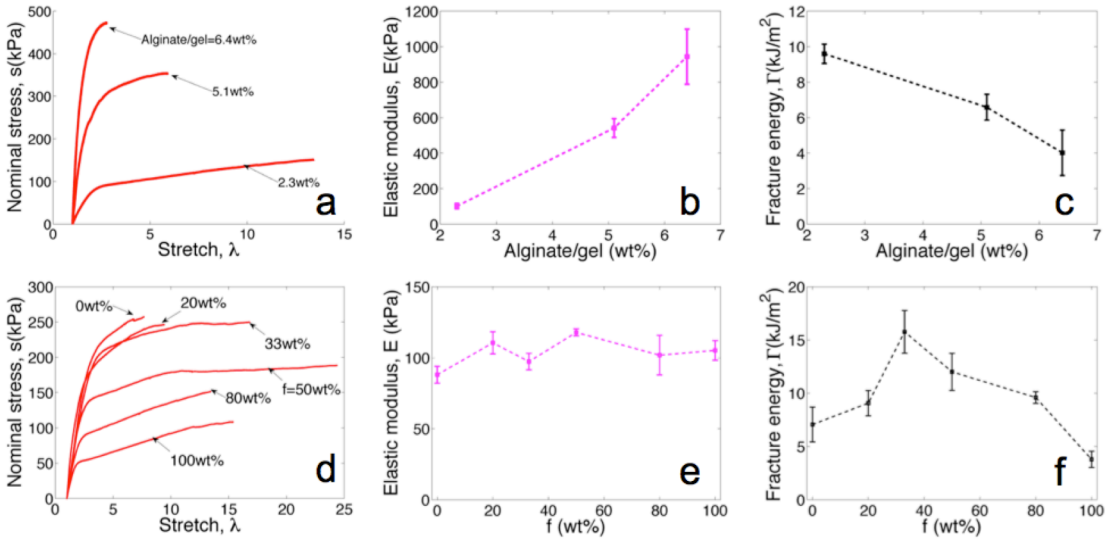

Figure 4.4 Properties of hybrid hydrogels. (**a**) Stress-stretch curves of gels of various concentrations of alginate. Each test was performed by pulling an unnotched sample to rupture. (**b**) Elastic modulus as a function of the concentration of alginate in the gel. (**c**) Fracture energy varies with the concentration of alginate. (**d**) Stress-stretch curves of gels of various fractions of short-chain alginate to the total alginate. (**e,f**) Elastic modulus (**e**) and fracture energy (**f**) vary with the fraction of short-chain alginate. Error bars show standard deviation; sample size $n = 4$.

samples. For the tensile tests of unnotched samples, as the concentration of alginate increases, the strength increases, but the rupture stretch decreases **(Figure 4.4a**). The nominal stress is the loading force divided by the cross-sectional area of the undeformed sample. The stretch is the current length divided by the initial length of undeformed sample. The elastic modulus is the slope of the initial portion of the stress-stretch curves. As the alginate content increases, the elastic modulus of the hydrogel increases (**Figure 4.4b**). The fracture energy of the hydrogel was measured by performing tensile tests on notched samples using a geometry known as the pure shear test.[24,93] The fracture energy of the hydrogel decreases with increasing alginate content (**Figure 4.4c**). Despite this reduction, the hydrogel with the maximum alginate content maintains a large fracture energy of 4,000 Jm^{-2}, while exhibiting a large elastic modulus of 1,000 kPa. As a result, this approach leads to stiff and tough hydrogels that contain excess mobile ions.

4.3 Decoupling stiffness and toughness

An obstacle to further improve the toughness of the hybrid hydrogels is an inverse relation between stiffness and toughness. We interpret this inverse relation between stiffness and toughness as follows. Increasing the alginate content not only raises the stiffness of the hydrogel, but also its strength (**Figure 4.4a**). The high strength, in turn, lowers the toughness of the hydrogel, because the region near the crack tip where energy is dissipated during crack growth decreases in size with increasing strength. The trade-off between strength and toughness is well recognized in materials science.[122,123]

Our new approach also breaks this inverse relation between stiffness and toughness.

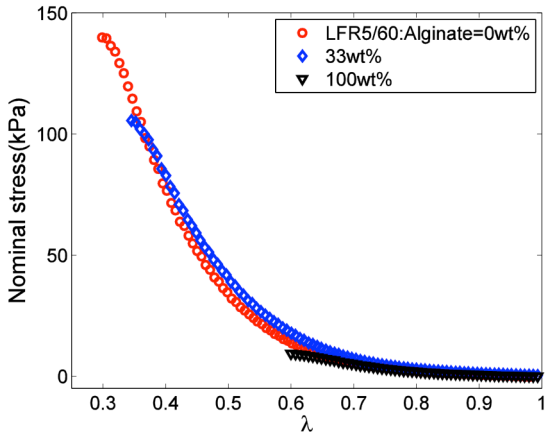

Figure 4.5 Stress-stretch curves of alginate hydrogels. The fraction of short-chain alginate is varied.

In alginate hydrogels, the chain length affects strength, but not stiffness (**Figure 4.5**). We performed a series of uniaxial compression tests on gel cylinders of 8 mm diameters. The AR-G2 rheometer was used. The rheometer platen approached the gel at a speed of 5 μm s^{-1} until a rise in force was detected, indicating contact between the platen and the gel. Upon contact, the displacement rate of the platen was increased to 20 μm s^{-1} until a pre-determined stretch ratio, typically 0.8-0.9, was achieved. The entire loading process was finished in less than two minutes to avoid any redistribution of solvent inside the gel, and thus maintain incompressibility. Both force and displacement were recorded continuously throughout the experiment. The chain length affects strength but not stiffness.

The same phenomenon occurs in alginate-polyacrylamide hydrogels. We varied the weight percentage of short-chain alginate in the gels, while fixing the total weight

percentage of alginate at 2.3 wt% and the ratio of $CaSO_4$ to alginate at 20 wt%. The strength of the hydrogel decreases as the fraction of short-chain alginate increases (**Figure 4.4d**), while the elastic modulus is independent of the fraction of short-chain alginate (**Figure 4.4e**).

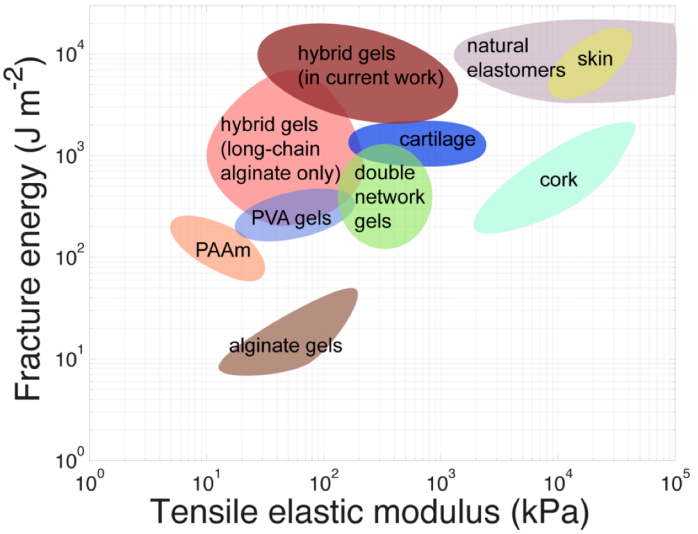

Figure 4.6 Fracture energies and tensile elastic moduli of various materials. The hybrid gels in the current work are compared with other soft materials, including hybrid gels with long-chain alginate only, double network hydrogels, polyvinyl alcohol hydrogels (PVA), cartilage, natural elastomers, skin, cork along with data for polyacrylamide hydrogels (PAAm) and alginate hydrogels.

The fracture energy reaches a maximum value of 16,000 J m^{-2} at an intermediate proportion of short- and long-chain alginates (**Figure 4.4f**). The maximum value of the fracture energy is a twofold improvement over the highest value reported before for alginate-polyacrylamide hydrogels with long-chain alginate only.[24]

In **Figure 4.6**, we present two Ashby charts for a variety of soft materials. It is perhaps the first time that a hydrogel containing around 90% water rivals natural elastomers in toughness. Materials include the hybrid gel prepared in this work, alginate-polyacrylamide gel using long-chain alginate only,[24] polyvinyl alcohol gel (PVA),[124] double network gel (DN),[103] polyacrylamide gel (PAAm),[24] alginate gel,[24] natural elastmoers,[125] along with cork, cartilage and skin.[126,127]

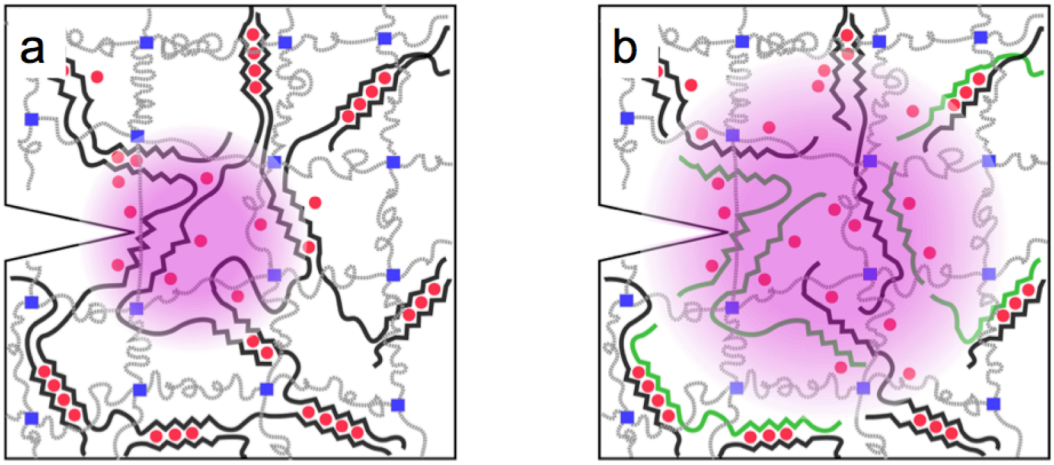

Figure 4.7 Effects of alginate chain length on the size of process zone. (**a**,**b**) Process zone around the root of the notch in alginate-polyacrylamide hydrogels containing long-chain alginate only (**a**), and containing both short- and long-chain alginates (**b**). Green solid lines represent short-chain alginate chains.

We interpret the observed relation between the fracture energy and the fraction of short-chain alginate as follows. In the alginate-polyacrylamide hydrogel containing only long-chain alginate, the strength is so high that only a small region around the root

of the notch is stressed enough to unzip ionic crosslinks, leading to a low fracture energy （**Figure 4.7a**). As the fraction of short-chain alginate increases, the strength decreases and the size of the region in which ionic crosslinks unzip grows, leading to an increase in fracture energy (**Figure 4.7b**). When the content of the short-chain alginate is too large, the strength of the alginate network is too low to effectively contribute to energy dissipation. Thus the fracture energy goes through a maximum at an intermediate fraction of short-chain alginate.

Furthermore, we can independently optimize the stiffness and toughness of a hydrogel by varying the molecular weight and crosslink density of the alginate (**Figure 4.8**). The ionic crosslink density affects greatly the properties of alginate-polyacrylamide hydrogels. We prepared two series of hybrid hydrogels (f = 100 wt% and f = 50 wt%) containing different $CaSO_4$ contents. The concentration of alginate (LFR5/60, LF20/40) was fixed at 2.3 wt%. Figure 4.8 illustrates the results of tensile tests along with the data reported by J.Y. Sun et al.[24] **Figure 4.8a** and **4.8b** illustrate the stress-stretch curves for the hybrid hydrogels with f = 100 wt% and f = 50 wt%, respectively. The elastic modulus increases with increasing ionic crosslink density (**Figure 4.8c**). The fracture energy is plotted in **Figure 4.8d**. The alginate network in the gel with *f = 100 wt%* is too weak to effectively contribute to energy dissipation, results in a low toughness. In the gels with *f = 0* or *50 wt%*, the fracture energy goes through a maximum value at a certain level of ionic crosslink density. By using both short- and long-chain alginate in alginate-polyacrylamide hydrogels, one can optimize stiffness and toughness independently.

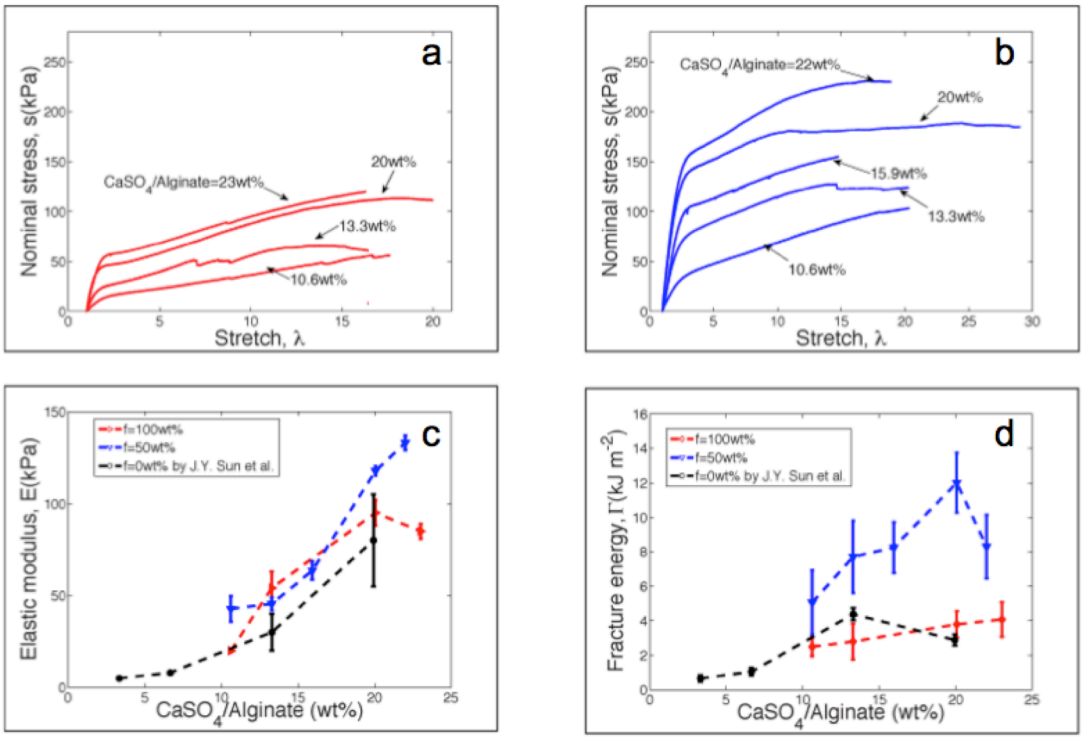

Figure 4.8 Effect of ionic crosslink density. (**a**,**b**) Stress-stretch curves were measured by tensile tests on the unnotched samples of hybrid hydrogels, *f*=100wt% (**a**), *f*=50wt% (**b**). (**c**) Elastic moduli as a function of ionic crosslinker input. (**d**) Fracture energy varies with the ionic crosslinker input. The data points labeled by 0wt% were cited from J.Y. Sun et al, which were measured on alginate-polyacrylamide hydrogels containing long-chain alginate only.[24]

4.4 Summary

The development of hydrogels for cartilage replacement and soft robotics has highlighted a challenge: load-bearing hydrogels need to be both stiff and tough. Several approaches have been reported to improve the toughness of hydrogels, but simultaneously achieving high stiffness and toughness remains difficult. Here we

report that alginate-polyacrylamide hydrogels can simultaneously achieve high stiffness and toughness. We combine short- and long-chain alginates to reduce the viscosity of pre-gel solutions, and synthesize homogeneous hydrogels of high ionic crosslink density. The resulting hydrogels can have elastic moduli of ~1 MPa and fracture energies of ~4,000 Jm^{-2}. Furthermore, this approach breaks the inverse relation between stiffness and toughness: while maintaining constant elastic moduli, these hydrogels can achieve fracture energies up to ~16 kJ m^{-2}. These stiff and tough hydrogels hold promises for the further development as load-bearing materials.

Chapter 5 Toughening hydrogels with crystallites

5.1 Introduction

Recent developments in the area of hydrogels promise to greatly expand their scope of applications.[23,24,98,109,128-130] Many applications require hydrogels to endure significant mechanical loads in aggressive environments. Examples range from biomedical applications such as artificial cartilage in tissue engineering,[104] to engineering applications such as swellable packers in the oil industry,[131] or artificial nerves and muscles in the nascent field of soft machines.[13] Substitutes for cartilage require high stiffness (1 MPa), high toughness (1,000 Jm^{-2}), and high water content (60-80 %).[108] Materials for oil packers require high stiffness, high strength, and chemical stability; they need to resist deformation, sustain sealing pressure (up to 34 MPa) and be stable in saline water.[131] Materials for artificial nerves and muscles require high resistance to mechanical damage,[107] and tolerance of concentrated electrolyte for ionic conductance.[13] Most hydrogels have low stiffness (~10 kPa), strength (~100 kPa) and toughness (~10 Jm^{-2});[22] and they may degrade in electrolyte solutions.[132] There is a strong need for mechanically robust hydrogels with good chemical stability.

Despite recent progress, developing hydrogels that are both mechanically robust and chemically stable is still a challenge.[22,25] Breaking covalent bonds in tough double network gels results in permanent and irreversible damage to the network.[103] Formation of hydrophobic associations is limited by low solubility of the hydrophobes.[110]

Hydrogen bonds have very low association strength in hydrogels due to competition of water for binding sites.[133] Ionic cross-links are particularly effective in toughening hydrogels – alginate-polyacrylamide hydrogels in which the alginate is cross-linked with calcium ions exhibit remarkably high toughness.[24,134] The ionic cross-link is, however, vulnerable to mobile ions, which are often encountered under physiological and engineering conditions,[13,104] and the performance of ionically cross-linked hydrogels degrades markedly in electrolyte solutions.[98,132]

As an alternative to ionic cross-links, the use of crystallites to cross-link a network has great potential to overcome these limitations: crystallites serve as physical cross-links that are reversible and stable when exposed to mobile ions. Polyvinyl alcohol (PVA) is an example of a polymer that can form crystallites. PVA is widely used and has seen extensive development for biomedical applications.[135,136] In 1975, Peppas discovered that a sequence of freeze and thaw cycles could produce PVA hydrogels where crystallites serve as cross-links.[135] Unfortunately, hydrogels synthesized using this method are compliant and brittle.[124] It is possible to achieve higher stiffness and toughness using a dry-anneal method, but only at the expense of a much lower water content.[137] Muratoglu and coworkers polymerized acrylamide monomers in the pores of a PVA hydrogel to form uncross-linked chains, and showed that the equilibrium water content of the resulting gels increased with acrylamide content, while the coefficient of friction, tear strength and creep resistance decreased.[136]

Here we propose that a hybrid network of a crystalline polymer and a covalently cross-linked hydrophilic polymer may form a hydrogel with robust mechanical properties and good chemical stability: the crystalline polymer can generate a large number of crystallites to serve as physical cross-links that are both stable and reversible; the covalently cross-linked hydrophilic polymer maintain the elasticity of the network during deformation and controls the swelling of the hydrogel. We describe one such hybrid hydrogel that combines extremely high stiffness, strength, and toughness. The hydrogel consists of a hydrophilic polyacrylamide (PAAm) polymer network that is covalently cross-linked and a PVA network that forms crystallites. We show that the PVA crystallites result in a high cross-link density, thus producing a gel of remarkable stiffness and strength. The crystallites unzip under deformation, dissipating energy in the process and yielding a hydrogel with exceptional toughness. After deformation, unzipped crystallites recover at room temperature due to the incompatibility of the two polymers in the gel. The hybrid hydrogel can achieve an elastic modulus of 5 MPa, a strength of 2.5 MPa, and a fracture energy of 14,000 Jm^{-2}. Moreover, these properties are stable, even in concentrated electrolyte solutions.

5.2 Experimental methods

The polyvinyl alcohol-polyacrylamide hydrogel was synthesized using the following protocol. Polyvinyl alcohol powder (PVA, Mw 89000-98000, hydrolysis >99%) was dissolved in distilled water at 90 ^{o}C; the mixture was stirred overnight until the solution became homogeneous. The PVA solution was then mixed with acrylamide

(AAm), N,N'-methylenebisacrylamide (MBAA), tetramethyl-ethylenediamine (TEMED) and ammonium persulfate (APS) in this sequence. The weights of TEMED and APS were fixed at 0.0055 and 0.006 times that of AAm, while the weight ratio of PVA versus AAm was varied. The mixture was placed in a glass mold (75 x 45 x 3 mm^3), and kept at room temperature overnight to complete the reaction.

After synthesis, the hydrogels were dried at room temperature. The dry gels were subsequently heated in a vacuum furnace (Symphony, VWR). The temperature was kept at 80°C for 3 hours and then increased to 120°C for 1 hour. The gel was then fully rehydrated in distilled water, which took approximately three days. The mass of the gel was measured before and after rehydration (m_{dry}, m_{wet}) using an analytical balance. The equilibrium water content was calculated using $1 - m_{dry} / m_{wet}$.

An Instron machine (model 3342 with a 1000 N load cell) was used for mechanical testing. A rectangular strip of gel (75 x 45 x 3 mm^3) was glued to two rigid acrylate clamps (75 x 20 x 1.5 mm^3). Both unnotched and notched samples were prepared for tensile tests. For notched samples, an edge crack of length 35mm was cut using a razor blade in the middle of the gauge section of the sample. The stretch rate was fixed at 2 min^{-1}. The signals of force and extension were recorded throughout the experiment.

Uniaxial compression tests were performed on gel cylinders of 5 mm diameters using the Instron machine. The upper platen approached the sample slowly until a rise in force was detected, indicating contact between the platen and the gel. Upon contact, the displacement rate of the platen was increased to 1 mm/min until a pre-determined

stretch ratio was achieved. The entire loading process was finished in less than five minutes to avoid any redistribution of solvent inside the gel, and thus maintain incompressibility. Both force and displacement were recorded continuously throughout the experiment.

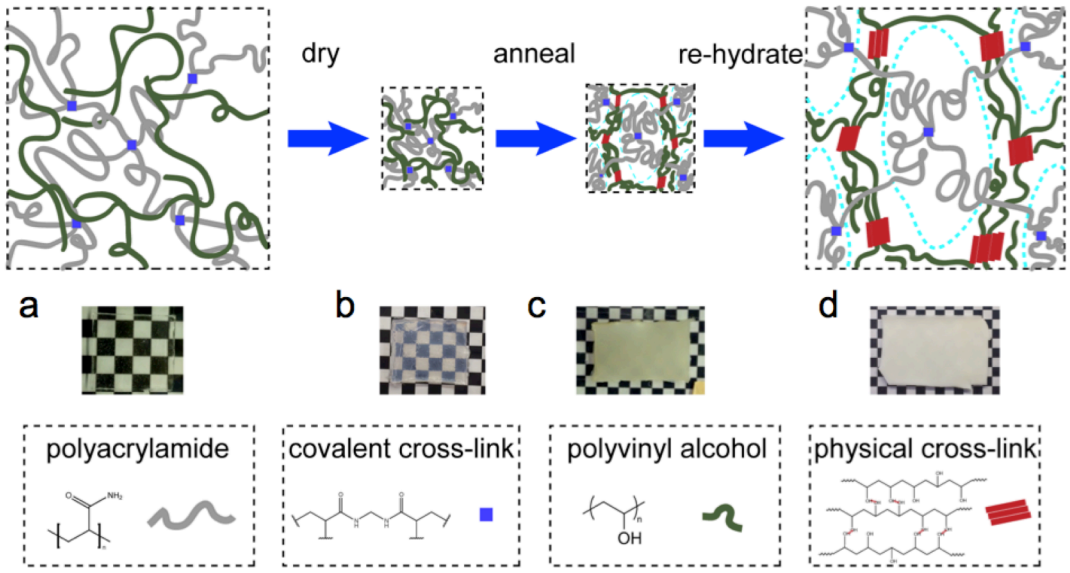

Figure 5.1 Synthesis and structure of the hybrid hydrogel. (**a**) Acrylamide forms a covalently cross-linked network (PAAm, gray lines) with N,N'-methylenebisacrylate (MBAA, blue squares). The gel is dried at room temperature (**b**), and then annealed at elevated temperature (**c**). Phase separation occurs (dashed cyan lines). Polyvinyl alcohol (PVA, green lines) forms a physically cross-linked network with crystallites (red blocks). (**d**) On rehydration in distilled water, the crystallized PVA-PAAm gel forms a hydrogel. Optical photographs of the gels were placed beneath the corresponding schematics.

5.3 Crystallites serving as reversible and yet stable crosslinks

We prepared the hybrid hydrogels in a simple three-step protocol (**Figure 5.1**). First, we form a cross-linked network of PAAm in the presence of PVA chains. Unlike the gel synthesized by Muratoglu et al., the PAAm chains are covalently cross-linked to increase the retraction force of the network and to prevent leakage of the polymer chains.[138]

Second, we dry and anneal the gel at elevated temperature. The drying process removes water and concentrates the PVA in the mixture. The annealing process enhances the mobility of PVA chains and promotes crystallization.[136,137] This step generates a much higher density of PVA crystallites than the freeze-thaw method developed by Peppas.[135] The resulting dry gel is translucent, indicative of phase separation; evidently PAAm and PVA are not mutually soluble.[139] In the final step, we re-hydrate the gel by immersing it in water for a period of time. The gel absorbs water and swells until it reaches equilibrium.

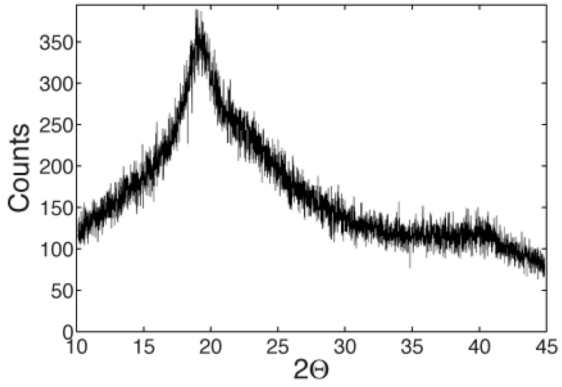

Figure 5.2 X-ray diffraction spectrum of dry PVA-PAAm gel.

X-ray diffraction measurements confirmed the formation of crystallites (**Figure 5.2**). We characterized the dry PVA-PAAm gels with the X-ray diffraction technique. The mass ratio of AAm to PVA in the hybrid gel was fixed at 1:1. The spectrum of the dry gel contains diffraction peaks at the 2Θ angles of 19°, 23° and 41°, indicating the formation of PVA crystallites.

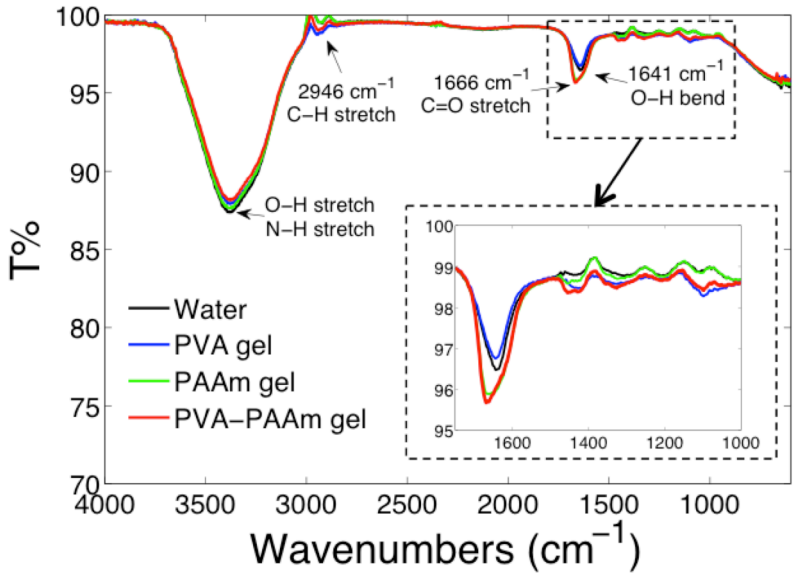

Figure 5.3 Fourier transform infrared spectrum (FTIR) of three gels and water. The inset shows the enlarged spectrum between 1750 cm^{-1} to 1000 cm^{-1}. Attenuated total reflectance (ATR) correction has been applied.

Fourier transform infrared spectroscopy confirmed that the PVA-PAAm hydrogel is essentially a superposition of PVA and PAAm hydrogels (**Figure 5.3**). We measured the Fourier transform infrared spectrum (FTIR) of three gels (PVA, PAAm and PVA-PAAm hybrid gels) with Perkin Elmer FT-IR. The mass ratio of AAm to PVA in the hybrid gel was fixed at 1:1, and its water content was 70.8%. Distilled

water was used as reference. A broad peak around 3390 cm^{-1} refers to stretching of N-H and O-H bonds, 2946 cm^{-1} of C-H stretch, 1666 cm^{-1} of C=O stretch and 1641cm^{-1} of O-H bend. Those peaks below 1400 cm^{-1} are the fingerprint regions related to C-C, C-O and C-N bonds. The spectrum of the hybrid gel is a superposition of those of PAAm and PVA gel, indicating the two polymers have no additional interaction.

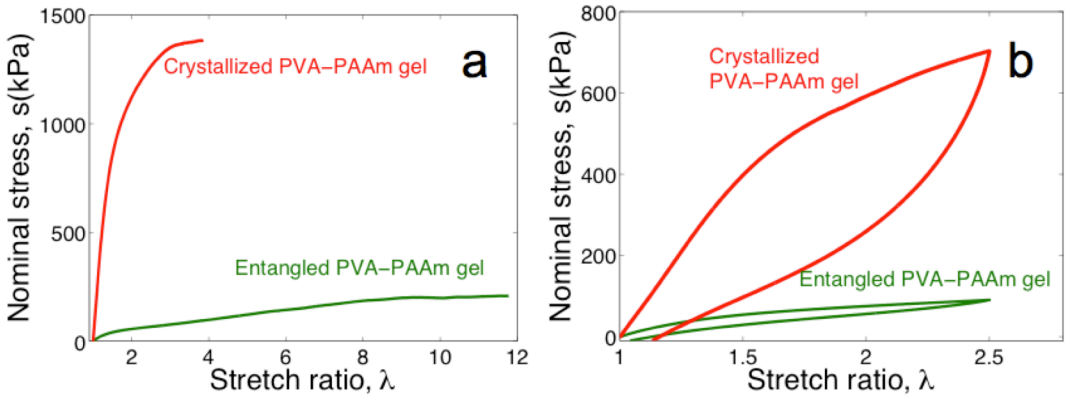

Figure 5.4 Crystallites as physical cross-links. (**a**) Stress-stretch curves of two types of gels. Each sample is stretched to rupture. The nominal stress is the applied force divided by the cross-sectional area of the undeform sample. The stretch ratio is the length of deformed sample divided by the initial length. (**b**) Loading-unloading curves of both gels. Each sample is stretched to a stretch ratio of 2.5.

To evaluate the mechanical behavior of the hybrid gels, we performed tensile experiments on two types of hydrogels: an entangled PVA-PAAm hydrogel and a crystallized PVA-PAAm hydrogel. The former was not subject to the dry-anneal step and the PVA chains in this gel were simply entangled in the cross-linked polyacrylamide network; the latter went through the standard three-step protocol.

Samples of both gels were stretched to rupture (**Figure 5.4a**). The nominal stress is the loading force divided by the cross-sectional area of the undeformed sample. The stretch ratio is the current length divided by the initial length of undeformed sample. The entangled PVA-PAAm hydrogel is compliant and soft. In contrast, the crystallized PVA-PAAm hydrogel is stiff and strong, evidently the result of a high density of physical cross-links. Each sample was stretched to a stretch ratio of 2.5 and then unloaded to its initial length (**Figure 5.4b**).

In the entangled PVA-PAAm hydrogel, the absence of crystallites results in relatively little hysteresis, and the sample behaves more or less elastically. In the crystallized PVA-PAAm hydrogel, on the other hand, the crystallites unzip and dissipate a significant amount of energy. This dissipated energy manifests as significant hysteresis in the stress-stretch curve, indicative of a very tough gel. This behavior is similar to that of pure PVA, for which the evolution of crystallites under deformation has been characterized with small-angle X ray scattering and is well documented in the literature.[140]

The unzipping of crystallites was further confirmed by the anisotropic swelling of gels after uniaxial deformation and the resulting anisotropic microstructure as revealed by confocal microscopy: the crystallites unzip preferentially in the deformation direction, allowing the gel to further expand in this direction on swelling (**Figure 5.5**). The fluorochrome dyes (5-DTAF) link with -OH groups on PVA chains. We excited the dyes with an Argon laser of 488nm band, and recorded images of 520nm band. Evidently, the PVA-rich phases are the bright regions in the images. When the gel is

deformed, crystallites unzip, and the cross-link density decreases. The deformed gel was submersed in distilled water and showed anisotropic swelling in the loading direction. As revealed by confocal microscopy, the microstructure of deformed gels elongates along the stretching direction (**Figure 5.5b**).

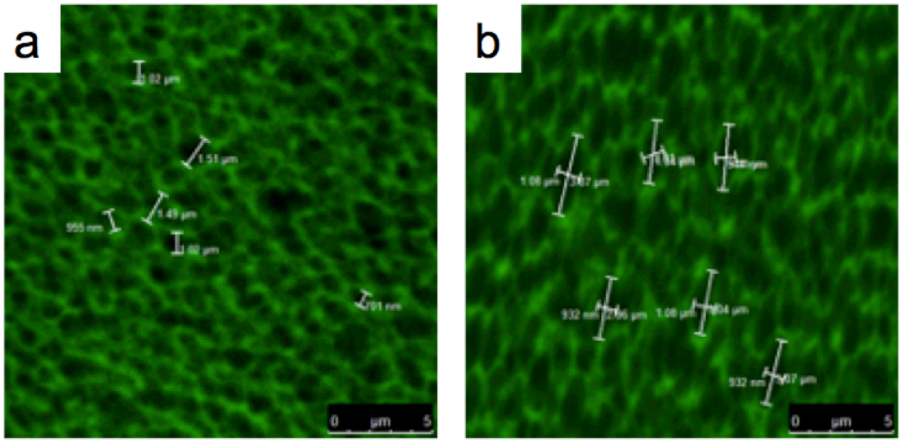

Figure 5.5 Morphology change of deformed gels. (**a**) Undeformed gel. (**b**) deformed gel after stretching. The inset indicates the stretching direction of specimen.

To evaluate the stability of the gels in electrolyte solutions, we performed tensile experiments on the PVA-PAAm gel and an alginate-PAAm, before and after soaking overnight in a saline solution (9 gL^{-1}). The results are shown in **Figure 5.6a**. The alginate-PAAm hydrogel is a tough gel formed by covalently and ionically cross-linked polymers. The electrostatic interactions between alginate chains and calcium ions form ionic cross-links that unzip and dissipate energy under deformation.[24] The sodium ions in the saline solution compete with the calcium ions for the binding sites on the alginate chains, resulting in an unzipping of the ionic cross-links. After soaking, the strength of the alginate-PAAm gel is significantly reduced and the gel has lost its

energy dissipation mechanism – the stress-stretch curve no longer shows any hysteresis.

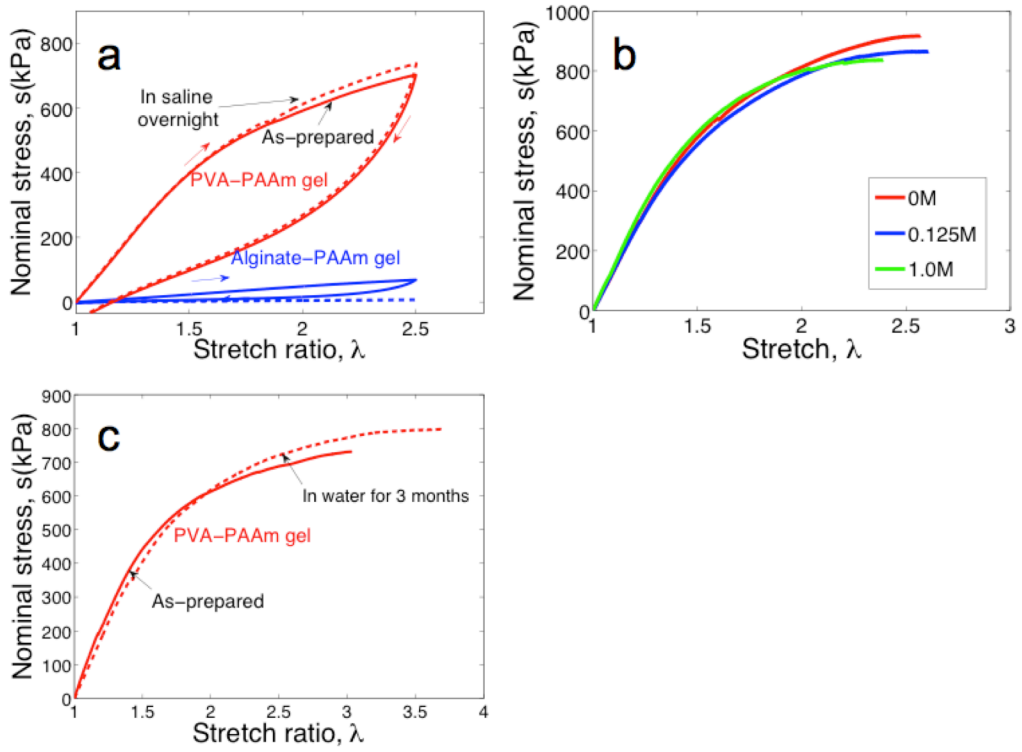

Figure 5.6 Crystallites as stable cross-links. (**a**) Effect of the saline solution. The loading-unloading curve of the gels stored in a saline solution (9 g/L) overnight (dashed line) is compared with that of the as-prepared gels (solid line). (**b**) Stress-stretch curves of the gels that have been soaked in electrolyte solutions containing different $CaCl_2$ concentrations, as labeled. (**c**) Long-term stability of the gels in water. The gels are stored in distilled water for a long period (3 months).

By contrast, soaking in saline has no effect on the stress-stretch curves of the PVA-PAAm gels, even in highly concentrated electrolyte solutions (**Figure 5.6b**). Unlike ionic cross-link, the crystallites in PVA do not rely on electrostatic interaction

and remain intact in electrolytes with a high content of monovalent ions. Furthermore, unlike alginate, the PVA network is not susceptible to hydrolysis: the mechanical properties of the PVA-based gel do not degrade after storing in distilled water for as long as three months (**Figure 5.6c**).

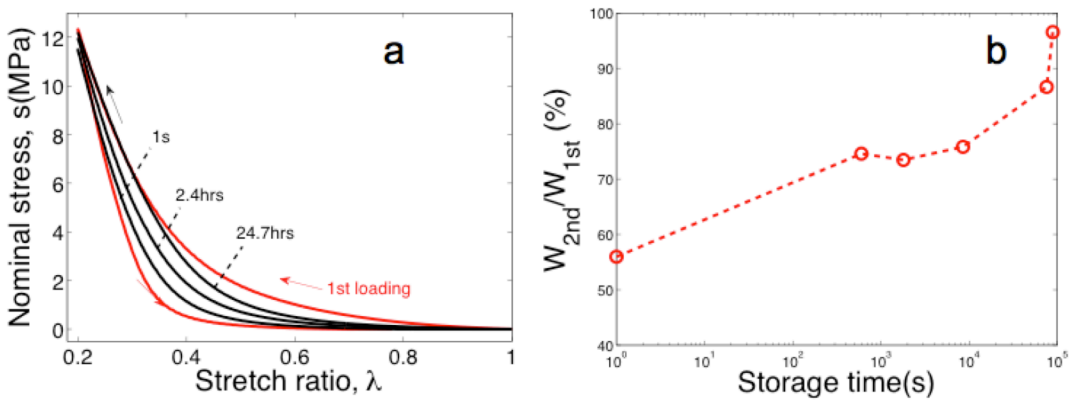

Figure 5.7 Crystallites as recoverable cross-links. (**a**) Recovery of samples stored at room temperature for different durations, as labeled. The samples are compressed to a stretch ratio of 0.2 (compressive strain 80%). (**b**) Recovery ration, i.e., work of the second loading, W_{2nd}, divided by that of the first loading, W_{1st}.

Recovery of the PVA-based gels was investigated by performing compression tests on cylindrical samples with a diameter of 5 mm. Each sample was first compressed to a stretch ratio of 0.2 and then unloaded. The sample was then stored at room temperature for various durations of time and subjected to another compression test (**Figure 5.7a**). We quantify the ability of the crystallites to reform by the recovery ratio, i.e., the work performed during the second compression test normalized by the work performed during the first test. The recovery ratio increases to more than 90% in less than 24 hours (**Figure 5.7b**). The phenomenon is understood as follows. As the

crystallites unzip under deformation, the covalently cross-linked network provides the force to re-store the original shape of the gel. Since PAAm and PVA are incompatible, there is a driving force for phase separation; the PVA chains aggregate and reform the crystallites at room temperature.[141]

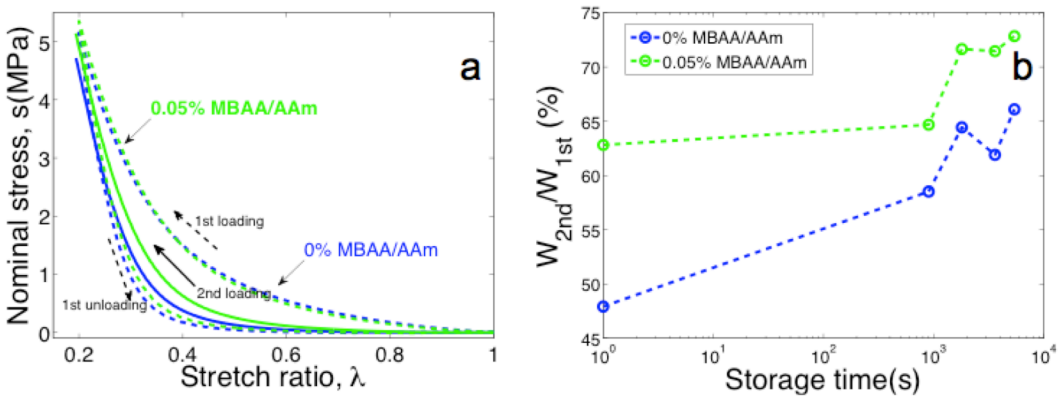

Figure 5.8 The covalent cross-links greatly affect the recovery process. (**a**) First loading-unloading cycle and second intermediate loading of the PVA-PAAm hydrogels with and without covalent cross-links (MBAA). The samples are compressed to a stretch ratio of 0.2 (compressive strain 80%). (**b**) The work of the second loading, W_{2nd}, divided by that of the first loading, W_{1st} as a function of storage duration at room temperature.

This process is relatively slow because of the large molecular weight of the PVA, but the rate of recovery increases with increasing covalent cross-link density (**Figure 5.8**). We prepared hybrid gels with and without covalent cross-links (MBAA/AAm), and performed compression tests with an Instron machine. The samples were in cylinder shape of diameter 12 mm. The loading curves of the first cycle for the two gels overlapped. The immediate 2nd loading tests revealed that the gel with covalent cross-links (0.05% MBAA/AAm) recovered more than the gel without covalent cross-

links (**Figure 5.8a**). The recovery ratio, defined as the ratio of the work of the first loading versus that of the second loading, is plotted against the storage duration of the gel at room temperature (**Figure 5.8b**). The covalent cross-links contribute to a retractive force in the deformed gel, which restore the undeformed shape, and enhance the recovery property.

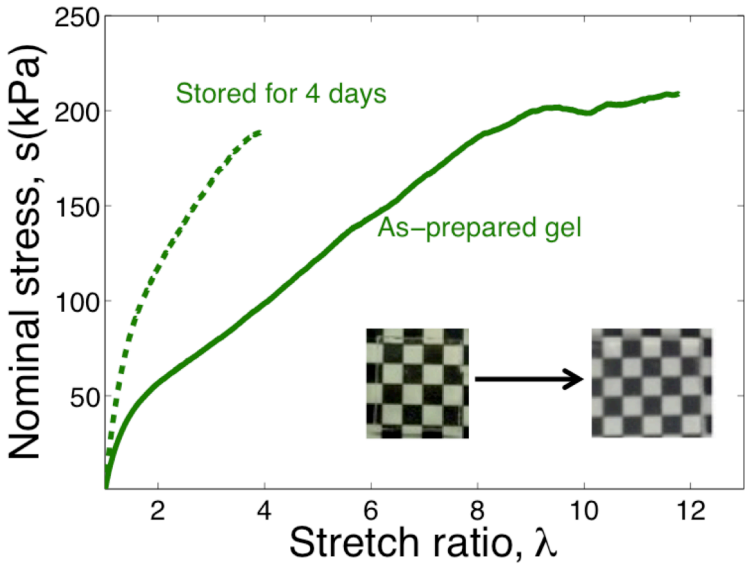

Figure 5.9 Phase separation with time. Stress-stretch curves of the two entangled PVA-PAAm gels. One sample has been stored at room temperature for 4 days. The inset shows the sample becomes opaque after storage at room temperature for 4 days.

A similar phenomenon is also observed in entangled PVA-PAAm hydrogel, which is initially transparent, but slowly turns translucent after storing at room temperature (**Figure 5.9**). We prepared and performed tensile tests on two entangled PVA-PAAm hydrogels. Both samples were stretched to rupture. One sample had been stored at room temperature for 4 days, while the other sample was as prepared. The as-prepared sample was fully transparent, and became opaque with storage time (Inset of

Figure 5.9). Accompanied with the transparency changed, the elastic modulus increased form 132 kPa to 257kPa. The results confirm that the PVA and PAAm are incompatible; two phases separate slowly with time; PVA crystallites are formed at room temperature.

5.4 Hydrogels with high mechanical performance and chemical stability

To evaluate the effect of acrylamide on the properties of the dry-annealed PVA-PAAm gel, we prepared a series of hydrogels with various ratios of acrylamide to (acrylamide plus polyvinyl alcohol) and performed tensile tests. As the acrylamide content increases, both the strength and stiffness of the hydrogel decreases (**Figure 5.10a** and **5.10b**). The fracture energy was measured by performing tensile tests on notched samples using a geometry known as the pure shear test.[24,84] Similar to the other mechanical properties, the fracture energy of the hydrogels decreases with increasing acrylamide content (**Figure 5.10c**). This trend is inversely correlated with the equilibrium water content (**Figure 5.10d**): as the acrylamide content of a gel increases, so does its affinity for water, and the gel absorbs more water.[41] In the limit of no acrylamide, the gel has very good mechanical properties, but its water content is low. At 25% acrylamide, the hydrogel has a relatively high water content of 62%, while maintaining a good combination of mechanical properties: an elastic modulus of 5 MPa, a strength of 2.5 MPa and a fracture energy of 14,000 Jm^{-2}.

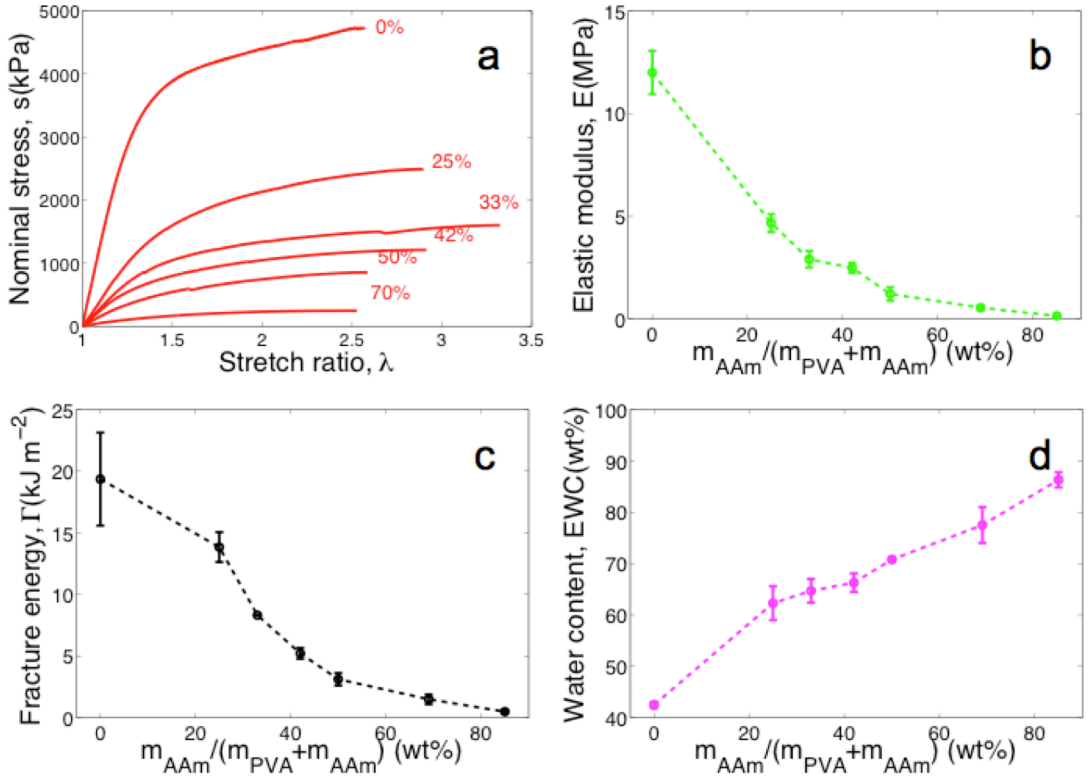

Figure 5.10 Composition greatly affects the properties of the hybrid gel. (**a**) Stress-stretch curves of hybrid gels of various weight percentages of acrylamide to (acrylamide plus polyvinyl alcohol), as labeled. (**b**) Elastic modulus, *E*, derived from the initial slope of the stress-stretch curves. (**c**) Fracture energy, Γ, as a function of the acrylamide content. (**d**) Water contents of the gels fully swollen in distilled water, *EWC*, plotted against the acrylamide content.

The mechanical behavior of these hybrid gels is well described by the rule of mixtures applied to the PVA and PAAm phases. We used the rule of mixtures to fit the data. The results show that the elastic modulus and fracture energy can be expressed as a series additon of the PVA and PAAm networks (**Figure 5.11**).

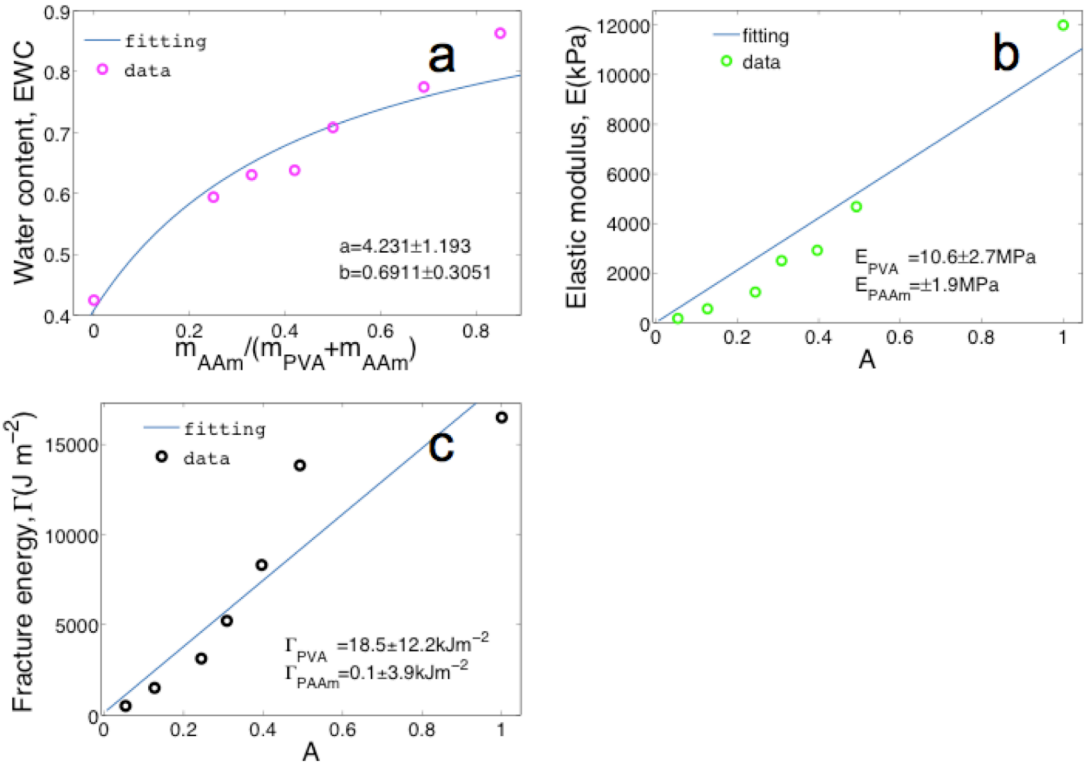

Figure 5.11 The properties of the hybrid gel follow the rule of mixtures. (**a**) Stress-stretch curves of gels of various weight percentages of acrylamide to (acrylamide plus polyvinyl alcohol), as labeled. (**b**) Fitting of equilibrium water content and the acrylamide content. (**c,d**) Elastic modulus and fracture energy were fitted with respect to the weight ratio of PVA-rich phase to the whole gel, *A*.

The PVA-rich and PAAm-rich phases are assumed to have constant contents of water. The equilibrum water content of the whole gel can be expressed as

$$EWC = 1 - \frac{1}{1 + ax + b(1-x)},$$

where x refers to the ratio of AAm to (AAm plus PVA), a and b refer to the weight ratio of water to polymer in the PAAm-rich and PVA-rich phases, respectively. This

equation fits the *EWC* data well (**Figure 5.11a**), indicating that the PAAm-rich phase contains ~81wt% water and the PVA-rich phase contains ~41 wt% water.

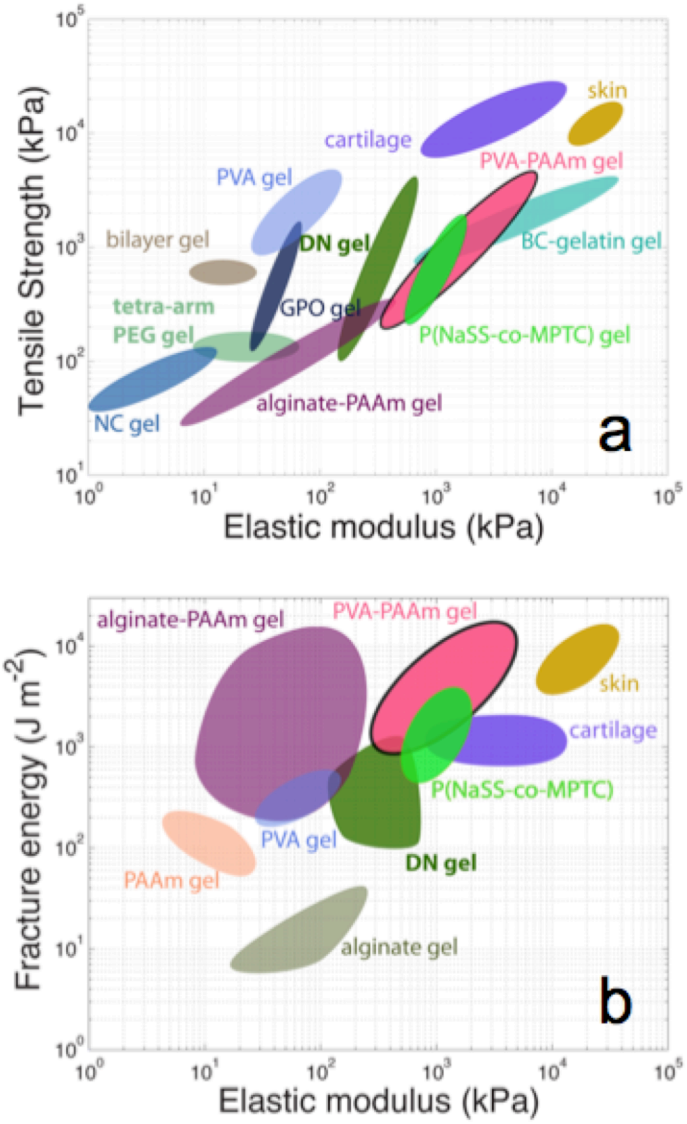

Figure 5.12 Material property charts for various soft materials. (**a**) Tensile strength versus elastic modulus. (**b**) Fracture energy versus elastic modulus.

Then we applied the rule of mixtures (**Figure 5.11c** and **5.11d**). With known water contents in the two phases, the weigth ratio of the PVA-rich phase to the whole

gel, designated as A, can be caculated. By assuming the PVA-rich and PAAm-rich phases have a similar density (1.0 gcm^{-3}), the rule of mixtures indicates

$$E = AE_{PVA} + (1-A)E_{PAAm},$$

$$\Gamma = A\Gamma_{PVA} + (1-A)\Gamma_{PAAm},$$

where the subscripts PVA and PAAm refer to the PVA-rich phase and PAAm-rich phase, respectively.

In **Figure 5.12**, we present two Ashby charts for a variety of soft materials. Materials include the gel prepared in this work (PVA-PAAm), polyvinyl alcohol gel (PVA),[124] double network gel (DN),[103] alginate-polyacrylamide gel,[24] sodium p-styrenesulphonate-co-3-(methaacryloylamino)propyl- trimethylammonium gel (NaSS-co-MPTC),[98] polyacrylamide gel (PAAm),[24] alginate gel,[24] nano-composite gel (NC),[128] tetra-arm polyethylene glycol gel (tetra-arm PEG),[130] hydrophobic bilayer gel,[97] graphene peroxide gel (GPO),[142] bacterial cellulose-gelatin gel (BC-gelatin) along with cartilage and skin.[126,127] In terms of strength and stiffness, PVA-PAAm hydrogels outperform most hydrogels, including alginate-polyacrylamide hydrogels and polyampholyte hydrogels (**Figure 5.12a**). Traditional PVA hydrogels prepared using freeze/thaw cycles are strong, but compliant and brittle with a toughness of only 500 Jm^{-2}.[124] Bacterial cellulose-gelatin hydrogels have high strength, but are brittle and rupture at small strains.[126] With respect to stiffness and fracture energy, PVA-PAAm hydrogels do better than all other hydrogels (**Figure 5.12b**). Considering that these gels contain 60-80% water, achieving such high strength and fracture resistance is quite remarkable.

5.5 Summary

Our results suggest that hydrogels with excellent mechanical performance and chemical stability can be prepared by combining hydrophilic and crystalline polymers. With appropriate processing, the crystalline polymer can form a high density of crystallites that serve as cross-links resulting in high stiffness, strength, and toughness; the network formed by the hydrophilic polymer maintains the shape of the hydrogel, provides a strong driving force to reform crystallites, and increases the equilibrium water content. The hydrogels remain stable in physiological solutions. This strategy has a large pool of material candidates. Beside polyvinyl alcohol, a variety of crystalline polymers can be used, including polyurethane,[143] polylactic acid, and polyethylene glycol.[144] The combination of high stiffness, high strength, fracture resistance and recoverability along with chemical stability, biocompatibility, facile synthesis, and low cost make these materials ideal candidates for many applications.

Chapter 6 Toughening hydrogels with strain-induced crystallization

6.1 Introduction

Great progress has been made in the field of tough hydrogels.[22-25,103] Their applications range from biomedical applications like cartilage replacement[145] to engineering applications such as soft robotics[106,107] and artificial muscles.[13] Conventional hydrogels are brittle, vulnerable to crack.[22] To improve the crack resistance, hydrogels need energy dissipating mechanisms. A widely used strategy for energy dissipation is breaking sacrificial bonds. Since the invention of double network gels, various kinds of sacrificial bonds have been explored, including covalent cross-links,[23] ionic cross-links,[24,98,134] hydrophobic association,[97] hydrogen bonds and crystallites.[96] Despite of those successes, this strategy has limitations. Complex and slow dynamics of polymer chains limit the recovery process.[24] An inevitable interdependence between mechanical properties limits the accessible properties.[134] In addition, this mechanism often leads to isotropic hydrogels,[23,24] while many structural applications require anisotropic structure. Vascular tissues, for instance, have higher stiffness in the circumferential direction than that in the axial direction.[146] Cartilage possesses a multi-layer anisotropic structure where collagen fibers align in different directions.[104] A new strategy is highly desirable for designing both toughness and anisotropy of hydrogels.

Here, we report a new mechanism of strain-induced crystallization for hydrogels. We report a strain-induced crystallizing hydrogel, forming with covalently crosslinked polyacrylamide (PAAm) and polyvinyl alcohol (PVA). We will show the PVA chains, entangled in the PAAm network, can re-orient and crystallize under stretching. Much like crystallizing rubber, the hybrid hydrogel show the dependence of the breaking stress on the crack size. This transition is attributed to alignment of PVA chain segments in a crystalline pattern under the orienting effect of the stretching. We will demonstrate the mechanism of strain-induced crystallization toughens the hydrogel effectively, leading to high fracture energy. Additionally, this mechanism leads to highly anisotropic hydrogels that exhibit shape-memory property and crack-deflection behavior. The new strategy holds promises for developing anisotropic tough hydrogels.

6.2 Strain-induced crystallization

Strain-induced crystallization is the main toughening mechanism of natural and synthetic elastomers.[147] As a toughening mechanism, the SIC has advantages over breaking sacrificial bonds. Firstly, the SIC process dissipates a significant amount of energy, and generates oriented crystallites, leading to high resistance to crack growth.[147-149] The fracture energy of natural and synthetic elastomers is on the order of 10^4 Jm^{-2}.[149] Secondly, this mechanism mainly occurs at large strains, such that a critical stretch ratio of 4.0 in case of natural rubber.[150] This attribute decouples the toughening effect from the cross-link density, and thus breaks the interdependence between stiffness and toughness. This decoupling enriches the accessible combinations of mechanical properties. Thirdly,

the SIC leads to a highly anisotropic structure at the crack tip. The anisotropy causes the crack growth to stop and even kink, which improves the crack growth resistance of materials.[150,151] Last, crystallization and melting of crystallites can be very fast. By elevating the temperature, the crystallites can be melted, and the material restores its initial state, resulting in a shape-memory behavior. Unlike breaking sacrificial bonds, the recovery process involves complex dynamics of polymer chains and crosslinkers. Those attributes inspire us to realize strain-induced crystallization in hydrogels, and explore its consequences.

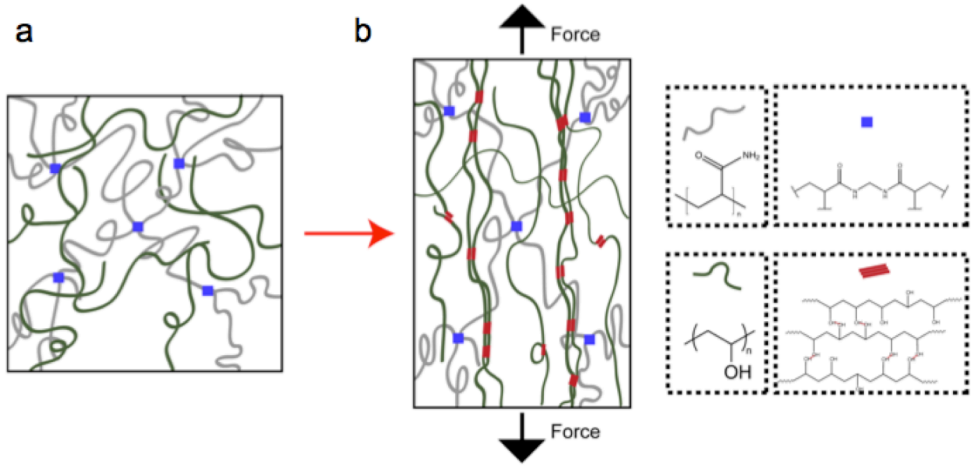

Figure 6.1 Schematic of entangled PVA-PAAm hydrogels. (**a**) PVA chains entangle in the cross-linked network of PAAm (grey lines). MBAA serves as covalent cross-links (blue squares). (**b**) When a force is applied, the hybrid network deforms, PVA chains reorient and form crystallites (red blocks).

Inspired by crystallizing rubber, we hypothesize that a strain-induced crystallizing hydrogel can be made by mixing crystalline polymer chains in a crosslinked polymer network. When a force is applied, the covalently crosslinked polymer network deform

affinely, which re-orients the crystalline polymer chains due to physical entanglements; the reoriented crystalline polymers get aligned, and form crystallites. Here we prepared such a hydrogel by polymerizing acrylamide monomers in the presence of polyvinyl alcohol polymer chains (**Figure 6.1**). A PVA chain carries an abundance of -OH groups, has high symmetry of configuration, and is highly flexible and capable of forming crystallites.[152] It has well documented that the dry PVA film is capable of strain-induced crystallization.[140,146]

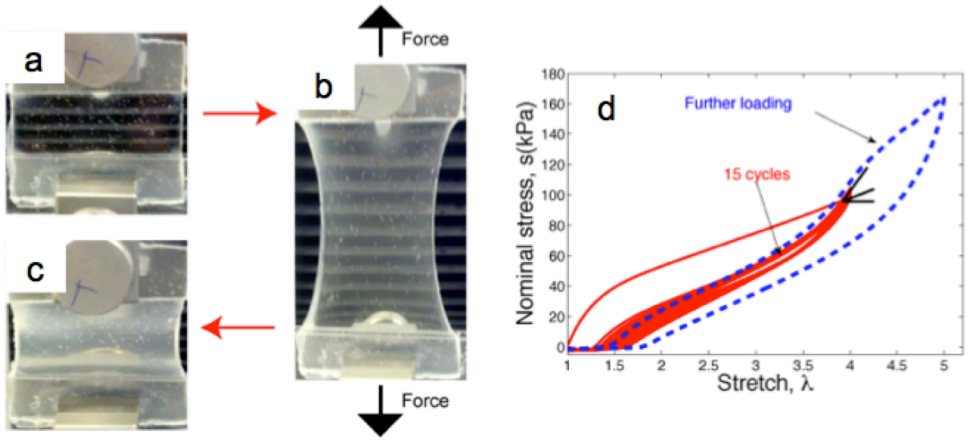

Figure 6.2 Strain-induced crystallization. The gel is transparent **(a)** before stretching, and becomes translucent **(b)** during and **(c)** after stretching. **(d)** Stress-stretch curves of the first 15 cycles (red solid line, maximum stretch ratio 4) and the 16th cycle (blue dashed line, maximum stretch ratio 5).

Experimental results confirm this hypothesis. We have prepared such a hybrid hydrogel, and performed cyclic loading tests. The original specimen was transparent, indicating no phase separation (**Figure 6.2a**). When the specimen was subject to cyclic loading of a maximum stretch 4 for 15 cycles, it became translucent (**Figure 6.2b** and **6.2c**). The nominal stress is the loading force divided by the cross-sectional area of the

undeformed sample, and the stretch is the current length relative to the initial length of the undeformed sample. The stress-stretch curves showed that the cyclic loading resulted in a large residue strain of ~50% (**Figure 6.2d**). The specimen was then stretched to a maximum stretch 5 in the 16th loading. During the last loading, the tangent modulus at stretch 4 was larger than that of the first loading.

The phenomena can be understood as follows. The hybrid gel contains the PVA chains entangled inside the PAAm network. When the gel is stretched, the PVA chains are deformed from their most probable configurations, most of them being elongated along the stretching direction. The configurational entropies of these chains consequently decrease, thus less entropy remains to be sacrificed in passing to the crystalline state, where the entropy can be taken as zero.[147] When $T\Delta S < \Delta H$, crystallization will occur and the gel will lose the transparency. The crystallites can serve as cross-linking points in a network, and fix the configuration of deformed network, resulting in the residue strain and the stiffening effect. The crystallization of PVA under deformation has been reported on dry PVA film and PVA nanofiber, and studied with characterization techniques like small-angle X-ray scattering.[140,153]

Next, we preformed mechanical tests to show the hybrid gel resembles natural rubbers that exhibit a characteristic dependence of the strength on the crack size. One consequence of strain-induced crystallization is an abrupt change of the strength on the crack size, due to a transition of failure mechanism from catastrophic failure to unstable crack growth. It has been extensively studied and well established in literature.[149,154] We hypothesize that if the hydrogel is capable of strain-induced crystallization, it might show

the same effect in analogy to natural rubber. To prove the hypothesis, we prepared strip test specimens (25 x 22 x 3 mm^3) of various sizes of edge cracks, and stretched them uniaxially to rupture.

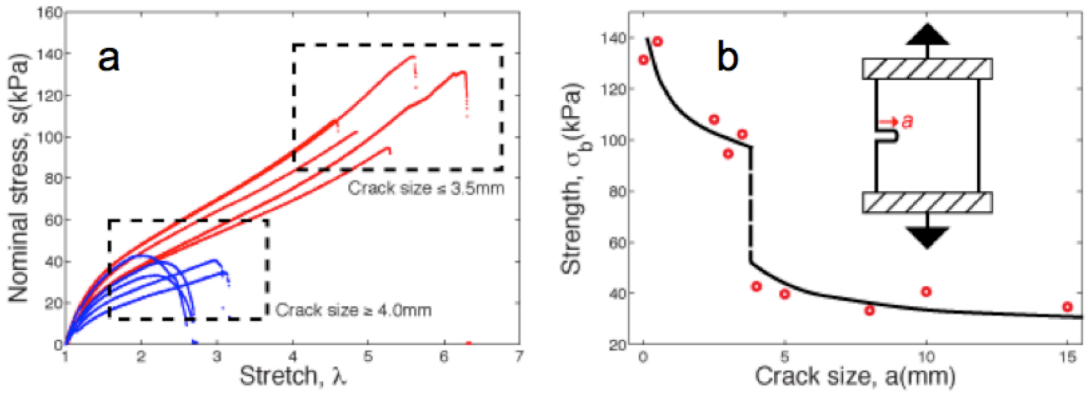

Figure 6.3 Dependence of the breaking stress with the crack size **(a)** Stress-stretch curves of gels of varied sizes of edge cracks. **(b)** Tensile strength of hybrid gel plotted versus the size of edge crack.

The stress-strain curves divide into two groups depending on the crack size (**Figure 6.3a**). The specimens of small crack size (a < 3.5mm) sustained large stretches of 5, and large stress of ~100kPa before rupture. In contrast, the specimens of larger crack ruptured at smaller strains and stresses. The breaking stress was plotted versus the crack size in **Figure 6.3b**. The strength decreases continuously with increasing crack size; but an abrupt drop of the breaking stress occurs at a critical crack size ($3.5mm < a_c < 4mm$). This transition was attributed to the change of failure mechanisms: when $c<c_{cr}$, the specimen sustains large strains and crystallization takes place in the bulk of the sample; while the crack is sufficiently large $c>c_{cr}$, severe stress concentration exists at the crack tip, the specimen ruptures at small strains, remaining non-crystalline, and thus the breaking stress drops sharply. The dependence of the breaking stress with the

crack size is analogous to that of the strength with the temperature.[154] Crystallization is prohibited when the temperature increases beyond a critical temperature. Evidently, this result resembles the behavior of strain-induced crystallizing elastomers like natural rubber.[149,154]

6.3 Toughening effects

Strain-induced crystallization has two-fold effects of toughening. First, the SIC process dissipates significant amount of energy, and thus raises the critical energy release rate for crack propagation. Second, this process can *in-situ* strengthen the gel with an anisotropic structure: the crystallites form preferentially along the loading direction, and thus halt crack growth in the plane perpendicular to the loading direction. Experiments showed the crack kinked 90 degree off the loading direction.

The SIC process can toughen the hydrogels effectively, and the toughening effect sensitively depends on the ratio of PVA versus AAm. We prepared the hybrid hydrogels containing fixed content of polymers (38wt%), and varied mass fractions of PVA to PVA plus AAm. **Figure 6.4a** illustrates the stress-strain curves for unnotched specimens. Each specimen was stretched to rupture. The elastic modulus was calculated from the initial portion of the stress-strain curves ($\lambda < 1.2$). **Figure 6.4b** shows a weak correlation between the elastic modulus and the mass fraction of PVA. This result indicates that both covalent crosslinks of PAAm and physical entanglements due to PVA chains contribute to the elastic modulus of the hybrid hydrogel. Pure shear tests were performed to measure the fracture energy of the hydrogels.[24,93] A notched specimen containing an edge crack

was gradually pulled to a critical stretch λ_c, when the crack starts to propagate. The critical stretch reached a maximum at 30wt% PVA (**Figure 6.4c**). A similar trend was observed for the measured fracture energy (**Figure 6.4d**).

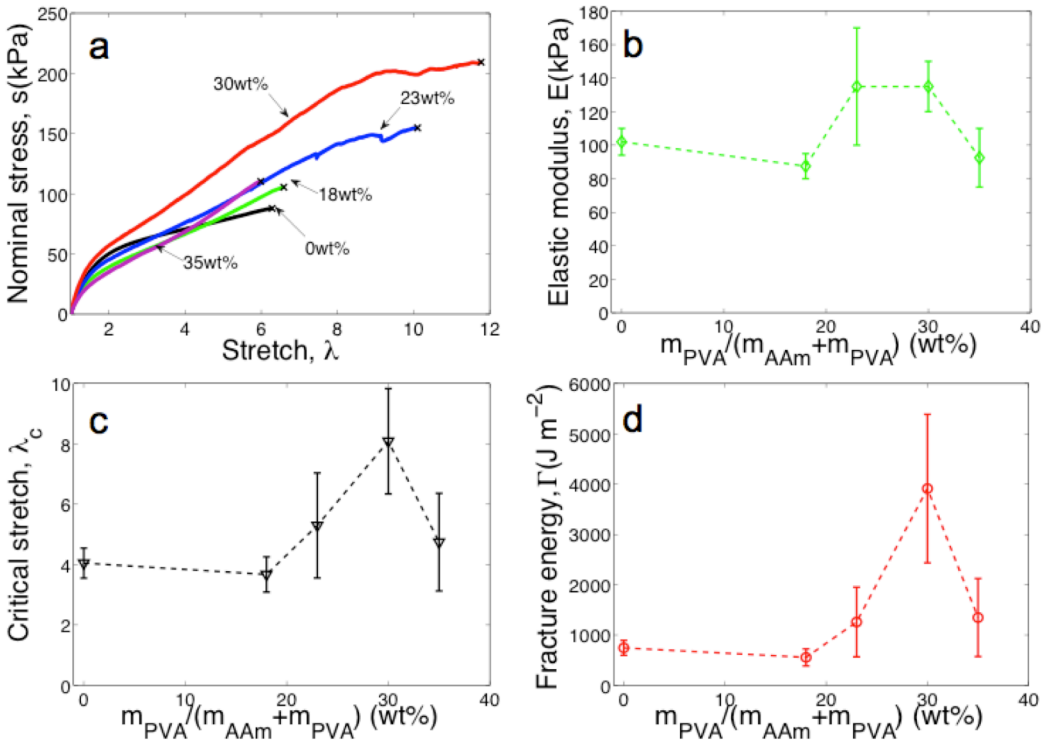

Figure 6.4 Composition affects mechanical behavior of the hybrid hydrogels. (**a**) Stress-stretch curves of gels of various ratios of m_{PVA} to (m_{PVA} plus m_{AAm}), as labelled. Unnotched specimens were stretched to rupture. (**b**) Elastic moduli, determined by the slope of initial portions of stress-stretch curves, plotted versus the mass fractions of PVA. (**c**) Critical stretches, measured by pulling notched specimens to rupture, plotted against the mass fraction. (**d**) Fracture energy, measured by the pure shear test, plotted versus the mass fraction.

The trend can be understood as follows. At the limit of high AAm content, the hybrid hydrogel is non-crystallizing, and thus the fracture energy is close to that of polyacrylamide.[24] At the other limit of low AAm content, the hybrid hydrogel lacks the

cross-linked PAAm network to re-orient PVA chains, and thus loses the effect of strain-induced crystallization. At intermediate content of PVA, a synergic effect of re-orientation and crystallization leads to an effective energy dissipation, as evident by a large fracture energy. We conclude that both polymers are essential for strain-induced crystallization: covalent crosslinked network contributes to re-orientation of polymer chains, and crystalline polymers contribute to crystallization and energy dissipation.

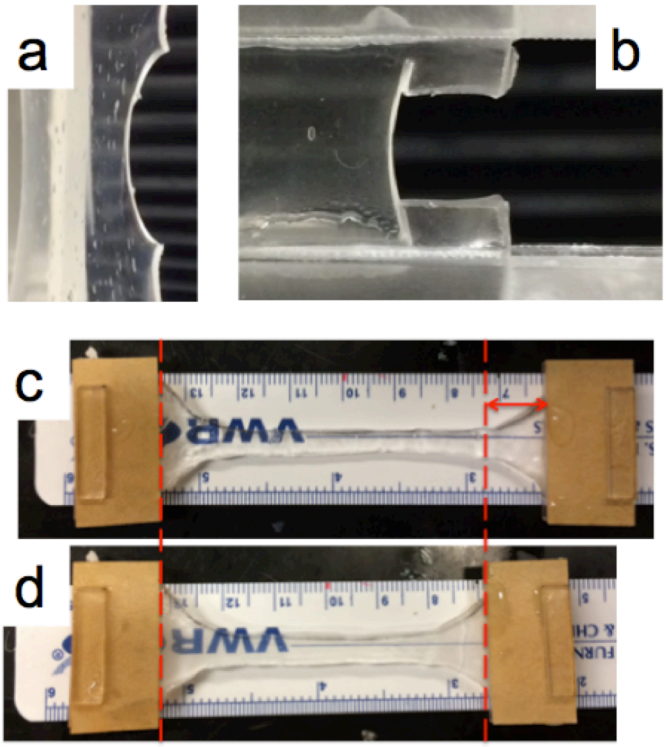

Figure 6.5 Anisotropic structure of the hybrid hydrogel leads to crack deflection and shape-memory behaviors. A specimen that has been pre-stretched contains an edge crack, and was subjected to a second run of cyclic loading. (**a**) The crack propagates in perpendicular to the loading direction. (**b**) The crack path after force is released. (**c**) A specimen which has been pre-stretched show a residue strain ~20%. (**d**) The specimen was heated, and restored the original shape, indicative of shape-memory behavior.

Next, we show that anisotropic structures created by the SIC enable unusual characteristics: crack kinking and shape memory behaviors. Although there exist many methods of making anisotropic hydrogels, most of them set the structure during synthesis.[155,156] For instance, J. P. Gong and coworkers applied shear stresses before polymerization, to align hydrophobic lamellar bilayers for anisotropic hydrogels.[156] Our hydrogels are capable of post-synthesis design. We first pre-stretched a specimen, and then unloaded, introduced an edge crack in the middle of the specimen. When subjected to a second loading, the specimen showed a unique behavior that the crack propagated along with the direction parallel to the loading direction (**Figure 6.5a**). After releasing the stress, the crack path clearly kink 90 degree along with the loading direction (**Figure 6.5b**). This phenomenon has been well studied in interfaces between two dissimilar materials.[157] In contrast, a notched specimen without pre-stretching failed by a running crack through the specimen.

Another outcome of the SIC process is shape-memory behavior. We prepared a specimen of dumbbell shape, and then stretched it to a maximum stretch 3. The resulting hydrogel showed a large residue strain ~24% (**Figure 6.5c**), which is attribute to the newborn crystallites fixing the deformed state of the hybrid hydrogel. The crystallites melt at elevated temperature. We treated the deformed specimen with a hot water of 95^{o}C. The specimen restored its initial shape very quickly (**Figure 6.5d**). The results demonstrate the strain-induced crystallizing hydrogel is capable of shape memory behavior. This attribute is independent of solvent diffusion, and thus enables fast actuation. In addition, it avoids the common process of pre-heating and subsequent

quenching to set the strain and restore the shape. For instance, a crystallizing rubber Morthane, containing carbon nanotubes, realizes remote control and large actuation force.[158]

6.4 Summary

In summary, we reported a new mechanism of strain-induced crystallization to toughen hydrogels. Crystalline polymer chains entangle inside a covalently crosslinked polymer network, forming a strain-induced crystallizing hydrogel. This design is to utilize the polymer network to impose deformation on the entangled crystalline polymers, and enable them to align, and crystallize. We demonstrated that such a hybrid hydrogel by mixing polyvinyl alcohol in a polyacrylamide hydrogel.

The family of strain-induced crystallizing hydrogels may be enlarged by selecting monomers and polymers with different structures. Many other polymers such as polyethylene oxide and poly(L-lactic acid) have the capacity to crystallize, and might be utilized into hybrid materials for improving mechanical properties. For instance, bio-nanocomposite fibers composed of polyethylene oxide exhibited strain-induced crystallization and high elongation.[144] The diversity of crosslinked networks and crystalline polymers creates a large pool of candidates for realizing this toughening mechanism of strain-induced crystallization

We showed that deformation sensitively affects mechanical properties and transparency of the hydrogel, and that the fracture behavior depends on the crack size. We further showed that the strain-induced crystallization toughens the hybrid effectively:

introducing energy dissipation, and creating anisotropic structure at crack tip. The new strategy holds promises for developing hydrogels with high mechanical performance and anisotropic structure.

Chapter 7 Adhesion between highly stretchable materials

7.1 Introduction

Adhesion is ubiquitous and important in many fields. In the field of biomedical engineering, intensive attention has been paid to develop adhesive materials for tissue adhesion and repair.[159-162] In the nascent field of soft robotics, the poor adhesion between different components limits the fabrication and performance of devices such as pneumatically-driven soft hands[163] and epidermal electronics.[10,164]

A class of ionic devices has been developed recently, which hold great promise for many applications, including transparent loudspeaker, active-noise-cancellation windows and transducers.[13] Those devices comprise of dielectric elastomers sandwiched by layers of salt-containing hydrogels. To maintain the physical integrity under deformation, the adhesion between dielectric elastomers and hydrogels is critical. Although both hydrogels and elastomers can sustain large strains, their laminate may fail due to interfacial debonding during operation. This chapter is to resolve two fundament and technical problems: how to characterize the adhesion between highly stretchable materials, and how to improve the adhesion.

To characterize the adhesion between highly stretchable materials, precise measurement technique is needed. Much attention has long focused on adhesion of metals, plastics and elastomers. The peel test and the lap shear test have been developed to study this phenomenon. The peel test has been applied to characterize the adhesion between hydrogels, and between medical tapes and skin.[165,166] However, these methods

have limitations. For the peel test, a considerable portion of the peel energy is dissipated through bending rather than through crack propagation.[167,168] The lap shear test typically reports the adhesive strength, e.g. the debonding force divided by the contact area; this quantity actually depends on the specimen geometry.[160,161,169] To this end, a more adequate parameter is the interfacial toughness, which only depends on the surface properties of materials.[170] Therefore, a method to measure the interfacial toughness between highly stretchable materials is desirable.

Strategies to improve the adhesion between highly stretchable materials need to be explored. There are various approaches to enhance interfacial interactions, including stimulus of electric field, double-network design of the interface, and addition of an electrolytic polymer liquid.[166,171,172] However, these methods are limited to specific material systems that can't be applied directly to hydrogel-elastomer laminates. A possible solution is to harness nanoparticles to form physical bonds at interface. Nanoparticles have been used as adhesives for gels.[173] This approach is analogous to the strategy of using nanoclays or nanoparticles to improve the toughness of hydrogels.[174,175] The method relies on the interaction between nanoparticles and polymer chains, which can be hydrogen bonding or ionic adsorption.[174,176] Thus, it may be applicable to the interface between hydrogels and elastomers.

In this chapter, we develop a method to characterize adhesion between highly stretchable materials, and apply it to determine the interfacial toughness of hydrogel-elastomer laminates. We show that the critical stretch decreases dramatically with increasing thickness of the hydrogel film, while the measured interfacial toughness keeps

constant. The interfacial toughness between VHB 4910 and PAAm hydrogel is $0.5Jm^{-2}$, due to the weak Van der Waal's interaction. Additionally, the interfacial toughness is independent of the crosslink density of the PAAm hydrogel. We further increase the interfacial toughness between VHB 4910 and PAAm hydrogel sevenfold, by adding silica nanoparticles at the interface. The adhesion between VHB 4910 and commonly used hydrogels with or without nanoparticle solution is also tested.

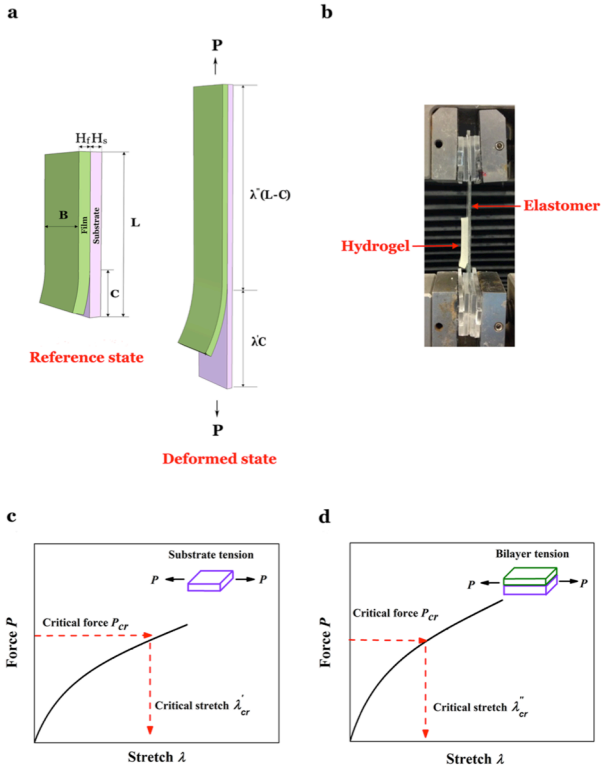

Figure 7.1 Interfacial toughness measurement. (**a**) The specimen in the reference state and the deformed state. (**b**) A laminate consisting of hydrogel film and elastomer substrate. (**c**) Stress-stretch relation of the substrate. The critical force P_{cr} when the crack starts to propagate is used to map the critical stretch λ'_{cr} for the detached substrate. (**d**) Stress-stretch relation of the attached laminate, used to determine critical stretch λ''_{cr} of the bilayer.

7.2 Analytical model for measuring interfacial toughness

The building block of ionic devices is a laminate of hydrogels and elastomers (**Figure 7.1a**). A piece of salt-containing hydrogel is attached on a layer of dielectric elastomer like VHB for ion conductance.[13,17] To simulate the working condition of ionic devices, we design a specimen in configuration of bilayer laminates (**Figure 7.1b**).

First we measure the stress-stretch relations of the film and the substrate separately. When a uniaxial force pulls the film, the nominal stress S_f in the film relates to the stretch λ through a curve $S_f(\lambda)$, and the area under this curve $W_f(\lambda)$ relates the nominal density of the free energy of the film to the stretch. Similarly, when a uniaxial force pulls the substrate, the nominal stress S_s in the substrate relates to the stretch λ through a curve $S_s(\lambda)$, and the area under this curve is the nominal density of the free energy in the film as a function of the stretch, $W_s(\lambda)$.

In the reference state, the laminate is undeformed: the thickness of the film is H_f, the thickness of the substrate is H_s, and the width of the film and substrate is B. In the deformed state, a force P pulls the substrate. Far behind the tip of the crack, the film is stress-free, and the substrate is in a state of uniaxial stress, with the stretch λ' determined by

$$BH_s S_s(\lambda') = P. \tag{7.1}$$

Far ahead the tip of the crack, the film and substrate are attached, and both have the same stretch λ'', determined by

$$BH_f S_f(\lambda'') + BH_s S_s(\lambda'') = P. \tag{7.2}$$

Now compare two specimens. Both specimens have the total length L in the reference state. One specimen has a crack of length C in the undeformed state, and potential energy in the deformed state. The potential energy equals to the strain energy minus the work done by external force. Therefore, the potential energy of the detached substrate is $C[BH_s W_s(\lambda') - P\lambda']$, and that of the bonded bilayer is $(L-C)[BH_f W_f(\lambda'') + BH_s W_s(\lambda'') - P\lambda'']$. The energy release rate is the reduction in the potential energy associated with unit increase of the crack area, giving that

$$G = H_f W_f(\lambda'') + H_s W_s(\lambda'') - H_s W_s(\lambda') + \frac{P}{B}(\lambda' - \lambda''). \tag{7.3}$$

In writing the potential energy, we have assumed that the detached substrate is in a homogeneous state of stretch λ', and the attached laminate is in a homogeneous state of λ''. In the region around the tip of the crack, however, the field is inhomogeneous. Because the crack is in a steady state, the inhomogeneous field in this region is identical in the two specimens. Consequently, this inhomogeneous field does not affect the calculation of the energy release rate.

In a limiting case that the substrate is much stiffer than the film, the attached film does not constrain the substrate, so that the stretch in the detached substrate is nearly the same as the stretch in the attached laminate, $\lambda' \approx \lambda''$. In this limiting case, the energy release rate reduces to

$$G = H_f W_f(\lambda'). \tag{7.4}$$

In another limiting case that the substrate is much softer than the film, the attached laminate does not deform, $\lambda'' = 1$, so that the energy release rate is entirely due to the detached substrate:

$$G = H_s\left[S_s(\lambda')\lambda' - W_s(\lambda')\right]. \tag{7.5}$$

These relations together relate the energy release rate to the applied force P. As the applied force increases to a critical value P_{cr}, the crack propagates in a steady state, and the energy release rate reaches the interfacial toughness. The critical applied force P_{cr} determines the critical stretches $\lambda_{cr}^{'}$ and $\lambda_{cr}^{''}$ in the detached substrate and the attached laminate by Equations 7.1 and 7.2, respectively (**Figure 7.1c** and **7.1d**). With known P_{cr}, $\lambda_{cr}^{'}$ and $\lambda_{cr}^{''}$, the interfacial toughness can be calculated by Equation 7.3.

7.3 Characterization of adhesion between hydrogels and elastomers

To determine the stress-stretch relations of the substrate and film, we performed uniaxial tensile tests on VHB 4910 and PAAm hydrogels, respectively. The crosslink density of the PAAm hydrogels was varied by controlling the input of cross-linker, MBAA; the mass ratio of the cross-linker to monomer is designated as N. Both VHB 4910 and PAAm hydrogels are highly stretchable (**Figure 7.2**). The nominal stress is the applied force divided by the cross-sectional area of undeformed sample. The stretch is the ratio of the length of deformed sample to that of undeformed sample. The stress-stretch relations of hydrogels strongly depend on the input of crosslinker (**Figure 7.2b**): the

slope of the initial portion of the stress-strain curves, e.g. the elastic modulus, increases with the input of crosslinker.

To verify the measured interfacial toughness is a material constant, we varied the thickness of hydrogel film, and performed the interfacial fracture tests. The interfacial toughness was determined by the experimental procedure as described above. **Figure 7.2c** illustrates the force-stretch relations of the bilayer laminates. The critical stretch decreases dramatically from H_f=*0.1mm* to H_f=*0.6mm*, and becomes indistinguishable for thick hydrogel films. The measured interfacial toughness is independent of the thickness of the hydrogel film (**Figure 7.2d**). It concludes that the interfacial toughness is indeed a material constant that depends only on the surface properties of the interface. Therefore, the interfacial toughness is an appropriate parameter to characterize the adhesive property of materials. The measured interfacial toughness is around 0.5 Jm^{-2}, indicative of a weak adhesion between PAAm hydrogel and VHB 4910. The low value reflects the fact that only weak Van der Waals' forces form at interface.

Despite of the low interfacial toughness between them, a large stretch can be obtained by simply reducing the hydrogel thickness. As shown in **Figure 7.3**, the critical stretch reaches λ_c =2.25 for the thin film of 0.1mm thickness. This phenomenon occurs because thinner samples have lower stiffness, and thus store less elastic energy for a given stretch. This result provides a useful guidance for the design of ionic devices: the laminates of thinner film may sustain larger stretches without changing the same interfacial toughness. This principle is consistent with the experimental results in

literature; epidermal electronics and transparent loudspeaker, for instance, have the attached films of thicknesses, only 30 μm and 100 μm, respectively.[10,13]

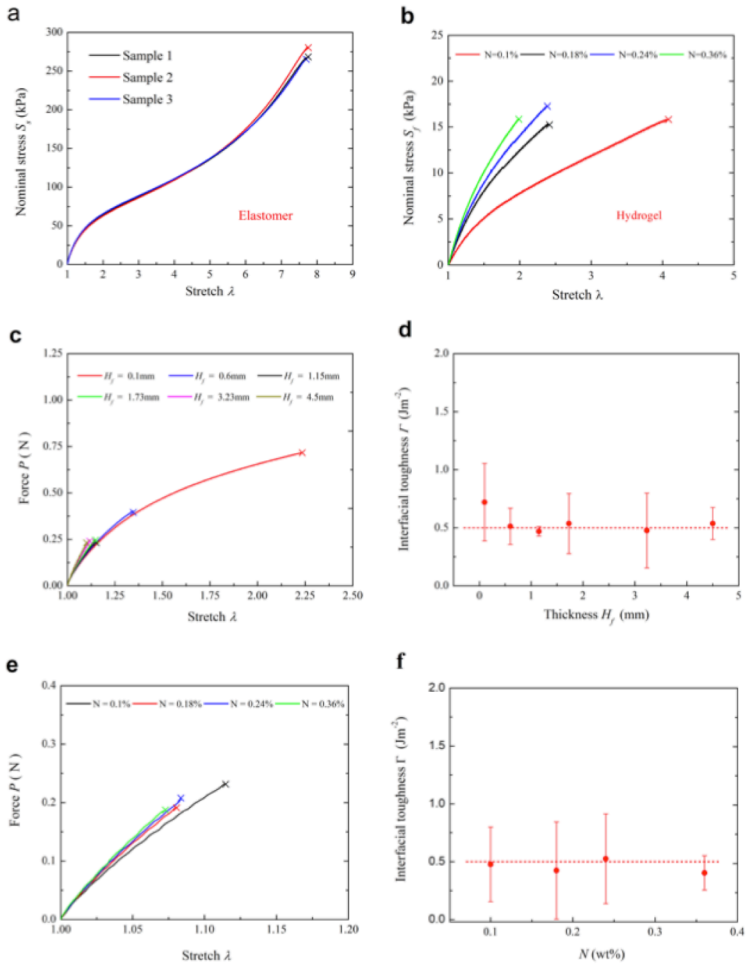

Figure 7.2 Effect of thickness and cross-link density of PAAm hydrogels. (**a**) The stress-stretch curves of VHB 4910. (**b**) The stress-stretch curves of PAAm hydrogels with different MBAA/AAm weight ratios *N*. (**c**) The force-stretch curves for bilayers as a function of hydrogel thickness. (**d**) The interfacial toughness Γ is independent of the thickness of PAAm hydrogel film. (**e**) The force-stretch curves of bilayer as a function of crosslink densities of hydrogels. (**f**) The interfacial toughness Γ is independent of crosslink densities of hydrogels.

Next, we studied the effect of cross-link density of the hydrogel on the interfacial toughness. The MBAA/AAm weight ratio was changed from 0.1% to 0.36% for 3mm-PAAm hydrogel film. **Figure 7.2e** shows the force-stretch relation for the bilayer of VHB 4910 and PAAm hydrogel with different cross-link densities. The interfacial toughness is independent of the cross-link densities of PAAm hydrogel (**Figure 7.2f**). Since no polymer chains of the hydrogel penetrate into VHB ribbon, the resistance for the interfacial crack propagation is only weak physical interaction. The interfacial crack can propagate without breaking polymer chains. Thus, the interfacial toughness does not depend on the cross-link density of the hydrogel.

Once the interfacial toughness is measured, we can predict the critical stretch at which the laminate debonds for a given geometry. One can set the critical energy release rate equals to the measured interfacial toughness, and solve for the critical stretches λ' and λ'' by combining Equations 7.1-7.3. Alternately, here we use Equation 7.4 for the laminates of VHB and PAAm hydrogel. The interfacial toughness between VHB and PAAm hydrogel is around 0.5 Jm^{-2}, Equation 7.4 for the limiting case can capture the relation of the critical stretch and thickness. When the hydrogel film is very thin compared to the VHB substrate, the attached film does not constrain the substrate, so that the stretch of the detached substrate is close to that of the attached laminate, $\lambda' \approx \lambda''$. When the hydrogel film is thick, the laminate debonds at small stretch, and λ' and λ'' are close. As a result, both the cases meet Equation 7.4. We compare the experimental data and the theoretical prediction by Equation 7.2 (**Figure 7.2c**). The Neo-Hookean model $W_f(\lambda) = \mu_f / 2 \cdot (\lambda^2 + 2/\lambda - 3)$ was applied to predict the critical stretch of the bilayer by

using the constant interfacial toughness Γ=0.5 Jm^{-2} (**Figure 7.2d**). The result shows a good agreement between experiment and theory.

Even though the adhesion is very weak, there is a simple rule of thumb: thinner films, better bonding, because for thin films a large critical stretch is needed to reach the critical energy release rate. Indeed the experiment showed that a thin film of 0.1mm sustained a large stretch >200% before debonding occurs (**Figure 7.3**).

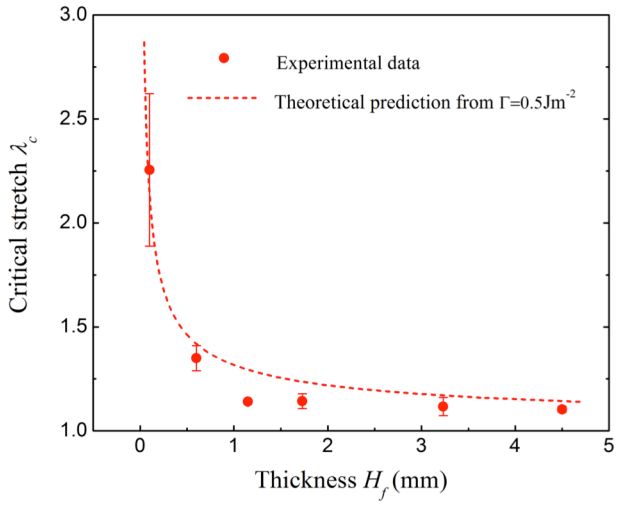

Figure 7.3 The experimental data and the theoretical prediction of the critical stretch using constant interfacial toughness for PAAm hydrogel film with different thicknesses.

7.4 Improve adhesion with nanoparticle solutions

The adhesion between VHB and hydrogels can be improved by adding nanoparticle solution at the interface. To increase the interfacial toughness, a toughening mechanism on the interface is needed. Recently, the silica nanoparticle solution has been used to glue two pieces of PDMA hydrogel.[173] We hypothesize that the same strategy can

be extended to the interface between elastomers and hydrogels, and that nanoparticles can adsorb the polymer chains from both elastomers and hydrogels, forming physical bonds. When a crack propagates, the physical bonds need to break, and thus dissipate energy (**Figure 7.4a**). We spread 20 μL of silica Ludox TM-50 colloidal nanoparticle solution at the interface between the VHB and PAAm hydrogel, and varied the MBAA/AAm weight ratio from 0.1% to 0.36%. The insets of **Figure 7.4b** show the surfaces of bonded and detached specimens that contain nanoparticles at interface. After debonding, nanoparticles present on both the surfaces of VHB and PAAm hydrogel. It indicates the existence of physical interactions between nanoparticles and VHB, and between nanoparticles and PAAm hydrogels.

Experiments confirmed our hypothesis that nanoparticles can toughen the interface. The interfacial toughness of PAAm hydrogel (N=0.1 %) increases from 0.5 Jm^{-2} to 3.5 Jm^{-2}, nearly 7 times after adding nanoparticles at interface. We also showed that this toughening effect strongly depends on the crosslink density of hydrogels (**Figure 7.4b**). As the crosslink density of hydrogels increases, the interfacial toughness decreases. For instance, nanoparticles has negligible effect on a highly crosslinked PAAm hydrogel (N=0.36%). This trend can be understood according to the Lake-Thomas theory.[177] Nanoparticles absorb polymer chains from the polymer network, whose elasticity determines the amount of absorbed polymer chains. Stiff hydrogels lead to large energy penalty for altering the network, and thus fewer polymer chains can be absorbed by nanoparticles. The decreasing amount of absorbed polymer chains leads to formation of fewer physical bonds, and dissipate less energy during crack propagation.[173]

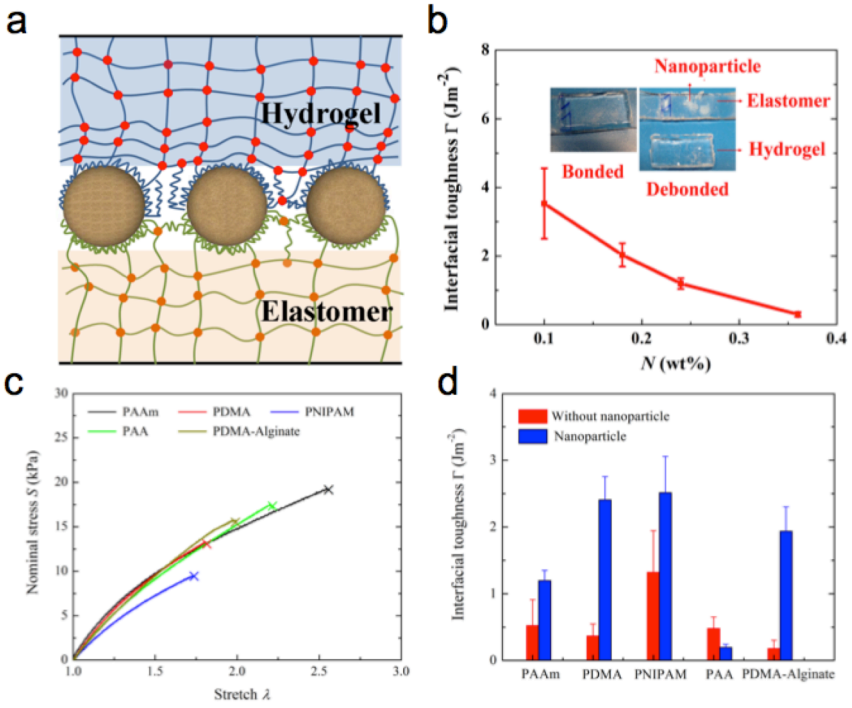

Figure 7.4 Effects of nanoparticles on the adhesion between elastomer and hydrogel. (**a**) Schematic of the interface between elastomer and hydrogel with nanoparticles. Polymer chains from elastomer and hydrogel are absorbed on the surface of nanoparticles (**b**) The interfacial toughness of VHB-nanoparticles-PAAm interface as a function of MBAA/AAm weight ratios. The photo insets depict the bonded and debonded specimens with nanoparticle. (**c**) The stress-stretch curves for different hydrogels with the same initial moduli. (**d**) The effect of nanoparticle on the interfacial toughness between VHB 4910 and different hydrogels, including poly(N,N-dimethylacrylamide) hydrogel (PDMA), poly(N-isopropylacrylamide) hydrogel (PNIPAM), polyacrylic acid hydrogel (PAA) and PDMA-alginate hybrid hydrogel.

The chemistry of polymer network strongly affects the adhesion, and the toughening effect of nanoparticles. We used our measurement techniques to access the adhesion between VHB dielectric elastomers and various hydrogels, and the toughening

effect of nanoparticles. The tested hydrogels include poly(N,N-dimethylacrylamide) (PDMA), poly(N-isopropylacrylamide) (PNIPAM), polyacrylic acid (PAA) and PDMA-Alginate. For a fair comparison, we controlled the crosslink density of each hydrogel, to exclude the effect of crosslink density. The stress-stretch curve confirmed that different hydrogels have the same initial modulus with that of PAAm hydrogel (N=0.24%), so does the crosslink density. The interfacial toughness between VHB and common hydrogels is indistinguishable ~1 Jm^{-2}, indicating that the adhesion is dominated by weak physical interactions (**Figure 7.4d**). The addition of nanoparticles shows a positive effect on the interfacial toughness between VHB and all these hydrogels, except the PAA hydrogel. In the case of PAA hydrogels, the reduction of interfacial toughness is due to the electrostatic repulsion between nanoparticles and PAA hydrogels.[52] Because the surface of silica nanoparticle is negatively charged,[178] and the polymer backbone of PAA hydrogel carry high density of negative charges at high pH (for Ludox TM-50, pH=9).

7.5 Summary

In this chapter, we studied the adhesion between hydrogels and elastomers, which critically limits the stretchability and reliability of ionic devices. We first developed analytical and experimental approaches to characterize the adhesion between highly stretchable materials. A criterion for crack propagation is that the energy release rate matches the interfacial toughness. We then applied this approach to measure the interfacial toughness between polyacrylamide hydrogels and VHB elastomers. The measured interfacial toughness is around 0.5 Jm^{-2}, and independent of the geometric

parameters. It reflects only weak van der Waals interactions form at interface. Despite of the low interfacial toughness, debonding can be retarded by simply reducing the hydrogel thickness. We also showed that adding energy dissipating mechanisms at interface can effectively improve interfacial toughness. A facial approach is adding nanoparticles at interface. The method is easy-to-implement and accurate that holds promise to apply on elastomers, gels and soft tissues.

Chapter 8 Conclusions

8.1 Summary

The emerging field of ionic devices promises to enable new generation of wearable and implantable devices that can match tissues mechanically, electrically and biologically. Before such devices come to life, there are the material constraints to overcome: hydrogels need to be ionically conductive to transmit electrical signals, and mechanically robust to sustain large deformation. The mechanical behavior of hydrogels and its coupling with ionic conductance are of scientific and technological significance.

We first developed a theoretical framework, and established a family of mechanical tests to characterize equations of state of gels. We proved that the polyacrylamide hydrogel behaves as an ideal elastomeric gel. The equations of state can be fully determined with 2-step mechanical tests: first determine the contribution due to stretching by compression or tensile tests, and then determine the osmotic pressure by free-swelling or constraint-swelling tests. The function of osmotic pressure is a single-variable function, and independent of cross-link density and experimental methods. Following the same strategy, we also studied the thermodynamic behavior of polyelectrolyte hydrogels. The model for polyelectrolyte hydrogels needs to invoke the osmotic pressure of ion distribution and non-Gaussian chain effect. We further extended this approach to an ionic liquid gel, polymethyl methacrylate ionogel. The polymethyl methacrylate ionogel is an ideal elastomeric gel. Only *2* material parameters are required for the equations of state for this ionogel: the elastic modulus and a single Flory

interaction parameter.

We then turned our attention to mechanical properties of hydrogels, developing new material systems and toughening mechanisms. We first improved the stiffness and toughness of alginate-polyacrylamide hydrogels. Combining short- and long-chain alginate breaks the inverse relation between stiffness and toughness: these hydrogels can achieve fracture energies up to ~16,000 Jm^{-2}, while maintaining constant elastic moduli. Additionally, the superior mechanical properties are compatible with excess mobile ions for ionic conductance. Using short-chain alginates reduces the viscosity of pre-gel solutions dramatically, and enables synthesis of homogeneous hydrogels with high ionic cross-link density. The resulting alginate-polyacrylamide hydrogels can achieve elastic moduli of ~1,000 kPa and fracture energies of ~4,000 Jm^{-2} simultaneously.

Next, we developed a new material system to achieve high mechanical performance and chemical stability simultaneously. The key is to replace ionic cross-links with crystallites. Polyvinyl alcohol-polyacrylamide hydrogels, containing both covalent crosslinks and crystallites, achieve extremely large elastic modulus (5 MPa), strength (2.5 MPa) and fracture energy (14,000 Jm^{-2}). The hydrophilic polyacrylamide network restores the shape of the hydrogel, increases the equilibrium water content and provides a strong driving force to reform crystallites. Crystallites serve as reversible and stable physical cross-links: crystallites keep stable in electrolyte solutions; they unzip, dissipate energy under deformation, and reform quickly after deformation. In addition, we have also discovered a new toughening mechanism for hydrogels: strain-induced crystallization. A cross-linked polymer network imposes deformation on the entangled

crystalline polymers, and enables them to align and crystallize. Strain-induced crystallization toughens hydrogels effectively, and creating anisotropic structure at the crack tip. This mechanism leads to unusual characteristics such as crack kinking and shape memory behavior.

We also studied the adhesive property of hydrogels. The adhesion between hydrogels and elastomers is critical for the performance and reliability of ionic devices, but is less studied. We adopted interfacial toughness to quantify this property. We developed a set of analytical and experimental methods to determine the interfacial toughness: an elastomer substrate of hydrogel-elastomer laminates is deformed until a pre-crack propagates through the interface. The measured interfacial toughness between polyacrylamide hydrogels and VHB elastomers is around 0.5 Jm^{-2}, independent of the geometry and the cross-link density of hydrogels. Despite of the low interfacial toughness, debonding can be retarded by reducing the hydrogel thickness. We also developed methods to improve the interfacial toughness. By adding nanoparticles at interface, the interfacial toughness can be increased sevenfold. This effect is due to formation physical bonds across the interface.

8.2 Suggestions for future work

To study mechanical behavior of hydrogels for the use of ionic devices, this dissertation has developed analytical and experimental approaches to characterize how the swelling of gels depends on applied forces, mechanical constraints, solvents, pH and salinity, synthesized new hydrogels to achieve unprecedented mechanical properties and

superior chemical stability, and developed experimental techniques to quantify and improve the adhesion of hydrogels. Although extensive efforts have been made here, there still remain ample of research opportunities.

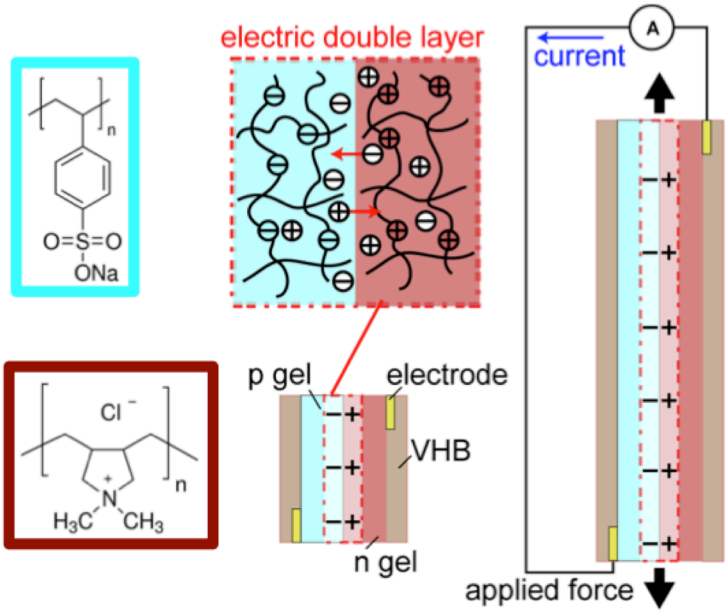

Figure 8.1 Hydrogel-based Stretchable electric double layer. A hydrogel junction consists of negatively and positively charged networks. When the junction deforms, the capacitance of the SEDL changes with deformation, resulting in transient current flows in external circuits.

First, the ionic devices demonstrated so far have been actuators and strain sensors. Their designs and functions are limited, in contrast to the large variety of available electronic devices. To expand the range of functionality, different device designs can be explored. The existing ionic strain sensor requires continuous monitoring by an external circuit, which in turn requires a constantly applied external voltage/current source. A better design is to utilize electric double layer to report signal to an external circuit. The operation principle is that applied strains deform the interfacial area, thus changing the

capacitance and inducing a charge transfer in the structure. This mechanism will eliminate the need of external power source, allow such a device to generate a transient signal that can be detected and processed by an external circuitry.

Second, there exist enormous opportunities to develop printing techniques for tough hydrogels. Fabrication of tough hydrogels has so far relied on manual assembly; printing techniques are needed to rapid-prototype hydrogels with fine features. While the hydrogels developed here limit by feature sizes (down to 1 mm) due to batch synthesis, printed soft materials can easily reach a sub-millimeter feature size. The synergy between tough hydrogels and printing techniques will open up a wide range of possibilities. Tough hydrogels enables high stretchability, crack resistance and reliability of the resulting ionic devices. Miniaturization by printing techniques enables the production of sensors desirable for specific applications such as tactile sensors and motion-sensing suits. Devices of small features can also improve the performance of ionic devices. For instance, ionic conductors of reducing thickness decrease the mechanical constraint of actuation and adhere better to dielectrics. In addition, rapid prototyping by printing enables fast, low-cost, mass production of ionic devices. Various design factors of hydrogels can be explored, including geometry, film alignment, and thickness.

Third, the developed materials and methods can also open up new research opportunities beyond ionic devices. In particular, a long-standing challenge in tissue engineering is cartilage replacement. The difficulty lies in a fundamental bottleneck: hydrogels mismatch cartilage in mechanical properties and anisotropic structure. Several composites of hydrogels and fillers have been reported, but have limitations: intrinsic

weakness of the hydrogels, and weak interaction between the hydrogels and the fillers. An emerging opportunity is to combine polyvinyl alcohol-based hydrogels and polyvinyl alcohol fibers. This thesis has established that polyvinyl alcohol-based hydrogels can achieve unprecedented mechanical properties and anisotropic structure. Although these hydrogels has lower tensile strength than that of cartilage, this gap can be filled by adding polyvinyl alcohol fibers. By controlling the melting process, these fibers can reform crystallites with the hydrogel matrix. Thus, the resulting materials can combine intrinsic properties of polyvinyl alcohol-based hydrogels, reinforcement effects with fibers, and synergy between matrix and fibers. These materials may lead to a material first time ever that mimics the cartilage.

With the rapid progress in the field of soft materials, hydrogels have achieved a wide range of properties that were unattained previously. It is hoped that this dissertation provides valuable methods and useful material systems that contribute to new applications of hydrogels.

Bibliography

1 Topol, E. J. Transforming medicine via digital innovation. *Sci. Transl. Med.* **2**, 16 (2010).

2 Steinhubl, S. R., Muse, E. D. & Topol, E. J. Can mobile health technologies transform health care? *JAMA* **310**, 2395-2396 (2013).

3 Walsh, J. A., Topol, E. J. & Steinhubl, S. R. Novel wireless devices for cardiac monitoring. *Circulation* **130**, 573-581 (2014).

4 Wagner, S. *et al.* Electronic skin: architecture and components. *Phys. E* **25**, 326-334 (2004).

5 Ramuz, M., Tee, B. C. K., Tok, J. B. H. & Bao, Z. Transparent, Optical, Pressure-Sensitive Artificial Skin for Large-Area Stretchable Electronics. *Adv. Mater.* **24**, 3223-3227 (2012).

6 Kaltenbrunner, M. *et al.* An ultra-lightweight design for imperceptible plastic electronics. *Nature* **499**, 458-463 (2013).

7 Hammock, M. L., Chortos, A., Tee, B. C. K., Tok, J. B. H. & Bao, Z. 25th Anniversary Article: The Evolution of Electronic Skin (E-Skin): A Brief History, Design Considerations, and Recent Progress. *Adv. Mater.* **25**, 5997-6038 (2013).

8 Minev, I. R. *et al.* Electronic dura mater for long-term multimodal neural interfaces. *Science* **347**, 159-163 (2015).

9 Xu, L. *et al.* 3D multifunctional integumentary membranes for spatiotemporal cardiac measurements and stimulation across the entire epicardium. *Nat. Commun.*, DOI: 10.1038/ncomms4329 (2014).

10 Kim, D.-H. *et al.* Epidermal electronics. *Science* **333**, 838-843 (2011).

11 Khang, D. Y., Rogers, J. A. & Lee, H. H. Mechanical buckling: Mechanics, metrology, and stretchable electronics. *Adv. Func. Mater.* **19**, 1526-1536 (2009).

12 Feng, X. *et al.* Stretchable ferroelectric nanoribbons with wavy configurations on elastomeric substrates. *ACS Nano* **5**, 3326-3332 (2011).

13 Keplinger, C. *et al.* Stretchable, Transparent, Ionic Conductors. *Science* **341**, 984-987 (2013).

14 Suo, Z. G., Zhao, X. H., Hong, W., Zhou, J. X. & Greene, W. H. A theory of large deformation in soft active materials. *P. Soc. Photo-opt. Ins.,* 692710 (2008)

15 Drury, J. L. & Mooney, D. J. Hydrogels for tissue engineering: scaffold design variables and applications. *Biomaterials* **24**, 4337-4351 (2003).

16 Langer, R. Drug delivery and targeting. *Nature* **392**, 5-10 (1998).

17 Sun, J. Y., Keplinger, C., Whitesides, G. M. & Suo, Z. Ionic skin. *Adv. Mater.* **26**, 7608-7614 (2014).

18 Bai, Y. *et al.* Transparent hydrogel with enhanced water retention capacity by introducing highly hydratable salt. *Appl. Phys. Lett.* **105**, 151903 (2014).

19 Marcombe, R. *et al.* A theory of constrained swelling of a pH-sensitive hydrogel. *Soft Matter* **6**, 784-793 (2010).

20 Cai, S. Q. & Suo, Z. G. Mechanics and chemical thermodynamics of phase transition in temperature-sensitive hydrogels. *J. Mech. Phys. Solids* **59**, 2259-2278 (2011).

21 Pharr, M., Sun, J. Y. & Suo, Z. G. Rupture of a highly stretchable acrylic dielectric elastomer. *J. Appl. Phys.* **111**, 104114 (2012).

22 Calvert, P. Hydrogels for Soft Machines. *Adv. Mater.* **21**, 743-756 (2009).

23 Gong, J. P., Katsuyama, Y., Kurokawa, T. & Osada, Y. Double-network hydrogels with extremely high mechanical strength. *Adv. Mater.* **15**, 1155-1158 (2003).

24 Sun, J. Y. *et al.* Highly stretchable and tough hydrogels. *Nature* **489**, 133-136 (2012).

25 Zhao, X. Multi-scale multi-mechanism design of tough hydrogels: building dissipation into stretchy networks. *Soft Matter* **10**, 672-687 (2014).

26 Cha, C., Kohman, R. H. & Kong, H. Biodegradable polymer crosslinker: independent control of stiffness, toughness, and hydrogel degradation rate. *Adv. Func. Mater.***19**, 3056-3062 (2009).

27 Lee, K. Y. & Mooney, D. J. Alginate: Properties and biomedical applications. *Prog. Polym. Sci.* **37**, 106-126 (2012).

28 Konda, A., Urayama, K. & Takigawa, T. Strain-rate-dependent poisson's ratio and stress of polymer gels in solvents revealed by ultraslow stretching. *Macromolecules* **44**, 3000-3006 (2011).

29 Cai, S. Q., Lou, Y. C., Ganguly, P., Robisson, A. & Suo, Z. G. Force generated by a swelling elastomer subject to constraint. *J. Appl. Phys.* **107**, 103535 (2010).

30 Hirokawa, Y. & Tanaka, T. Volume Phase-Transition in a Nonionic Gel. *J. Chem. Phys.* **81**, 6379-6380 (1984).

31 Tanaka, T., Nishio, I., Sun, S. T. & Uenonishio, S. Collapse of gels in an electric field. *Science* **218**, 467-469 (1982).

32 Ohmine, I. & Tanaka, T. Salt effects on the phase-transition of ionic gels. *J. Chem. Phys.* **77**, 5725-5729 (1982).

33 Tanaka, T. *et al.* Phase-transitions in ionic gels. *Phys. Rev. Lett.* **45**, 1636-1639 (1980).

34 Lee, K. Y. & Mooney, D. J. Hydrogels for tissue engineering. *Chem. Rev.* **101**, 1869-1880 (2001).

35 Beebe, D. J. *et al.* Functional hydrogel structures for autonomous flow control inside microfluidic channels. *Nature* **404**, 588-590 (2000).

36 Cai, S. Q. & Suo, Z. G. Equations of state for ideal elastomeric gels. *EPL* **97**, 34009 (2012).

37 Hong, W., Zhao, X. H., Zhou, J. X. & Suo, Z. G. A theory of coupled diffusion and large deformation in polymeric gels. *J. Mech. Phys. Solids* **56**, 1779-1793 (2008).

38 Flory, P. J. & Rehner, J. Statistical mechanics of cross-linked polymer networks II Swelling. *J. Chem. Phys.* **11**, 521-526 (1943).

39 Flory, P. J. & Rehner, J. Statistical mechanics of cross-linked polymer networks I Rubberlike elasticity. *J. Chem. Phys.* **11**, 512-520 (1943).

40 Huggins, M. L. Solutions of long chain compounds. *J. Chem. Phys.* **9**, 440-440 (1941).

41 Li, J. Y., Hu, Y. H., Vlassak, J. J. & Suo, Z. G. Experimental determination of equations of state for ideal elastomeric gels. *Soft Matter* **8**, 8121-8128 (2012).

42 Day, J. C. & Robb, I. D. Thermodynamic parameters of polyacrylamides in water. *Polymer* **22**, 1530-1533 (1981).

43 Livney, Y. D. *et al.* Interactions of glucose and polyacrylamide in solutions and gels. *J. Polym. Sci., Part B: Polym. Phys.* **41**, 3053-3063 (2003).

44 Mallam, S., Horkay, F., Hecht, A. M. & Geissler, E. Scattering and swelling properties of inhomogeneous polyacrylamide gels. *Macromolecules* **22**, 3356-3361 (1989).

45 Hochberg, A., Tanaka, T. & Nicoli, D. Spinodal line and critical-point of an Acrylamide gel. *Phys. Rev. Lett.* **43**, 217-219 (1979).

46 Dubrovskii, S. A., Afanaseva, M. V., Lagutina, M. A. & Kazanskii, K. S. Comprehensive characterization of superabsorbent polymer hydrogels. *Polym. Bulletin* **24**, 107-113 (1990).

47 Suzuki, A. & Tanaka, T. Phase transition in polymer gels induced by visible light. *Nature* **346**, 345-347 (1990).

48 Liu, Z. S. & Calvert, P. Multilayer hydrogels as muscle-like actuators. *Adv. Mater.* **12**, 288-291 (2000).

49 Yoshioka, Y. & Calvert, P. Electrically stimulated hydrogel as microactuators. *Abstr. Pap. Am. Chem. S.* **221**, 387 (2001).

50 Agarwal, A. K., Nammi, K., Kaczmarek, K. A., Tyler, M. E. & Beebe, D. J. A hybrid natural/artificial electrostatic actuator for tactile stimulation. *Eng. Med. Biol. Soc. Ann.*, 341-345 (2002).

51 Li, J., Suo, Z. & Vlassak, J. J. A model of ideal elastomeric gels for polyelectrolyte gels. *Soft matter* **10**, 2582-2590 (2014).

52 Ricka, J. & Tanaka, T. Swelling of ionic gels - quantitative performance of the donnan theory. *Macromolecules* **17**, 2916-2921 (1984).

53 Lifson, S. & Katchalsky, A. The electrostatic free energy of polyelectrolyte solutions. 2. Fully stretched macromolecules. *J. Polym. Sci.* **13**, 43-55 (1954).

54 Michaeli, I. & Katchalsky, A. Potentiometric titration of polyelectrolyte gels. *J. Polym. Sci.* **23**, 683-696 (1957).

55 Prudnikova, K. & Utz, M. Electromechanical characterization of polyelectrolyte gels by indentation. *Macromolecules* **43**, 511-517 (2010).

56 Rubinstein, M., Colby, R. H., Dobrynin, A. V. & Joanny, J. F. Elastic modulus and equilibrium swelling of polyelectrolyte gels. *Macromolecules* **29**, 398-406 (1996).

57 Dubrovskii, S. A. & Rakova, G. V. Elastic and osmotic behavior and network imperfections of nonionic and weakly ionized acrylamide-based hydrogels. *Macromolecules* **30**, 7478-7486 (1997).

58 Skouri, R., Schosseler, F., Munch, J. P. & Candau, S. J. Swelling and elastic properties of polyelectrolyte gels. *Macromolecules* **28**, 197-210 (1995).

59 Arruda, E. M. & Boyce, M. C. A 3-dimensional constitutive model for the large stretch behavior of rubber elastic materials. *J. Mech. Phys. Solids* **41**, 389-412 (1993).

60 Boyce, M. C. & Arruda, E. M. Constitutive models of rubber elasticity: A review. *Rubb. Chem. Techn.* **73**, 504-523 (2000).

61 Gent, A. N. A new constitutive relation for rubber. *Rubb. Chem. Techn.* **69**, 59-61 (1996).

62 Horgan, C. O. & Saccomandi, G. Constitutive models for compressible nonlinearly elastic materials with limiting chain extensibility. *J. Elasticity* **77**, 123-138 (2004).

63 Lu, T. Q. *et al.* Dielectric elastomer actuators under equal-biaxial forces, uniaxial forces, and uniaxial constraint of stiff fibers. *Soft Matter* **8**, 6167-6173 (2012).

64 Webber, R. E., Creton, C., Brown, H. R. & Gong, J. P. Large strain hysteresis and mullins effect of tough double-network hydrogels. *Macromolecules* **40**, 2919-2927 (2007).

65 Chen, B. *et al.* Highly Stretchable and transparent ionogels as nonvolatile conductors for dielectric elastomer transducers. *ACS Appl. Mater. Interfaces **6**, 7840-7845* (2014).

66 Lodge, T. P. A unique platform for materials design. *Science* **321**, 50-51 (2008).

67 Quartarone, E. & Mustarelli, P. Electrolytes for solid-state lithium rechargeable batteries: recent advances and perspectives. *Chem. Soc. Rev.* **40**, 2525-2540 (2011).

68 Suzuki, K. *et al.* A planar rhombic charge-separated tetrasilacyclobutadiene. *Science* **331**, 1306-1309 (2011).

69 Liu, X., Wu, D., Wang, H. & Wang, Q. Self-recovering tough gel electrolyte with adjustable supercapacitor performance. *Adv. Mater.* **26**, 4370-4375 (2014).

70 Ahn, S. K. *et al.* Development of dye-sensitized solar cells composed of liquid crystal embedded, electrospun poly(vinylidene fluoride-co-hexafluoropropylene) nanofibers as polymer gel electrolytes. *ACS Appl. Mater. Interfaces* **4**, 2096-2100 (2012).

71 Cho, J. H. *et al.* High-capacitance ion gel gate dielectrics with faster polarization response times for organic thin film transistors. *Adv. Mater.* **20**, 686-690 (2008).

72 Lee, K. H. *et al.* "Cut and stick" Rubbery ion gels as high capacitance gate dielectrics. *Adv. Mater.* **24**, 4457-4462 (2012).

73 Cho, J. H. *et al.* Printable ion-gel gate dielectrics for low-voltage polymer thin-film transistors on plastic. *Nat. Mater.* **7**, 900-906 (2008).

74 Peng, B., Zhu, J., Liu, X. & Qin, Y. Chemical potentiometric response of ion-selective membranes with ionic liquids as ion-exchanger and plasticizer. *Sen. Actuators, B* **133**, 308-314 (2008).

75 Riisagera, A., Fehrmanna, R., Haumannb, M. & Wasserscheidb, P. Supported ionic liquids: versatile reaction and separation media. *Topics in catalysis* **40**, 91-102 (2006).

76 McDonagh, C., Burke, C. S. & MacCraith, B. D. Optical chemical sensors. *Chem. Rev.* **108**, 400-422 (2008).

77 Shvedene, N. V. *et al.* Ionic liquids plasticize and bringi-sensing ability to polymer membranes of selective electrodes. *Electroanalysis* **18**, 1416-1421 (2006).

78 Yoon, J., Lee, H. J. & Stafford, C. M. Thermoplastic elastomers based on ionic liquid and poly(vinyl alcohol). *Macromolecules* **44**, 2170-2178 (2011).

79 Harner, J. M. & Hoagland, D. A. Thermoreversible gelation of an ionic liquid by crystallization of a dissolved polymer. *J. Phys. Chem. B* **114**, 3411-3418 (2010).

80 Visentin, A. F. & Panzer, M. J. Poly(ethylene glycol) diacrylate-supported ionogels with consistent capacitive behavior and tunable elastic response. *ACS Appl. Mater. Interfaces* **4**, 2836-2839 (2012).

81 Susan, M. A. B. H., Kaneko, T., Noda, A. & Watanabe, M. Ion gels prepared by in situ radical polymerization of vinyl monomers in an ionic liquid and their characterization as polymer electrolytes. *J. Am. Chem. Soc.* **127**, 4976-4983 (2005).

82 Ueno, K., Hata, K., Katakabe, T., Kondoh, M. & Watanabe, M. Nanocomposite ion gels based on silica nanoparticles and an ionic liquid: ionic transport, viscoelastic properties, and microstructure. *J. Phys. Chem. B* **112**, 9013-9019 (2008).

83 He, Y., Boswell, P. G., Bühlmann, P. & Lodge, T. P. Ion gels by self-assembly of a triblock copolymer in an ionic liquid. *J. Phys. Chem. B* **111**, 4645-4652 (2007).

84 Lake, G. J. & Thomas, A. G. Strength of highly elastic materials. *Proc. R. Soc. London, Ser. A* **300**, 108-119 (1967).

85 Neouze, M.-A., Bideau, J. L., Gaveau, P., Bellayer, S. & Vioux, A. Ionogels, new materials arising from the confinement of ionic liquids within silica-derived networks. *Chem. Mater.* **18**, 3931-3936 (2006).

86 Klingshirn, M. A. *et al.* Gelation of ionic liquids using a cross-linked poly (ethylene glycol) gel matrix. *Chem. Mater.* **16**, 3091-3097 (2004).

87 Izak, P., Hovorka, Š., Bartovský, T., Bartovska, L. & Crespo, J. Swelling of polymeric membranes in room temperature ionic liquids. *J. Mem. Sci.* **296**, 131-138 (2007).

88 Yamamoto, S., Ejaz, M., Tsujii, Y. & Fukuda, T. Surface interaction forces of well-defined, high-density polymer brushes studied by atomic force microscopy: 2. Effect of graft density. *Macromolecules* **33**, 5608-5612 (2000).

89 Hu, Y. H., Chen, X., Whitesides, G. M., Vlassak, J. J. & Suo, Z. G. Indentation of polydimethylsiloxane submerged in organic solvents. *J. Mater. Res.* **26**, 785-795 (2011).

90 Gu, Y. *et al.* High Toughness, High conductivity ion gels by sequential triblock copolymer self-assembly and chemical cross-linking. *J. Am. Chem. Soc.* **135**, 9652-9655 (2013).

91 Prasad, K., Kaneko, Y. & Kadokawa, J. i. Novel gelling systems of κ-, ι-and λ-carrageenans and their composite gels with cellulose using ionic liquid. *Macromol. biosci.* **9**, 376-382 (2009).

92 Zhang, S., Lee, K. H., Frisbie, C. D. & Lodge, T. P. Ionic conductivity, capacitance, and viscoelastic properties of block copolymer-based ion gels. *Macromolecules* **44**, 940-949 (2011).

93 Rivlin, R. S. & Thomas, A. G. Rupture of rubber. 1. Characteristic energy for tearing. *J. Polym. Sci.* **10**, 291-318 (1953).

94 Zhang, S., Lee, K. H., Sun, J., Frisbie, C. D. & Lodge, T. P. Viscoelastic properties, ionic conductivity, and materials design considerations for poly (styrene-b-ethylene oxide-b-styrene)-based ion gel electrolytes. *Macromolecules* **44**, 8981-8989 (2011).

95 Gent, A. N. & Tobias, R. H. Threshold tear strength of elastomers. *J. Polym. Sci. Part B Polym. Phys.* **20**, 2051-2058 (1982).

96 Li, J., Suo, Z. & Vlassak, J. J. Stiff, strong, and tough hydrogels with good chemical stability. *J. Mater. Chem. B* **2**, 6708-6713 (2014).

97 Haque, M. A., Kurokawa, T., Kamita, G. & Gong, J. P. Lamellar bilayers as reversible sacrificial bonds to toughen hydrogel: Hysteresis, self-recovery, fatigue resistance, and crack blunting. *Macromolecules* **44**, 8916-8924 (2011).

98 Sun, T. L. *et al.* Physical hydrogels composed of polyampholytes demonstrate high toughness and viscoelasticity. *Nat. Mater.* **12**, 932-937 (2013).

99 Illeperuma, W. R., Sun, J.-Y., Suo, Z. & Vlassak, J. J. Force and stroke of a hydrogel actuator. *Soft Matter* **9**, 8504-8511 (2013).

100 Flory, P. J. & Rehner, J. Effect of deformation on the swelling capacity of rubber. *J. Chem. Phys.* **12**, 412-414 (1944).

101 Zhang, S., Sun, N., He, X., Lu, X. & Zhang, X. Physical properties of ionic liquids: database and evaluation. *J. Phys. Chem. Ref. Data* **35**, 1475-1517 (2006).

102 Wang, X., Nie, Y., Zhang, X., Zhang, S. & Li, J. Recovery of ionic liquids from dilute aqueous solutions by electrodialysis. *Desalination* **285**, 205-212 (2012).

103 Gong, J. P. Why are double network hydrogels so tough? *Soft Matter* **6**, 2583-2590 (2010).

104 Huey, D. J., Hu, J. C. & Athanasiou, K. A. Unlike bone, cartilage regeneration remains elusive. *Science* **338**, 917-921 (2012).

105 Shepherd, R. F. *et al.* Multigait soft robot. *Proc. Natl. Acad. Sci.* **108**, 20400-20403 (2011).

106 Martinez, R. V. *et al.* Robotic tentacles with three-dimensional mobility based on flexible elastomers. *Adv. Mater.* **25**, 205-212 (2013).

107 Martinez, R. V., Glavan, A. C., Keplinger, C., Oyetibo, A. I. & Whitesides, G. M. Soft actuators and robots that are resistant to mechanical damage. *Adv. Func. Mater.* **24**, 3003-3010 (2014).

108 ChinPurcell, M. V. & Lewis, J. L. Fracture of articular cartilage. *J. Biomech. Eng.-T ASME* **118**, 545-556 (1996).

109 Henderson, K. J., Zhou, T. C., Otim, K. J. & Shull, K. R. Ionically cross-linked triblock copolymer hydrogels with high strength. *Macromolecules* **43**, 6193-6201 (2010).

110 Tuncaboylu, D. C., Sari, M., Oppermann, W. & Okay, O. Tough and self-healing hydrogels formed via hydrophobic interactions. *Macromolecules* **44**, 4997-5005 (2011).

111 Koutroupi, K. S. & Barbenel, J. C. Mechanical and failure behavior of the stratum corneum. *J. Biomech.* **23**, 281-287 (1990).

112 Darnell, M. C. *et al.* Performance and biocompatibility of extremely tough alginate/polyacrylamide hydrogels. *Biomaterials* **34**, 8042-8048 (2013).

113 Liao, I., Moutos, F. T., Estes, B. T., Zhao, X. & Guilak, F. Composite three-dimensional woven scaffolds with interpenetrating network hydrogels to create functional synthetic articular cartilage. *Adv. Func. Mater.***23**, 5833-5839 (2013).

114 Webber, R. E. & Shull, K. R. Strain dependence of the viscoelastic properties of alginate hydrogels. *Macromolecules* **37**, 6153-6160 (2004).

115 Draget, K. I., Simensen, M. K., Onsoyen, E. & Smidsrod, O. Gel strength of Ca-limited alginate gels made in-situ. *Hydrobiologia* **261**, 563-569 (1993).

116 Draget, K. I., Braek, G. S. & Smidsrod, O. Alginic acid gels - the effect of alginate chemical composition and molecular weight. *Carbonhydr. Polym.* **25**, 31-38 (1994).

117 Kuo, C. K. & Ma, P. X. Ionically crosslinked alginate hydrogels as scaffolds for tissue engineering: part 1. Structure, gelation rate and mechanical properties. *Biomaterials* **22**, 511-521 (2001).

118 Kong, H. J., Kaigler, D., Kim, K. & Mooney, D. J. Controlling rigidity and degradation of alginate hydrogels via molecular weight distribution. *Biomacromolecules* **5**, 1720-1727 (2004).

119 Johnson, F. A., Craig, D. Q. M., Mercer, A. D. & Chauhan, S. The effects of alginate molecular structure and formulation variables on the physical characteristics of alginate raft systems. *Int. J. Pharm.* **159**, 35-42 (1997).

120 Skjåk-Bræk, G., Grasdalen, H. & Smidsrød, O. Inhomogeneous polysaccharide ionic gels. *Carbonhydr. Polym.***10**, 31-54 (1989).

121 Yang, C. H. *et al.* Strengthening alginate/polyacrylamide hydrogels using various multivalent cations. *ACS Appl. Mater. Interfaces* **5**, 10418-10422 (2013).

122 Tvergaard, V. & Hutchinson, J. W. The relation between crack-growth resistance and fracture process parameters in elastic plastic solids. *J. Mech. Phys. Solids* **40**, 1377-1397 (1992).

123 Ritchie, R. O. The conflicts between strength and toughness. *Nat. Mater.* **10**, 817-822 (2011).

124 Zhang, L., Zhao, J., Zhu, J. T., He, C. C. & Wang, H. L. Anisotropic tough poly(vinyl alcohol) hydrogels. *Soft Matter* **8**, 10439-10447 (2012).

125 Gent, A. N., Kim, H. J. Tear strength of stretched rubber. *Rubb. Chem. Techno.* **51**, 34-44 (1978).

126 Nakayama, A. *et al.* High mechanical strength double-network hydrogel with bacterial cellulose. *Adv. Func. Mater.* **14**, 1124-1128 (2004).

127 Wegst, U. G. K. & Ashby, M. F. The mechanical efficiency of natural materials. *Philos. Mag.* **84**, 2167-2181 (2004).

128 Haraguchi, K. & Takehisa, T. Nanocomposite hydrogels: A unique organic-inorganic network structure with extraordinary mechanical, optical, and swelling/de-swelling properties. *Adv. Mater.* **14**, 1120-1124 (2002).

129 Bakarich, S. E., Beirne, S., Wallace, G. G. & Spinks, G. M. Extrusion printing of ionic–covalent entanglement hydrogels with high toughness. *J. Mater. Chem. B* **1**, 4939-4946 (2013).

130 Sakai, T. *et al.* Design and fabrication of a high-strength hydrogel with ideally homogeneous network structure from tetrahedron-like macromonomers. *Macromolecules* **41**, 5379-5384 (2008).

131 Kleverlaan, M., van Noort, R. H. & Jones, I. Deployment of swelling elastmoer packers in Shell E&P. *SPE/IADC Drilling Conference,* Society of Petroleum Engineers (2005).

132 Kamata, H., Akagi, Y., Kayasuga-Kariya, Y., Chung, U.-i. & Sakai, T. "Nonswellable" hydrogel without mechanical hysteresis. *Science* **343**, 873-875 (2014).

133 Appel, E. A., del Barrio, J., Loh, X. J. & Scherman, O. A. Supramolecular polymeric hydrogels. *Chemical Society Reviews* **41**, 6195-6214 (2012).

134 Li, J., Illeperuma, W. R., Suo, Z. & Vlassak, J. J. Hybrid Hydrogels with Extremely High Stiffness and Toughness. *ACS Macro Lett.* **3**, 520-523 (2014).

135 Hassan, C. M. & Peppas, N. A. Structure and applications of poly(vinyl alcohol) hydrogels produced by conventional crosslinking or by freezing/thawing methods. *Adv. Polym. Sci.* **153**, 37-65 (2000).

136 Bodugoz-Senturk, H., Macias, C. E., Kung, J. H. & Muratoglu, O. K. Poly (vinyl alcohol)–acrylamide hydrogels as load-bearing cartilage substitute. *Biomaterials* **30**, 589-596 (2009).

137 Cha, W. I., Hyon, S. H., Oka, M. & Ikada, Y. Mechanical and wear properties of poly(vinyl alcohol) hydrogels. *Macromol. symp.* **109**, 115-126 (1996).

138 Bodugoz-Senturk, H. *et al.* The effect of polyethylene glycol on the stability of pores in polyvinyl alcohol hydrogels during annealing. *Biomaterials* **29**, 141-149 (2008).

139 Mishra, S., Bajpai, R., Katare, R. & Bajpai, A. On the mechanical strength of biocompatible semi-IPNs of polyvinyl alcohol and polyacrylamide. *Microsyst. Technol.* **14**, 193-198 (2008).

140 Miyazaki, T., Hoshiko, A., Akasaka, M., Shintani, T. & Sakurai, S. SAXS studies on structural changes in a poly (vinyl alcohol) film during uniaxial stretching in water. *Macromolecules* **39**, 2921-2929 (2006).

141 Holloway, J. L., Lowman, A. M. & Palmese, G. R. The role of crystallization and phase separation in the formation of physically cross-linked PVA hydrogels. *Soft Matter* **9**, 826-833 (2013).

142 Zhang, L. *et al.* High strength graphene oxide/polyvinyl alcohol composite hydrogels. *J. Mater. Chem.* **21**, 10399-10406 (2011).

143 Wu, J., Ge, Q. & Mather, P. T. PEG− POSS multiblock polyurethanes: synthesis, characterization, and hydrogel formation. *Macromolecules* **43**, 7637-7649 (2010).

144 Gaharwar, A. K. *et al.* Highly Extensible Bio-Nanocomposite Fibers. *Macromol. Rapid Commun.* **32**, 50-57 (2011).

145 Ronken, S. *et al.* Double-network acrylamide hydrogel compositions adapted to achieve cartilage-like dynamic stiffness. *Biomech. Model. Mechanobiol.* **12**, 243-248 (2013).

146 Millon, L. E., Nieh, M.-P., Hutter, J. L. & Wan, W. SANS characterization of an anisotropic poly (vinyl alcohol) hydrogel with vascular applications. *Macromolecules* **40**, 3655-3662 (2007).

147 Flory, P. J. Thermodynamics of crystallization in high polymers. I. Crystallization induced by stretching. *J. Chem. Phys.***15**, 397 (1947).

148 Gent, A. Crystallization and the relaxation of stress in stretched natural rubber vulcanizates. *Trans. Faraday Soc.* **50**, 521-533 (1954).

149 Gent, A. N. *Engineering with Rubber: How to Design Rubber Components*. Hanser Publications, Cincinnati, Ohio, USA (2001).

150 Trabelsi, S., Albouy, P.-A. & Rault, J. Crystallization and melting processes in vulcanized stretched natural rubber. *Macromolecules* **36**, 7624-7639 (2003).

151 Trabelsi, S., Albouy, P.-A. & Rault, J. Stress-induced crystallization around a crack tip in natural rubber. *Macromolecules* **35**, 10054-10061 (2002).

152 Hassan, C. M. & Peppas, N. A. Structure and morphology of freeze/thawed PVA hydrogels. *Macromolecules* **33**, 2472-2479 (2000).

153 Yano, T. *et al.* Orientation of poly (vinyl alcohol) nanofiber and crystallites in non-woven electrospun nanofiber mats under uniaxial stretching. *Polymer* (2012).

154 Thomas, A. G., Whittle, J. M. Tensile rupture of rubber. *Rubber Chem. Technol.* **43**, 222-228 (1970).

155 Yang, W., Furukawa, H. & Gong, J. P. Highly extensible double-network gels with self-assembling anisotropic structure. *Adv. Mater.* **20**, 4499-4503 (2008).

156 Haque, M., Kamita, G., Kurokawa, T., Tsujii, K. & Gong, J. P. Unidirectional alignment of lamellar bilayer in hydrogel: One-dimensional swelling, anisotropic modulus, and stress/strain tunable structural color. *Adv. Mater.* **22**, 5110-5114 (2010).

157 Suo, Z. G. & Hutchinson, J. W. Sandwich test specimens for measuring interface crack toughness. *Mater. Sci. Eng.: A* **107**, 135-143 (1989).

158 Koerner, H., Price, G., Pearce, N. A., Alexander, M. & Vaia, R. A. Remotely actuated polymer nanocomposites—stress-recovery of carbon-nanotube-filled thermoplastic elastomers. *Nat. Mater.* **3**, 115-120 (2004).

159 Wu, C. J., Wilker, J. J. & Schmidt, G. Robust and adhesive hydrogels from cross-linked poly (ethylene glycol) and silicate for biomedical use. *Macromol. Biosci.* **13**, 59-66 (2013).

160 Barrett, D. G., Bushnell, G. G. & Messersmith, P. B. Mechanically robust, negative-swelling, mussel-inspired tissue adhesives. *Adv. Healthcare Mater.* **2**, 745-755 (2013).

161 Brubaker, C. E. & Messersmith, P. B. Enzymatically degradable mussel-inspired adhesive hydrogel. *Biomacromolecules* **12**, 4326-4334 (2011).

162 Peak, C. W., Wilker, J. J. & Schmidt, G. A review on tough and sticky hydrogels. *Colloid Polym. Sci.* **291**, 2031-2047 (2013).

163 Ilievski, F., Mazzeo, A. D., Shepherd, R. F., Chen, X. & Whitesides, G. M. Soft robotics for chemists. *Angew. Chem.* **123**, 1930-1935 (2011).

164 Bauer, S. *et al.* 25th Anniversary Article: A soft future: From robots and sensor skin to energy harvesters. *Adv. Mater.* **26**, 149-162 (2014).

165 Laulicht, B., Langer, R. & Karp, J. M. Quick-release medical tape. *Proc. Natl. Acad. Sci.* **109**, 18803-18808 (2012).

166 PingáGong, J. Robust bonding and one-step facile synthesis of tough hydrogels with desirable shape by virtue of the double network structure. *Polym. Chem.* **2**, 575-580 (2011).

167 Brown, H. R. Adhesion between polymers. *IBM J. Res. Dev.* **38**, 379-389 (1994).

168 Gent, A. & Hamed, G. Peel mechanics of adhesive joints. *Polym. Eng. Sci.* **17**, 462-466 (1977).

169 Simson, J., Crist, J., Strehin, I., Lu, Q. & Elisseeff, J. H. An orthopedic tissue adhesive for targeted delivery of intraoperative biologics. *J. Orthop. Res.* **31**, 392-400 (2013).

170 Kendall, K. The adhesion and surface energy of elastic solids. *J Phys. D: Appl. Phys.* **4**, 1186 (1971).

171 Asoh, T.-A. & Kikuchi, A. Electrophoretic adhesion of stimuli-responsive hydrogels. *Chem. Commun.* **46**, 7793-7795 (2010).

172 Tamagawa, H. & Takahashi, Y. Adhesion force behavior between two gels attached with an electrolytic polymer liquid. *Mater. Chem. Phys.* **107**, 164-170 (2008).

173 Rose, S. *et al.* Nanoparticle solutions as adhesives for gels and biological tissues. *Nature* **505**, 382-386 (2013).

174 Haraguchi, K. & Takehisa, T. Nanocomposite hydrogels: a unique organic-inorganic network structure with extraordinary mechanical, optical, and swelling/de-swelling properties. *Adv. Mater.* **14**, 1120 (2002).

175 Carlsson, L., Rose, S., Hourdet, D. & Marcellan, A. Nano-hybrid self-crosslinked PDMA/silica hydrogels. *Soft Matter* **6**, 3619-3631 (2010).

176 Haraguchi, K., Li, H.-J., Matsuda, K., Takehisa, T. & Elliott, E. Mechanism of forming organic/inorganic network structures during in-situ free-radical polymerization in PNIPA-clay nanocomposite hydrogels. *Macromolecules* **38**, 3482-3490 (2005).

177 Lake, G. & Thomas, A. The strength of highly elastic materials. *Proc. R. Soc. London, Ser. A* **300**, 108-119 (1967).

178 Vertegel, A. A., Siegel, R. W. & Dordick, J. S. Silica nanoparticle size influences the structure and enzymatic activity of adsorbed lysozyme. *Langmuir* **20**, 6800-6807 (2004).